Title
Taxonomies, Functions, and Applications of Rice-Associated Microbiome

Permalink
https://escholarship.org/uc/item/23r0h9jc

Author
Liechty, Zachary Seth

Publication Date
2021

Peer reviewed|Thesis/dissertation

Taxonomies, Functions, and Applications of Rice-Associated Microbiome

By

ZACHARY SETH LIECHTY
DISSERTATION

Submitted in partial satisfaction of the requirements for the degree of

DOCTOR OF PHILOSOPHY

in

Plant Biology

in the

OFFICE OF GRADUATE STUDIES

of the

UNIVERSITY OF CALIFORNIA

DAVIS

Approved:

Venkatesan Sundaresan, Chair

Philipp Zerbe

Alan Bennett

Committee in Charge

2021

i

TABLE OF CONTENTS

ACKNOWLEDGEMENTS

I would like to thank Professor Venkatesan Sundaresan for his continued support throughout my time in graduate school and for pushing me to become independent in thought and confident in my abilities in the lab. I also would not have been able to accomplish what I have without the mentorship and friendship of more experienced graduate students and postdocs, especially Joseph Edwards, Christian Santos-Medellín, and Ryan Melnyk. Thank you to other graduate and undergraduate students who helped in running experiments, including Esteban Veliz, David Mikhail, Bao Nguyen, Lynne Hagelthorn, Aaron Rosenfeld and Eva Muljono. Thank you to my dissertation committee, Philipp Zerbe and Alan Bennett for their thoughts and suggestions regarding my research. Thank you to Chenxin Li, Debra Skinner, and Chris Brooks for their friendship and for talking through experiments and analysis with me. Thank you to my D&D group for the much-needed escapes from reality. Thank you to my wife, Katie Liechty, and my children, Henry and Calvin Liechty, for the joy they brought me that carried me through these years and thank you to the rest of my family for their love and support.

ABSTRACT

Plant-associated microbes form complex interactions within their microbial community as well as with the host, affecting processes such as nutrient and carbon cycling, abiotic stress protection, and disease resistance. Understanding the interactions of the host and host-associated microbiomes could potentially aid plant health in a variety of ways and is therefore of interest to the plant science community. Rice is a unique system to study plant-microbe interactions because of flooded conditions in which it is cultivated. This anoxic environment leads to a host of anaerobic microbial taxa associating with the rice host which harbor functions dependent on the anoxic conditions, including methanogenesis. In this thesis, I describe three studies where we profile the taxonomies and functions of rice-associated microbiomes and demonstrate how the knowledge gained from these methods can be applied in discovering microbial isolates that are beneficial to the plant host.

In the first chapter, I present a study that characterizes the microbiomes of a high- and a low-methane-emitting rice cultivar throughout the growing season. We found that the high methane emitting cultivar had a higher relative abundance of methanogenic archaea in the rhizosphere, and additionally had a greater abundance of taxa associated with fermentation, which could be responsible for producing methanogenic precursor molecules.

In the second chapter, I present a study that characterizes the effects of drought and recovery on the microbiome. We found that a *Streptomyces* taxa became the most abundant member of the endosphere community during and after drought, and that this member was prevalent in rice samples from various locations. We cultured a corresponding isolate and demonstrated that it had similar qualities to the *Streptomyces* from the study (it was endophytic and increased in relative abundance under drought stress) and promoted root growth,

demonstrating the enrichment of this microbe under drought could potentially mitigate drought effects.

In the third chapter, I present a study demonstrating the effects of nitrogen on the microbiome in three different soils by profiling both the taxonomies and functions through genome-resolved metagenomics. We found that the response of rice-associated microbiomes to the nitrogen fertilizer was largely soil specific, though there were general increases in Gammaproteobacteria and decreases in Actinobacteria in response to nitrogen. Profiling the metagenome demonstrated that nitrogen fertilizer increased the abundance of genes related to aromatic compound degradation, fermentation, and methanogenesis. We also recovered 60 metagenome assembled genomes, which to our knowledge is the first such dataset of its kind in rice, and can be a valuable resource to further understanding the dynamics of microbes associating with rice.

Chapter 1

Comparative Analysis of Root Microbiomes of Rice Cultivars with High and Low Methane Emissions Reveals Differences in Abundance of Methanogenic Archaea and Putative Upstream Fermenters

Zachary Liechty[a], Christian Santos-Medellín[a], Joseph Edwards[a], Bao Nguyen[a], David Mikhail[a], Shane Eason[b], Gregory Phillips[b], Venkatesan Sundaresan[a,c]

[a]Department of Plant Biology, University of California, Davis, Davis, California, USA
[b]Department of Agriculture, Arkansas State University, Jonesboro, Arkansas, USA
[c]Department of Plant Sciences, University of California, Davis, Davis, California, USA

Abstract

Rice cultivation worldwide accounts for ~7 to 17% of global methane emissions. Methane cycling in rice paddies is a microbial process not only involving methane producers (methanogens) and methane metabolizers (methanotrophs) but also other microbial taxa that affect upstream processes related to methane metabolism. Rice cultivars vary in their rates of methane emissions, but the influence of rice genotypes on methane cycling microbiota has been poorly characterized. Here, we profiled the rhizosphere, rhizoplane, and endosphere microbiomes of a high-methane-emitting cultivar (Sabine) and a low-methane-emitting cultivar (CLXL745) throughout the growing season to identify variations in the archaeal and bacterial communities relating to methane emissions. The rhizosphere of the high-emitting cultivar was enriched in methanogens compared to that in the low emitter, whereas the relative abundances of methanotrophs between the cultivars were not significantly different. Further analysis of cultivar-sensitive taxa identified families enriched in the high emitter that are associated with methanogenesis-related processes. The high emitter had greater relative abundances of sulfate-

reducing and iron-reducing taxa which peak earlier in the season than methanogens and are necessary to lower soil oxidation reduction potential before methanogenesis can occur. The high emitter also had a greater abundance of fermentative taxa which produce methanogenesis precursors (acetate, CO_2, and H_2). Furthermore, the high emitter was enriched in taxa related to acetogenesis which compete with methanogens for CO_2 and H_2. These taxa were enriched in a spatio-specific manner and reveal a complex network of microbial interactions on which plant genotype-dependent factors can act to affect methanogenesis and methane emissions.

Author Contributions

The initial project was conceptualized by VS, JE, SE, and GP. The field experiment was overseen by SE and GP in Arkansas. Samples were processed, and 16S region was sequenced by ZL, JE, CS-M, and BN. Sequences were processed and data was analyzed by ZL. ZL conceptualized and carried out the aerenchyma experiment, including the processing and analysis of pycnometer and cross sectioning results. DM analyzed performed image analysis on root section images.

Comparative Analysis of Root Microbiomes of Rice Cultivars with High and Low Methane Emissions Reveals Differences in Abundance of Methanogenic Archaea and Putative Upstream Fermenters

Zachary Liechty,[a] Christian Santos-Medellín,[a] Joseph Edwards,[a] Bao Nguyen,[a] David Mikhail,[a] Shane Eason,[b] Gregory Phillips,[b] Venkatesan Sundaresan[a,c]

[a]Department of Plant Biology, University of California, Davis, Davis, California, USA
[b]Department of Agriculture, Arkansas State University, Jonesboro, Arkansas, USA
[c]Department of Plant Sciences, University of California, Davis, Davis, California, USA

Christian Santos-Medellín and Joseph Edwards contributed equally to this work.

ABSTRACT Rice cultivation worldwide accounts for ~7 to 17% of global methane emissions. Methane cycling in rice paddies is a microbial process not only involving methane producers (methanogens) and methane metabolizers (methanotrophs) but also other microbial taxa that affect upstream processes related to methane metabolism. Rice cultivars vary in their rates of methane emissions, but the influence of rice genotypes on methane cycling microbiota has been poorly characterized. Here, we profiled the rhizosphere, rhizoplane, and endosphere microbiomes of a high-methane-emitting cultivar (Sabine) and a low-methane-emitting cultivar (CLXL745) throughout the growing season to identify variations in the archaeal and bacterial communities relating to methane emissions. The rhizosphere of the high-emitting cultivar was enriched in methanogens compared to that in the low emitter, whereas the relative abundances of methanotrophs between the cultivars were not significantly different. Further analysis of cultivar-sensitive taxa identified families enriched in the high emitter that are associated with methanogenesis-related processes. The high emitter had greater relative abundances of sulfate-reducing and iron-reducing taxa which peak earlier in the season than methanogens and are necessary to lower soil oxidation reduction potential before methanogenesis can occur. The high emitter also had a greater abundance of fermentative taxa which produce methanogenesis precursors (acetate, CO_2, and H_2). Furthermore, the high emitter was enriched in taxa related to acetogenesis which compete with methanogens for CO_2 and H_2. These taxa were enriched in a spatio-specific manner and reveal a complex network of microbial interactions on which plant genotype-dependent factors can act to affect methanogenesis and methane emissions.

IMPORTANCE Rice cultivation is a major source of anthropogenic emissions of methane, a greenhouse gas with a potentially severe impact on climate change. Emission variation between rice cultivars suggests the feasibility of breeding low-emission rice, but there is a limited understanding of how genotypes affect the microbiota involved in methane cycling. Here, we show that the root microbiome of the high-emitting cultivar is enriched both in methanogens and in taxa associated with fermentation, iron, and sulfate reduction and acetogenesis, processes that support methanogenesis. Understanding how cultivars affect microbes with methanogenesis-related functions is vital for understanding the genetic basis for methane

Address correspondence to Venkatesan Sundaresan, sundar@ucdavis.edu.

3

emission in rice and can aid in the development of breeding programs that reduce the environmental impact of rice cultivation.

KEYWORDS endosphere, fermentation, methane, methanogenesis, microbiome, rhizoplane, rhizosphere, rice, root

Methane (CH_4), a potent greenhouse gas, has 28 times the global warming potential of CO_2 (1). A major source of anthropogenic CH_4 emissions is rice cultivation, which accounts for approximately 7 to 17% of the global CH_4 sources (25 to 100 terragrams [Tg] of CH_4 per year) (2–4). Methane is produced by facultative anaerobic archaea in the rice rhizosphere, which subsist predominantly on carbon sources originating from the rice plant, such as root exudate (5, 6). After production in the rhizosphere, CH_4 diffuses into the root airspaces (aerenchyma) and is transported through the plant and into the atmosphere. Up to 80% of the CH_4 produced in soils of paddy fields was found to be transported into the atmosphere through the aerenchyma of rice plants (7). Methanogens interact positively and negatively with several microbial taxa that influence the rate of methanogenesis. Methanogens cannot directly consume complex root exudates but rather rely on the fermentative activity of syntrophic microbes to produce methanogenic precursor molecules such as acetate, H_2, and CO_2 (8, 9). On the other hand, methanotrophic bacteria oxidize CH_4 and reduce the amount of CH_4 emitted by up to 60% (10). Methanogens can also be outcompeted by microbes that consume the same precursor molecules, such as anaerobic respiring microbes that reduce nitrate, sulfate, and iron (9, 11).

An effort to mitigate the environmental impact of rice cultivation using a transgenic approach has been reported (12). An alternate approach is to exploit natural variation in CH_4 emissions between rice genotypes. A survey of different rice cultivars identified varieties that exhibit divergence in CH_4 emissions through the growing season, with up to 2-fold variation in average seasonal CH_4 emissions between the high- and low-emitting cultivars (13). Understanding the underlying causes behind these genotype-mediated differences in CH_4 emissions could lead to mitigation strategies to curb the environmental cost of rice cultivation. Genotypic variation has been shown to directly affect the microbial composition of methanogens and methanotrophs, and low emitters have been reported to have an increased abundance of methanotrophs (14, 15). However, these studies were limited to only estimating methanogen and methanotrophs and did not survey the compositional profiles of all bacteria and archaea in the root microbiomes. By profiling full bacterial and archaeal communities, we can identify variations in the abundances not only of methanogens and methanotrophs but also in other microbes fulfilling the above-mentioned niches related to methanogenesis. We have previously demonstrated that the rice root microbiome exhibits a reproducible dependence on plant genotype (16, 17). Rice microbiomes are also spatially structured in compositionally distinct compartments, namely, the rhizosphere (soil directly influenced by root activity), the rhizoplane (surface of the root), and the endosphere (interior of the root) (16–18). The composition of root microbiomes also shifts throughout the life cycle of rice plants, with individual members displaying reproducible temporal patterns across geographic regions and growing seasons (18, 19). Such highly dynamic spatiotemporal trends emphasize the need to incorporate these sources of variation when exploring the root-associated taxa related to the processes around methanogenesis.

Here, we characterized microbial differences between low- and high-CH_4-emitting rice cultivars through the growing season by in-depth 16S rRNA sequence analysis of their root microbiomes. Based on previous studies by Simmonds et al. (13), we selected the low-emission hybrid CLXL745 and the high-emission cultivar Sabine, which display divergent CH_4 emissions late in the season postheading (13). We investigated whether the variation in CH_4 emissions might be due to either a greater abundance of methanogens, upstream fermenters, and syntrophs in the rhizosphere of Sabine or a greater abundance of methanotrophs in the endosphere or rhizosphere of CLXL745. We also

characterized the aerenchyma development in these two cultivars under controlled-growth conditions. We conclude that the cultivars do not differ significantly in aerenchyma or in relative abundance of methanotrophs but that the high-emitting microbiome has an increased relative abundance of methanogenic microbes, as well as compartment-specific consortia of microbes associated with fermentation, sulfate and iron reduction, and acetogenesis.

RESULTS

The hybrid rice cultivar CLXL745 has been shown to consistently emit less CH_4 than do other cultivars in a variety of locations and conditions (13, 20–22), whereas Sabine, an inbred cultivar grown in the southeastern rice-producing region of the United States, has been shown to emit significantly more CH_4 than CLXL745, particularly later in the season (13). In this study, we utilized an experiment in which the two cultivars were grown in an Arkansas field and sampled every 2 weeks over approximately 4 months, constituting the entire life cycle of the plants (18). At each time point, the bulk soil, rhizosphere, rhizoplane, and endosphere were sampled. The rhizosphere and endosphere samples were previously sequenced and analyzed to investigate the dynamics of temporal succession of the microbiome over a growing season (18); however, an in-depth analysis of cultivar variation, particularly in regard to CH_4 metabolism, had not been performed in that study. Here, we included additionally sequenced samples from the experiment corresponding to the rhizoplane, which represents a critical plant-soil interface, and integrated the previously published raw sequence data from the endosphere and rhizosphere to perform the new analyses detailed below.

The microbial compositions of the root compartments vary throughout the growing season between Sabine and CLXL745. Permutational multivariate analysis of variance (PERMANOVA) on Bray-Curtis dissimilarities revealed that compartment, time point, and cultivar were significant main effects and that the interactions between time point and cultivar and between time point and compartment were significant as well (see Table S1A in the supplemental material). To further confirm that the cultivar effect was apparent in each compartment, the data were subsetted by compartment, and PERMANOVA was run on each compartment individually (Table S1B to D). Cultivar and time point were found to be significant in each compartment. To examine if the variation between cultivars in each compartment could be confounded by the location of the plots, PERMANOVA was run on bulk soil samples to check if bulk soils from plots growing CLXL745 varied from bulk soils growing Sabine. The "cultivar effect" (meaning plots growing each cultivar) was not significant, indicating that the variation observed in the compartments is not due to their plots of origin (Table S1E). Principal-coordinate analysis showed the separation of compartments along the first axis, with rhizoplane samples falling between rhizosphere and endosphere samples (Fig. S1A). This observation followed patterns observed in rice microbiome samples in previous studies (16, 18). Furthermore, the rhizoplane samples showed similar temporal dynamics previously elaborated on by Edwards et al. (18). Namely, the microbiota composition of the rhizoplane stabilizes once the plants reach the reproductive stage (Fig. S1C) and have similar temporal shifts in taxa, such as a seasonal increase in *Deltaproteobacteria* (Fig. S1D). Although these samples were omitted from the previous experiment, these analyses show that the rhizoplane microbiota is not aberrant in its composition or successional patterns.

A canonical analysis of principal coordinates (CAP) was used to identify variation between cultivars. Since the relative effect size of compartment is large, this variable was partialled out. The results confirmed the significance of the cultivar effect and cultivar-time interaction identified in the above-mentioned PERMANOVA (Fig. 1A and S1B and Table S1F). The first principal-coordinate axis correlated with time, and the second principal-coordinate axis displayed variation due to cultivar. A continual increase in the divergence between the cultivars was observed, although this effect was much larger in the rhizoplane and endosphere than in the rhizosphere (Fig. 1A).

5
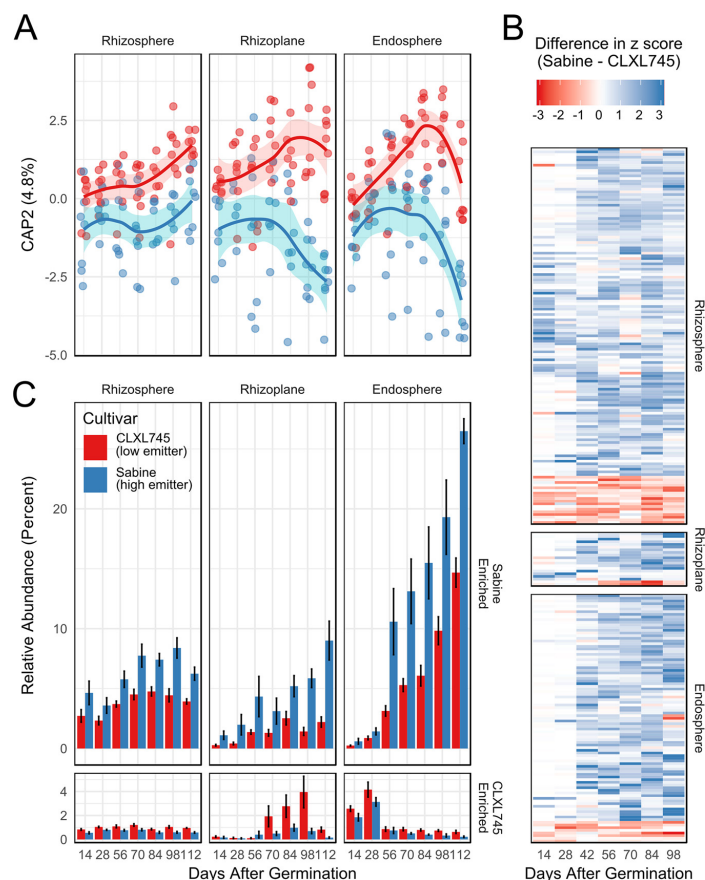
FIG 1 Cultivar significantly shapes the root microbiome. (A) Canonical analysis of principal coordinates controlling for compartment effects. Points are individual samples, whereas the line denotes the cultivar average. The shaded ribbon denotes the standard error ($n = 6$ to 8). The x axis represents days after germination and corresponds to the x axis in panel C. (B) The difference in Z-scores of each OTU identified as significant ($P < 0.05$) in the likelihood ratio test. Each column represents one time point, and each row is an individual OTU within the compartment denoted on the right. The Z-score is calculated within the OTU across all time points within both cultivars. The difference was calculated by subtracting the Z-score of CLXL745 from Sabine, meaning that positive numbers (blue) are enriched in Sabine over CLXL745, and negative numbers (red) are enriched in CLXL745. White indicates no difference in Z-score. (C) Cumulative relative abundance of Sabine-enriched and CLXL745-enriched OTUs within each compartment. OTUs were defined as Sabine or CLXL745 enriched by averaging the seasonal fold change at each time point between the two cultivars for each OTU in the LRT-derived list. Error bars indicate the standard error ($n = 6$ to 8).

To identify operational taxonomic units (OTUs) whose relative abundances differ between cultivars, a likelihood ratio test (LRT) was performed. We found 141, 20, and 93 OTUs that significantly contributed to cultivar variation in the rhizosphere, rhizoplane, and endosphere communities, respectively (false-discovery rate [FDR], <0.05) (Fig. 1B and Data Set S1). The majority of these cultivar-sensitive OTUs showed no abundance differences between cultivars until after 28 days postgermination, confirming the patterns observed in the CAP analysis (Fig. 1B). The average seasonal log fold change revealed that most of these cultivar-sensitive OTUs were Sabine enriched (123/141 in the rhizosphere, 18/20 in the rhizoplane, and 85/93 in the endosphere).

6

FIG 2 Cultivars vary significantly in methanogen abundances in the rhizosphere but not methanotroph abundance in any compartment. (A) Seasonal trends of OTUs 139580 and 706555, the two methanogens in the list of cultivar-sensitive OTUs detected in the rhizosphere. The colored line indicates the average relative abun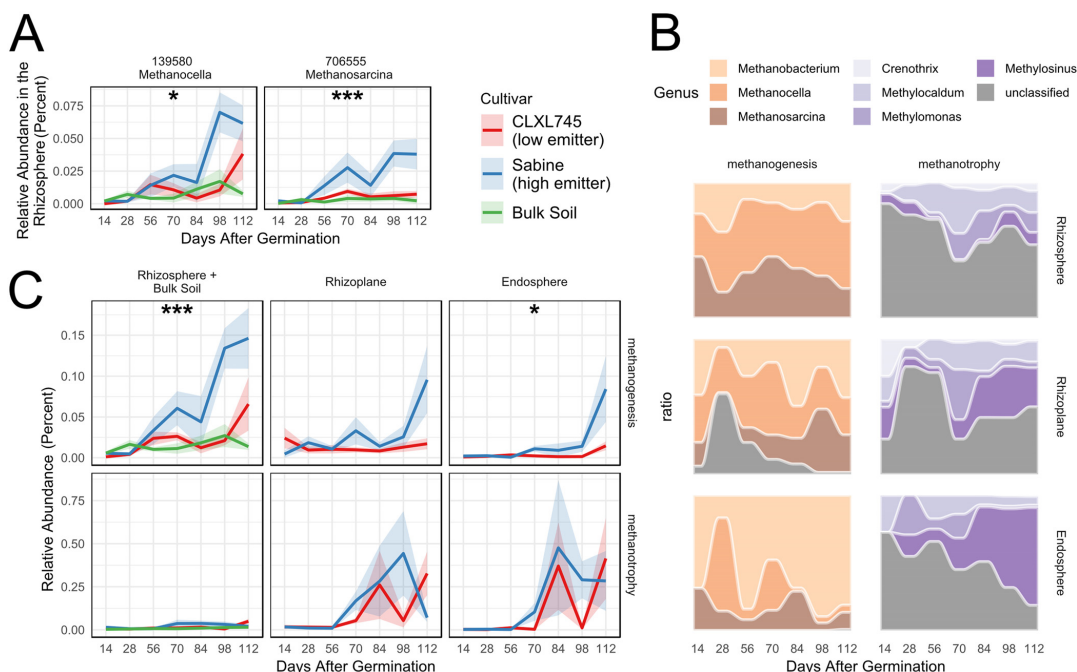dance, and the colored ribbon indicates the standard error ($n = 6$ to 8). Asterisks indicate that the OTU was significant in the likelihood ratio test (*, $P < 0.05$; **, $P < 0.01$; ***, $P < 0.001$). Statistical comparisons were only performed between Sabine and CLXL745 samples, and the bulk soil is shown for reference. (B) Total relative abundances of methanogenic archaea and methanotrophic bacteria as defined by FAPROTAX. The shaded colored ribbon indicates the standard error ($n = 6$ to 8). Asterisks indicate that the cultivar term was significant in the ANOVA on variance-stabilized data (*, $P < 0.05$; **, $P < 0.01$; ***, $P < 0.001$). Statistical comparisons were only performed between Sabine and CLXL745 samples. (C) Seasonal shifts in methanogen and methanotroph compositions within each compartment. Color indicates the average relative proportion of methanogens or methanotrophs across both cultivars.

Looking at their cumulative relative abundances further revealed that the magnitude of difference between cultivars increased throughout the growing season within the Sabine-enriched OTUs (Fig. 1C). The Sabine-enriched OTUs also increased in relative abundance throughout the growing season, indicating that many of these OTUs established themselves later in the growing season. These data show that the difference between cultivars becomes more pronounced later in the season, and this difference is driven largely by Sabine-enriched late colonizers.

OTUs involved in methanogenesis contribute to the variation between cultivars in each compartment. Predictive software, such as the Functional Annotation of Prokaryotic Taxa (FAPROTAX), can be used to identify OTUs in a data set which are likely to display a phylogenetically linked trait of interest. We used FAPTROTAX, which has recently been applied to the rice rhizosphere (23), to identify putative taxa associated with methanogenesis and methanotrophy. FAPROTAX identified methanogenesis-associated OTUs belonging to the genera *Methanocella*, *Methanosarcina*, and *Methanobacterium*. Two methanogenesis-associated OTUs from the genera *Methanocella* and *Methanosarcina* (OTUs 139580 and 706555, respectively) were identified as significant contributors to cultivar variation in the rhizosphere samples (Fig. 2A). Both OTUs had a higher average abundance in Sabine over CLXL745, and this variation was greater later in the season during the growth stages where these cultivars have been shown to be most divergent in CH_4 emissions (13). No methanotrophic OTUs were significantly differentially abundant between cultivars in any compartment.

7

The cumulative relative abundances of OTUs associated with methanogenesis and methanotrophy were also compared using analysis of variance (ANOVA) with linear models on data that were variance stabilized using DESeq2 (Fig. 2B and Table S2). Methanogens were significantly enriched in the rhizosphere of Sabine at 98 and 112 days after germination ($P < 0.05$). Methanogen- and methanotroph-associated OTU compositions also changed throughout the season and between compartments (Fig. 2C). *Methanocella* and *Methanosarcina* OTUs were most prominent in the rhizosphere, decreased in abundance in the rhizoplane, and were depleted to an even greater degree in the endosphere. *Methanobacterium* OTUs followed the opposite trend, becoming more prominent from the exterior of the root inward. Similarly, *Methylosinus* OTUs became the more prominent methanotrophs from the exterior of the root in. In the endosphere, *Methylosinus* OTUs increased in prominence throughout the season as well (Fig. 2C).

Although differences in methanogen relative abundances were identified between the cultivars in the rhizosphere, it is possible that the relative abundance comparisons between cultivars do not correlate to absolute abundances. For example, one cultivar might support a diverse microbiome with increased microbial load in the rhizosphere compared to another cultivar causing OTUs with relatively lower abundance to have a larger absolute abundance. The absolute abundances of methanogens and methanotrophs are likely to be a better indicator of cultivar effects on CH_4 emissions. To test if the relative abundances of methanogens and methanotrophs observed correlate with the absolute abundances, we performed quantitative PCR (qPCR) on a methanogen-specific region of the 16S rRNA gene and the alpha subunit of the methane monooxygenase gene (*pmoA*), which is necessary for methanotrophy. This procedure also allowed us to assess whether the absolute abundances of methanogens and methanotrophs varied between cultivars. Since the final two time points showed the greatest differences in cumulative methanogen relative abundances in the rhizospheres of the two cultivars, qPCR was performed on the bulk soil and rhizosphere samples of both cultivars at these time points (Fig. S2A). The bulk soil samples were subsetted by plots growing each cultivar to check if the plots of origin could be affecting the abundances of these markers in our samples; neither marker varied between bulk soils originating from plots growing different cultivars (ANOVA, $P = 0.3462$ for the methanogen-specific 16S rRNA marker and $P = 0.8469$ for the *pmoA* marker), so for further analysis, these samples were not distinguished from each other. The final time point was found to have significant differences between Sabine and both the bulk soil and CLXL745 for the methanogen marker. There was no significant difference between cultivars in *pmoA* abundance (Fig. S2). Furthermore, there was a significant positive correlation between the corresponding methanogen relative abundances from 16S rRNA gene amplicon libraries and absolute abundances from qPCR ($r = 0.480$, $P = 0.001$) but not a significant correlation between methanotroph 16S relative abundance and *pmoA* abundance ($r = 0.131$, $P = 0.425$). This result validated the use of 16S rRNA gene amplicon relative abundances to compare methanogen compositions in this context and confirmed that the high-CH_4-emitting cultivar had an increased abundance of methanogens over the low emitter. Although there was a weak correlation between the OTUs associated with methanotrophy identified through FAPROTAX and the *pmoA* abundances, both measures confirm that methanotroph abundances do not vary between cultivars.

Overrepresented families enriched in Sabine are associated with methanogenesis-related processes. Since there was a significant enrichment of methanogens in the rhizosphere of the high emitter over the low emitter, we hypothesized that other cultivar-sensitive OTUs might be playing a role in the upstream processes related to methanogenesis (i.e., fermentation, syntrophy, etc.). To examine this, hypergeometric tests were performed within each compartment to determine which taxa at each taxonomic rank were overrepresented in the cultivar-sensitive OTUs to identify taxa that are enriched in these lists more than expected by chance (Data Set S2). The methanogenic class *Methanomicrobia* (the class containing methanogenic archaea) was notably overrepresented in the rhizosphere, with two of five *Methanomicrobia* OTUs
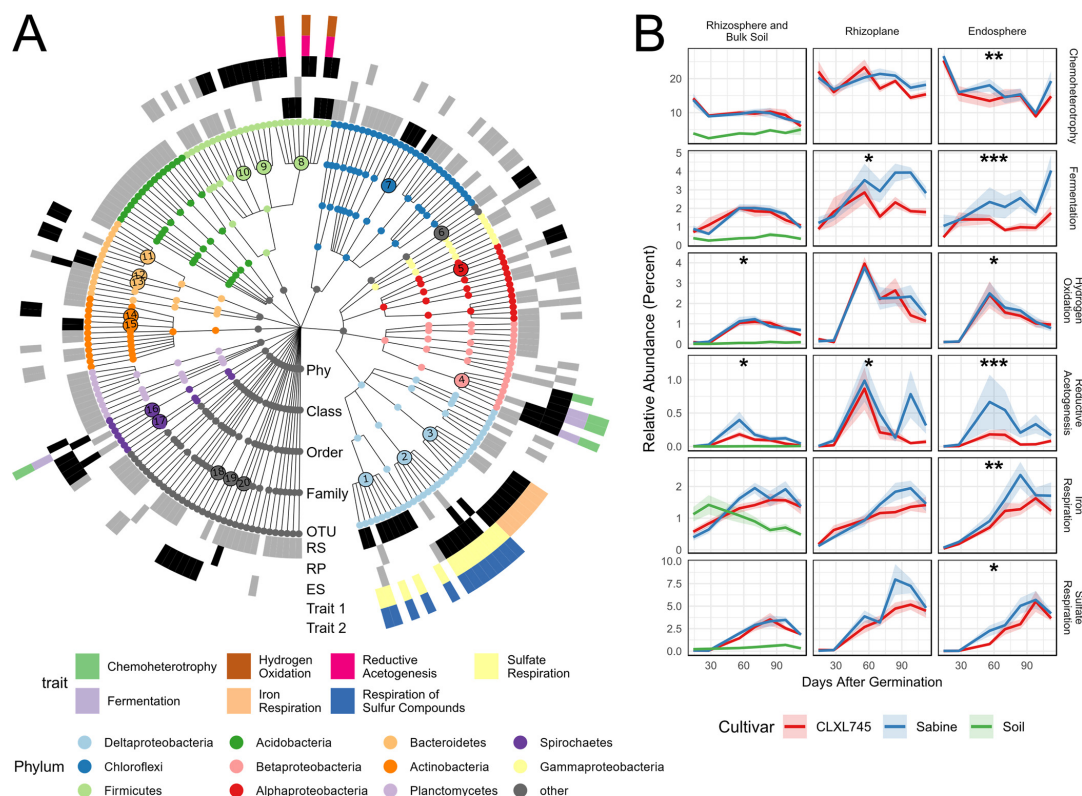
8

FIG 3 Overrepresented families in the set of cultivar-sensitive OTUs are associated with various anaerobic metabolic traits. (A) Taxonomy dendrogram displaying cultivar-sensitive OTUs in any compartment ($P < 0.05$). The color of each dot represents the phylum (Phy) to which it belongs. A gray or black box in the first three rings indicates that that OTU is cultivar sensitive in the rhizosphere, rhizoplane, or endosphere going from the inside out (RS, rhizosphere; RP, rhizoplane; ES, endosphere). Additionally, a black box means that OTU belongs to a family that is overrepresented among the cultivar-sensitive OTUs in that compartment. The larger numbered circles in the dendrogram are indicative of families that are overrepresented in at least one compartment (hypergeometric test, $P < 0.05$). The corresponding families are found at the end of this text block. The outer two rings indicate traits associated with overrepresented families assigned using FAPROTAX. (B) Relative abundances of all OTUs associated with the traits identified in panel A. The colored shaded ribbon represents the standard error ($n = 6$ to 8). Asterisks indicate that the cultivar term was significant in the ANOVA on variance-stabilized data (*, $P < 0.05$; **, $P < 0.01$; ***, $P < 0.001$). OTUs associated with respiration of sulfur compounds were not included because this list did not vary from the OTUs associated with sulfate respiration. The overrepresented families represented by the numbered circles in panel A correspond to the following families: 1, *Syntrophobacteraceae*; 2, *Desulfovibrionaceae*; 3, *Geobacteraceae*; 4, *Rhodocyclaceae*; 5, unclassified family in the order Ellin329; 6, *Helicobacteraceae*; 7, *Anaerolineaceae*; 8, *Veillonellaceae*; 9, *Ruminococcaceae*; 10, unclassified family in the order *Clostridiales*; 11, unclassified family in the order *Bacteroidales*; 12, BA008; 13, *Bacteroidaceae*; 14, *Cellulomonadaceae*; 15, *Nakamurellaceae*; 16, *Spirochaetaceae*; 17, *Sphaerochaetaceae*; 18, TG3-1; 19, *Ignavibacteriaceae*; and 20, *Phormidiaceae*.

(OTUs 139580 and 706555 discussed above) present in the list of cultivar-sensitive OTUs ($P < 0.05$). At the family level, the rhizosphere, rhizoplane, and endosphere had five, five, and 14 families overrepresented in the cultivar-sensitive OTUs, respectively (Fig. 3A and Data Set S2). Almost all OTUs belonging to these overrepresented families had greater relative abundance in Sabine than in CLXL745 (Fig. S3).

FAPROTAX was again used to identify functions associated with overrepresented families. Only traits assigned to more than one OTU were further considered, but the full list of functional trait assignments can be found in Data Set S1. The overrepresented families mentioned above in all three compartments were associated with sulfate respiration (*Syntrophobacteraceae* in the rhizosphere and *Desulfovibrionaceae* in the rhizoplane and endosphere) (Fig. 3A). Families in both the rhizosphere and the endosphere were associated with reductive acetogenesis and hydrogen oxidation (the genus *Sporomusa* within *Veillonellaceae* in both the rhizosphere and endosphere)

9

TABLE 1 Fermentative functions associated with overrepresented families in the list of cultivar-sensitive OTUs[a]

Overrepresented taxon	Compartment(s)	Fermentative process (reference)	Source
Rhodocyclaceae	RP, ES	Genus *Propionivibrio* (ES, 3/6 OTUs; RP, 2/3 OTUs) ferments sugars, dicarboxylic acids, sugar alcohols, and aspartate to produce propionate and acetate (68)	FAPROTAX
Spirochaetaceae	RP	Genus *Spirochaeta* (RP, 1/2 OTUs) produces acetate, ethanol, CO_2, and H_2 as fermentative end products (69); previously identified as enriched in endosphere and associated with cellulose degradation (16)	FAPROTAX
Cellulomonadaceae	ES	Genus *Actinotalea* (ES, 2/2 OTUs) contains isolates that are cellulose degrading and acetate and formate producing (70)	Literature search
Veillonellaceae	RS, RP, ES	Many isolates produce acetate and propionate as fermentative end products (71)	Literature search
Desulfovibrionaceae	RP, ES	Produce acetate, CO_2, and H_2 through fermentation of lactate and pyruvate (72); *Desulfovibrio* spp. (RP, 2/2 OTUs; ES, 7/7 OTUs) have been characterized to have a syntrophic association with *Methanobacterium* spp., the most abundant methanogens in the endosphere (50)	Literature search
BA008	RS	Produce acetate, propionate, formate, and H_2 through fermentation (73)	Literature search
Anaerolineaceae	RS	"Semisyntrophic," in that coculture with methanogens significantly stimulated growth (74); produce acetate through fermentation (53)	Literature search
Syntrophobacteraceae	RS	Genus *Syntrophobacter* (RS, 5/8 OTUs) act syntrophically with methanogens using H_2/formate shuttling (75); acetate produced by *Syntrophobacteraceae* consumption of propionate is preferentially consumed by *Methanosarcina* spp. (35)	Literature search

[a]RS, rhizosphere; RP, rhizoplane; ES, endosphere.

(Fig. 3A). Families in the rhizoplane and endosphere were associated with fermentation and chemoheterotrophy (*Rhodocyclaceae* in both the rhizoplane and endosphere and *Spirochaetaceae* additionally in the rhizoplane) (Fig. 3A). The endosphere additionally contained members of a family associated with iron respiration (*Geobacteraceae*) (Fig. 3A). Although these traits were found to be associated with certain overrepresented families within the cultivar-sensitive OTUs, we wanted to test whether the overall trends of microbes associated with these traits were different between the cultivars in each compartment (Fig. 3B). The data were variance stabilized using DESeq2, and linear models in conjunction with ANOVA were used to identify significant differences. We found taxa associated with reductive acetogenesis, hydrogen oxidation, fermentation, chemoheterotrophy, iron respiration, and sulfur respiration to vary significantly in relative abundance across cultivars and compartments (Table S2). Additional literature was searched to find other functions associated with the overrepresented families of the rhizosphere (Table 1).

Clustering analysis identifies OTUs that show seasonal patterns similar to those of methanogen OTUs. Previous studies have used 16S rRNA gene amplicon data to identify OTUs that cluster with methanogen OTUs in samples in rice paddies or in wetlands that were geographically or compartmentally separated (16, 24, 25). We performed a time series-based clustering using global alignment kernels on the cultivar-sensitive OTUs within the rhizosphere to identify consortia of OTUs that showed similar temporal and cultivar-specific patterns (Fig. S4 and Data Set S1). Methanogenic archaea partitioned to cluster 2, which contained 31 OTUs in total. Eleven of the 31 OTUs in the cluster were of the class *Anaerolineae*, two of which are of the genus *Anaerolinea* (from the overrepresented family *Anaerolineaceae*), two from the genus *Caldilinea*, three from the order SBR1031, three from the order GCA004, and one from the order WCHB1-50.

Sabine-enriched OTUs generally show an enrichment in the rhizosphere compared to bulk soil samples. Although rhizosphere OTUs can be classified as enriched in either CLXL745 (low emitter) or Sabine (high emitter), the question remains whether the enrichment of these OTUs in one cultivar is due to an increase in abundance in that
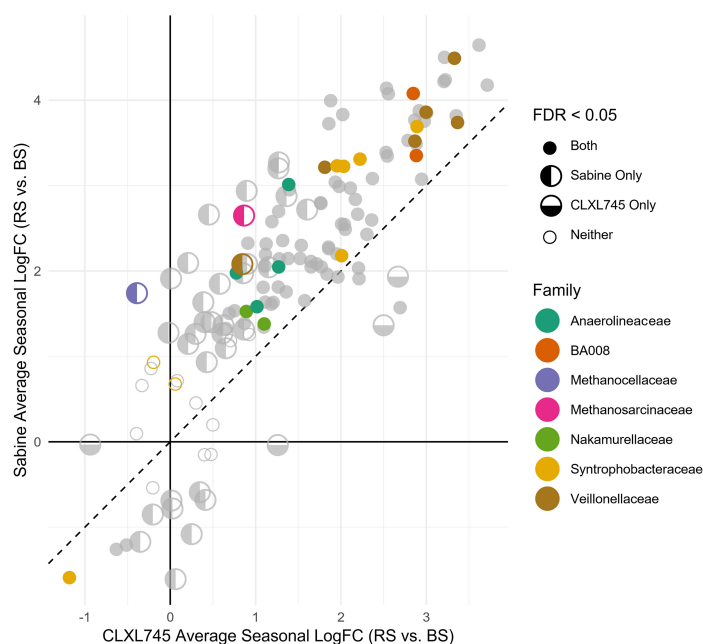
10

FIG 4 Cultivar-sensitive OTUs are enriched or depleted in a greater degree in the rhizosphere of Sabine than the rhizosphere of CLXL745 when compared to bulk soils (BS) from their respective plots. Each circle represents one OTU that significantly differs between cultivars in the rhizosphere. Colored dots represent the five families that are overrepresented in the list of cultivar-sensitive OTUs in the rhizosphere compared to the total community (hypergeometric test, $P < 0.05$), and the two methanogenic families are represented in the same list. A full circle indicates that that OTU is significantly depleted or enriched in the rhizospheres of both cultivars compared to bulk soil. A half circle filled on the left indicates significant enrichment or depletion in the rhizosphere of Sabine compared to bulk soil but not CLXL745. A half circle filled on the bottom indicates the opposite. An empty circle indicates that neither cultivar is significantly enriched or depleted compared to bulk soil. FC, fold change.

cultivar compared to bulk soil or to a depletion in the other cultivar compared to bulk soil. To examine this question, the cultivar-sensitive OTUs on our list were compared between the rhizosphere samples of each cultivar and the bulk soil samples originating from corresponding plots (i.e., rhizospheres from CLXL745 plots compared to bulk soils from CLXL745 plots). The majority of these OTUs had a greater abundance in the rhizosphere of both cultivars than in bulk soil, and the majority of these rhizosphere-enriched OTUs were also enriched in the rhizosphere of Sabine over CLXL745 (Fig. 4). Conversely, OTUs that are depleted in rhizospheres are less abundant in the rhizosphere of Sabine than in that of CLXL745 (Fig. 4). This indicates that Sabine had a larger influence over both those OTUs that are enriched and those OTUs that are depleted. Both methanogen OTUs showed significant enrichment in the rhizosphere of Sabine compared to bulk soil, whereas the methanogens in the rhizosphere of CLXL745 compared to the bulk soil were not significantly different (Fig. 4). All overrepresented families in the rhizosphere LRT-derived list discussed above were also enriched in the rhizosphere over the bulk soil. The *Syntrophobacteraceae* followed a bimodal distribution, with OTUs 620224, 591709, and New.ReferenceOTU1528 showing much less enrichment in the rhizosphere than in the bulk soil.

Root airspace measurements of cultivars display a complex relationship with microbial taxa distribution and CH$_4$ emissions. An unexpected result of the trait-based analysis described above was an enrichment of microbes associated with fermentation in the endosphere of the high-emitting Sabine over the low-emitting

11
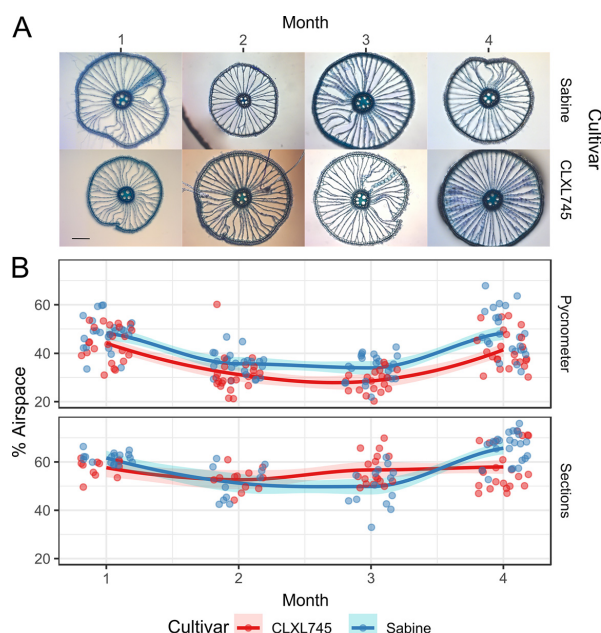
FIG 5 Airspaces of Sabine and CLXL745 over time. (A) Cross-sections indicative of those used to quantify the airspace in panel B. All images are at the same magnification. Black scale bar = 100 μm. (B) Percent airspace calculated using pycnometers (top) and area of sections (bottom). Dots in the top graph represent individual pycnometer measurements (n = 3 per plant). Dots in the bottom graph represent measurements from individual cross-sections of roots (n = 3 to 5 per root). Lines are the average of each sample (determined by averaging the subsamples). The shaded ribbons indicates the standard error (n = 4).

CLXL745. Since the endosphere is a relatively aerobic environment, and the fermentation processes that support methanogens are anaerobic, we hypothesized that the observed variation might be due to either structural variation of the root between cultivars allowing for greater activity of anaerobic metabolism or to an increased substrate availability in the anaerobic or microaerobic sections of the root. In support of the first hypothesis, Jiang et al. found that in a comparison of two cultivars, a higher-performing cultivar had a greater airspace than did a lower-yielding cultivar, which could account for increased oxygen diffusion into the root and potentially an increase in methanotrophy (14).

We therefore investigated whether Sabine had a reduced airspace compared to CLXL745, resulting in more anaerobic/microaerobic environments where fermentation can occur. To test this, we measured aerenchyma in both cultivars during four monthly time points throughout the life cycle in a greenhouse experiment. The proportion of root space occupied by the aerenchyma was measured by two methods (26). The first method was direct observation of cross-sections of similar-sized mature roots of the two cultivars (Fig. 5A). The second method was indirect measurement, using the pycnometer method, which measures total airspace volumes in a selection of roots; the volumes were used to compute the proportional airspace in that selection of roots (Fig. 5B).

We used ANOVA and linear modeling to determine significant factors affecting aerenchyma variation using both methods (Table S3). Conflicting results were obtained, which are likely due to the differences in measurement types, wherein the cross-sections and the pycnometer measure the proportional air capacities of individual

12

mature roots and of the total roots, respectively. For example, the pycnometer measurements can be influenced by factors such as increased tillering, which produces a greater fraction of younger roots with undeveloped aerenchyma. The cross-section measurements indicated that there were no significant differences in aerenchyma sizes between the cultivars, i.e., roots of similar diameter did not differ in aerenchyma area in the cross-sections. We did observe a significant difference in the volume percentages between the cultivars in the pycnometer measurements (Table S3). However, using this assay, the high-emission cultivar Sabine showed a proportionately greater aerenchyma volume than did CLXL745, which is the opposite of the result expected, both from our hypothesis and from the predictions of Jiang et al. (14).

DISCUSSION

Microbial variation between cultivars suggests an increased relative abundance of methanogens in the high-CH$_4$-emitting Sabine. In this study, we investigated the possible factors underlying differences in CH$_4$ emissions between the high-emission rice cultivar Sabine and the low-emission rice variety CLXL745. We identified two methanogen OTUs belonging to the genera *Methanocella* and *Methanosarcina* that were enriched in the rhizosphere of Sabine compared to the rhizosphere of CLXL745. Both of these OTUs showed greater variation in relative abundance during the end of the season, which correlated with increased variation in CH$_4$ emissions posttransition to the reproductive stage (Fig. 2) (13). Total methanogen relative abundance was shown to be significantly enriched in the Sabine rhizosphere over the CLXL745 rhizosphere during the final two time points. This divergence notably correlates with the seasonal divergence in CH$_4$ emissions, which is most prominent later in the season (13). These findings were confirmed by qPCR, validating the conclusions drawn from the analysis of the relative abundances of the 16S rRNA gene sequences. Furthermore, it was demonstrated that these two methanogenic OTUs were significantly increased in the rhizosphere of Sabine over bulk soil, whereas CLXL745 did not vary from bulk soil (Fig. 4). This further supports the hypothesis that the methanogens are truly enriched in the rhizosphere of the high emitter and not depleted in the rhizosphere of the low emitter.

Methanocella spp., hydrogenotrophic methanogens formerly known as Rice Cluster I have been shown to incorporate more plant-derived carbon than do other methanogenic groups (27). The inclusion of this taxon among the enriched methanogens could be indicative of differences in the exudation of plant carbon sources to be a large contributor to the differences in methanogen abundances. *Methanosarcina* spp. are able to utilize all three methanogenic pathways (utilization of H$_2$ and CO$_2$, methylated compounds, and acetate) (4). *Methanosarcina* spp. have a low affinity for acetate but outcompete the strictly acetoclastic methanogens *Methanosaeta* spp. at higher temperatures, typical of those occurring during the growing season in this study (28, 29). *Methanosarcina* spp. are also thought to dominate over *Methanosaeta* spp. at higher acetate concentrations, which could be the case in the organic carbon-rich rhizosphere (30). *Methanosarcina* spp. can oxidize acetate, producing the necessary components for hydrogenotrophic methanogenesis (31). Thus, it is reasonable that in this study, especially in the absence of strictly acetoclastic methanogens (Fig. 2C), that the increased abundance of *Methanosarcina* OTUs could utilize hydrogen and CO$_2$ or acetate to produce CH$_4$, or it could enable the oxidization of acetate to further promote hydrogenotrophic methanogenesis by *Methanocella* spp.

Contrary to other studies investigating methanotrophs in rice hybrids, we observed no variation between cultivars in methanotroph relative abundances using 16S rRNA sequencing or in absolute abundances using qPCR on the *pmoA* gene. Furthermore, the cultivars did not vary in methanotrophic syntrophs in the way they varied in methanogenic syntrophs. For example, laboratory isolation or enrichment of methanotrophs is often accompanied by species in the genus *Hyphomicrobium* (32). *Hyphomicrobium* spp. can remove methanol, an inhibitor to methanotrophic growth. Although present in our data set, no *Hyphomicrobium* OTUs were present in the cultivar-sensitive lists.

13

Although methanotrophs abundances did not vary across cultivars, they did vary across compartments. Notably, type I methanotrophs (*Methylocaldum*, *Methylosinus*, and *Crenothrix* spp.) were in greater relative abundance in the rhizosphere, whereas type II methanotrophs (*Methylosinus* spp.) were more abundant in the endosphere. It has been shown that high concentrations of CH_4 in soil stimulate type I but not type II methanotrophs, which supports our results (33). In addition, *Methylosinus* spp. may be enriched within the endosphere due to their ability to utilize methanol, which is produced by demethylation of pectin in the cell walls of plants (34).

Although the qPCR results comparing the relative abundances of methanogens and absolute abundances of the methanogen-specific 16S rRNA correlated significantly, the results for methanotrophs were less clear due to the weak correlation between 16S rRNA relative abundance and *pmoA* absolute abundance. A previous study indicated that the community composition of methanotrophs varies drastically when sequenced with methanotroph-specific 16S rRNA genes or *pmoA* genes, which could contribute to the variation seen here (33). It is also possible that the assignment of OTUs associated with methanotrophy with FAPROTAX missed previously uncharacterized methanotrophs. Furthermore, FAPROTAX can only identify associations if OTUs are classified at the family or genus level, so methanotrophic OTUs not classified at these levels would be missed. This demonstrates some of the limitations of assigning traits based on 16S rRNA gene amplicon data and should be taken into consideration when considering the other trait associations discussed in this study.

Trait-based analysis suggests an increase in anaerobic microbial metabolism across all compartments in Sabine, leading to better conditions for methanogenesis. Since methanogen OTUs are enriched in the rhizosphere of the high emitter, we were able to identify patterns of microbial succession associated with processes upstream of methanogenesis. Two factors could lead to an increased abundance of methanogenesis, the availability of precursor substrates, and a highly reduced environment. Anaerobic metabolism involving iron and sulfate is more energetically favorable than methanogenesis, meaning that these electron acceptors must be depleted before methanogenesis can occur (9, 11). For example, it has been demonstrated in rice paddies that the addition of sulfate can reduce CH_4 emissions by 70% (35). Our study found overrepresented families associated with both sulfate reduction (*Syntrophobacteraceae* in the rhizosphere and *Desulfovibrionaceae* in the rhizoplane and endosphere) and iron reduction (*Geobacteraceae* in the endosphere). The overall seasonal trends of taxa were associated with iron reduction peaking earlier in the season (70 days postgermination), followed by a peak in sulfate reduction (98 days postgermination) and a continued increase in the relative abundances of methanogens throughout the growing season (Fig. 2B and 3B). This follows the theoretical progression of electron acceptor usage, since the reduction of iron is more favorable than the reduction of sulfate, which is more favorable than methanogenesis. An increase in these activities earlier in the season (as suggested by the association of overrepresented families with these traits) could lead to more favorably reduced conditions earlier on in the season for methanogenesis to occur.

An increased methanogen relative abundance could also be stimulated by an increased substrate availability. Some microbes can ferment carbon inputs to a variety of carbon sources, including organic acids, alcohols, propionate, acetate, H_2, and CO_2, the last three of which can be used as the substrates for methanogenesis. The production of acetate and propionate is particularly notable, because 70% and 23% of emitted CH_4 goes through acetate and propionate as intermediates, respectively (35, 36). A study comparing high- and low-CH_4-emitting cultivars has found a greater abundance of acetate in the rhizosphere of the high emitter, further confirming the importance of acetate as an important intermediate (37). Our study identified several taxa associated with fermentation, as summarized in Table 1 and Fig. 6. Furthermore, the seasonal trends of the cumulative OTUs associated with fermentation are significantly greater in the endosphere and rhizoplane of Sabine than in those of CLXL745. This increased abundance of fermentation-associated OTUs could be indicative of a

14
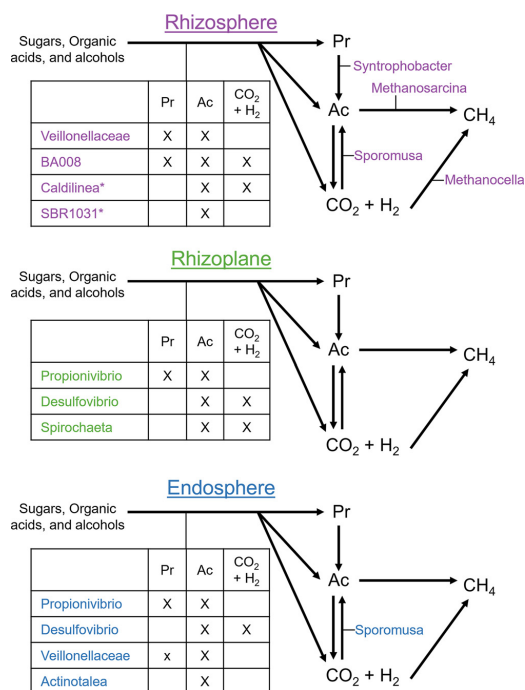
FIG 6 A summary of potential metabolic roles carried out by microbes enriched in Sabine (high emitter) over CLXL745 (low emitter). The table shows fermentative end products of taxa listed on the left, as discussed in the text. All microbes listed are from enriched families, except those indicated by an asterisk, which are taxa that clustered with methanogens in the rhizosphere. Pr, propionate; Ac, acetate.

greater abundance of methanogenic precursor molecules which could stimulate methanogenesis.

We hypothesized that this increase in fermentation-associated OTUs was due to a greater microaerobic/anaerobic sections of the Sabine root due to a less-developed root airspace; however, we found no significant difference in the proportion of root cross-sections occupied by aerenchyma and a significantly greater proportion of aerenchyma volume in Sabine. This result differs from our expectations, as well as from the model of Jiang et al. (14), which would predict that the higher-yielding/lower-emission cultivar CLXL745 will have proportionally greater aerenchyma space than the lower-yielding/higher-emission cultivar Sabine. Our data further diverge from the results of Jiang et al. (14) in changes in methanogens and methanotroph abundances, in that we found an increase in methanogen abundance in our high-emitting cultivar, whereas they found an increase in methanotroph abundance in their low-emitting cultivar. We conclude that the genetic factors involved in genotype-dependent fermentative OTU abundance in our study are unlikely to act by a simple mechanism involving control of root porosity. In our study, we focused on root airspace due to recent reports that variation in airspace between hybrids and other rice cultivars influence CH_4 emission (14). In addition, other morphological and physiological traits have also been correlated with CH_4 emissions, including above- and below-ground biomass (38), root exudation rate (39), and variation in the root-shoot transition zone (40). These traits could be affecting the composition of methanogenic, methanotrophic, or other related taxa and are physiological factors that could be further studied between these cultivars.

Another interesting trait associated with some overrepresented families of both the rhizosphere and endosphere was reductive acetogenesis (Fig. 3). Acetogens use the

15

Wood-Ljungdahl pathway to produce acetate from CO_2 and H_2 (41). This would put them in competition with hydrogenotrophic methanogens, such as *Methanocella* spp., due to utilization of the same substrates; however, methanogenesis is more energetically favorable than is acetogenesis, meaning that acetogens would be outcompeted and must resort to other modes of metabolism (41). Interestingly, microbes that act acetogenically in culture will oxidize acetate, running the Wood-Ljungdahl pathway in reverse, when in the presence of a syntroph (41, 42). In both the rhizosphere and the endosphere, *Sporomusa* is an overrepresented genus associated with acetogenesis. This genus has previously been observed in experiments studying the incorporation of CO_2 into acetate on rice roots (43). However, when *Sporomusa* spp. are grown in the presence of *Desulfovibrio* spp., which is also an overrepresented genus in the endosphere, no acetate is formed, and methanol is oxidized to CO_2 and H_2 (42). This is indicative that the *Sporomusa* spp. in these samples might be performing activities other than acetogenesis which could further promote methanogenesis. It is noteworthy that taxa associated with acetogenesis peak in the middle of the season across all compartments, which does not follow the trend of methanogens during that time period, with whom they theoretically could be competing for substrates. Many acetogens have high metabolic flexibility and are additionally able to ferment, which could cause this initial peak (44).

It is surprising that taxa associated with methanogenesis, fermentation, and acetogenesis are enriched in the aerobic endosphere of one cultivar over the other, considering that these are anaerobic processes. This is also not the first time we have observed strictly anaerobic taxa in the endosphere compartment; Edwards et al. (16) identified an enrichment of methanogenic *Methanobacterium* OTUs in the endosphere, which we again see in this study (Fig. 2). Furthermore, a study has recently shown that *Methanobacterium* OTUs were more enriched in the endosphere of rice plants than in other native plant species growing in the same field, indicating that *Methanobacterium* spp. have a unique interaction with rice (45). Previous studies have correlated the activity of superoxide dismutase with oxygen tolerance in some taxa, including *Methanobacterium,* as well as some anaerobic taxa discussed above (e.g., *Desulfovibrio* and *Propionivibrio*) (46–48). However, *Methanosarcina* OTUs, which have also been shown to have a tolerance to oxygen via superoxide dismutase (49), are enriched in the rhizosphere but not the endosphere, indicating that the above-mentioned taxa are able to persist in the endosphere due to other unknown factors.

To summarize, multiple enriched families in all three compartments of Sabine over CLXL745 have been associated with fermentation and the production of propionate, acetate, CO_2, and H_2. Interestingly, some of the enriched taxa have been previously found to be associated with methanogenic archaea. The rhizosphere of Sabine is enriched with *Syntrophobacter* OTUs, isolates of which have been shown to degrade propionate to acetate and have been closely associated with *Methanosarcina* spp. (35), of which one OTU is also enriched in the rhizosphere (35). The Sabine endosphere is enriched for *Desulfovibrio* OTUs, which is associated both with the acetogens of *Sporomusa* spp. as well as the dominant endosphere methanogens, *Methanobacterium* spp. (42, 50). This demonstrates the potential for unique consortia in each compartment contributing to an increase in abundance of methanogenic substrates for the corresponding archaea.

Clustering analysis reveals a potential syntrophic relationship between the class *Anaerolineae* and methanogens. In addition to OTUs that are generally overrepresented in one cultivar over the other, clustering analysis allows us to identify OTUs that potentially interact more directly with methanogens. Previous studies have identified OTUs that cluster with methanogens that are spatially separated; this allows for the identification of OTUs related to methanogens across a much larger diversity of environments, including across diverse plant compartments and geographic locations (16, 24, 25). Clustering across a season will identify OTUs more specifically linked to methanogen metabolism as substrate availability and soil redox potential change over time. Some of the taxonomies of methanogen-clustering OTUs have previously been

16

identified as methanogen clustering or CH_4 production clustering in other experiments over a variety of conditions, including the phylum *Planctomycetes*, order iii1-15, *Geobacter*, *Sphingomonas*, family *Ignavibacteriaceae*, class *Phycisphaerae*, and *Anaerolineae* families *Anaerolineaceae*, A4b, and SHA-31 (16, 24, 25).

However, these studies did not show significant positive correlations or clustering with other taxa identified in this study, including multiple families of the class *Anaerolineae*. The *Anaerolineae* family *Caldilinea* isolates have been shown to produce acetate, CO_2, and H_2 through fermentation (51, 52). Genome sequences from the uncultured SBR1031 have been shown to contain key genes in pathways necessary for acetate production through fermentation (53). These results show that temporal clustering identifies key taxa that cooccur with methanogens and could produce fermentation products that were not identified in previous spatial clustering analyses. Specifically, the presence of 11 OTUs in the class *Anaerolineae* out of a total 30 OTUs in the cluster suggest that this class could have a syntrophic relationship with methanogens.

In conclusion, this study utilized a high-emission cultivar and a low-emission cultivar to investigate the relationships between emission differences and the abundances of CH_4-cycling microbes in their root-associated microbiomes. The high-CH_4-emitting cultivar, Sabine, had an increased relative abundance of methanogens, as well as taxa associated with upstream processes related to methanogenesis (fermentation, acetogenesis, and iron and sulfate reduction) but no significant differences in methanotrophs relative to the low emitter CLXL745. The enrichment of fermentative microbes in the endosphere of the high emitter does not arise from reduced airspace in the roots, suggesting that the cultivars vary in the abundances of fermentation-associated taxa due to increased substrate availability in the exudates from the roots of the high emitter. The identity of these upstream taxa and the factors that control their abundance could provide avenues for efforts to manipulate plant influence over the microbiome to reduce CH_4 emissions in rice.

MATERIALS AND METHODS

Compartment separation, sample processing, and sequence processing have recently been published in *Bio-Protocols*, and a more in-depth explanation of the 16S rRNA gene amplicon pipeline can be found there (54).

Arkansas field experiment sampling and DNA extraction. Samples were grown in 8 different plots with 4 plots per cultivar. Two individual plants were collected from each plot at each time point and treated as individual replicates for a total of 8 replicates per factor combination. Bulk soils were also sampled from the same 8 plots. The rhizosphere and endosphere data used in this paper were previously published by Edwards et al. (54). The rhizoplane samples were not included in that study, though the samples were collected at the same time as the endosphere and rhizosphere samples and frozen at −80°C. These samples were not included in the original study because the authors were unsure if the samples would be compromised in transport and were not necessary for the temporal dynamics explored in that paper. Due to the significant insight rhizoplane samples could add to the taxa involved in methane dynamics, the rhizoplane samples were sequenced to check for quality to include in further analysis. Rhizoplane samples corresponding to 42 days after germination were compromised before library preparation, so all samples corresponding to that time point were removed in downstream analyses. Further information about the field setup and sample collection can be found in the paper by Edwards et al. (54). Rhizoplane samples were thawed at room temperature, and extractions were performed using the Mo Bio PowerSoil DNA isolation kits.

16S rRNA gene amplicon library preparation. Libraries were prepared using dual-index primers, as previously described (16, 18, 55). PCR was performed using the Qiagen HotStar HiFidelity polymerase kit. Touchdown PCR was used to amplify the samples with the following steps: 95°C for 5 min, 35 cycles of 95°C for 45 s, 50°C for 1 min, and 72°C for 1 min, and 72°C for 10 min. A negative control was included for each sample to identify contamination, which was identified using a 1% agarose gel. AMPure beads were used to remove the primer dimer, and the Qubit high-sensitivity (HS) assay kit was used to quantify the concentrations. Samples were pooled, gel purified, and sequenced using the Illumina MiSeq machine on a 2 × 250 paired-end run.

Sequence processing. The rhizoplane paired-end reads were combined with the rhizosphere and endosphere paired-end reads and demultiplexed with custom scripts (https://github.com/RiceMicrobiome/Edwards-et-al.-2014/tree/master/sequencing_scripts). PANDAseq was used to align the endosphere, rhizosphere, and rhizoplane reads (56). Sequences with ambiguous bases and reads over 275 bp were discarded. OTUs were clustered at 97% using UCLUST (57). An open-reference strategy was used against the 13_8 Greengenes 16S rRNA sequence database (58). OTUs with a name beginning with "New.ReferenceOTU" or "New.CleanUp.ReferenceOTU" were generated during the *de novo* clustering stage of the open-reference algorithm. Chloroplast and mitochondrial OTUs were then removed, and

17

OTUs occurring in less than 5% of the samples were removed as well. Sequencing depths varied from 3,985 to 161,535 reads, with a median of 37,239 reads. OTUs were divided by the sequencing depth and multiplied by 1,000 to form relative abundances in units of per mille for analysis. However, all plot relative abundances are shown in percentages. Some samples had large spikes of *Gammaproteobacteria* in all compartments; however, the spikes did not correlate across compartments so were likely introduced through contamination. These spikes were largely made up of a single OTU, 839235 of the family *Aeromonadaceae*, which has been found in much lower abundances in another data set, which averaged 0.017% across all samples (17). Therefore, samples that had a relative abundance of *Gammaproteobacteria* two standard deviations greater than the mean were removed. No more than 2 samples were removed from any factor combination, meaning that the replicates per factor combination ranged from 6 to 8 samples.

qPCR quantification. The weights of the original rhizosphere samples were not recorded during the original sampling, so the remaining frozen rhizosphere samples were thawed and reextracted using the Mo Bio PowerSoil DNA isolation kit. The protocol was followed as normal, but the initial weight was recorded before the extractions were performed. The thawed rhizosphere samples were briefly dried in an oven, and approximately 100 mg (dry weight) was extracted. Three samples did not have enough remaining sample to be extracted ($<$50 mg) and were excluded from the extraction. The qPCR method was derived from previously published methods for methanogen quantification using methanogen-specific 16S rRNA primers (12). The samples were diluted 1/10 to reduce the effects of PCR inhibitors. Previously published methanogen-specific primers were used (MET630F, GGATTAGATACCCSGGTAGT; MET803R, GTTGARTCCAATTAAACCG) (12). A PCR-cloned 16S rRNA gene fragment extracted from environmental samples was used as a standard. Triplicates of each sample were run, and replicates that disagreed with the other two replicates were excluded. The gene copy number of each sample was calculated using the values from the serially diluted standard. Those copy numbers were corrected to reflect the DNA copy number per gram of dried soil. The qPCRs were prepared with Bio-Rad iTaq Universal SYBR green Supermix, and the qPCR program for methanogen-specific 16S rRNA region was that reported by Su et al. (12), as follows: 95°C for 7 min, followed by 54 cycles of 40 s at 95°C, 1 min at 60°C, and 40 s at 72°C. The melting curve was from 65°C to 95°C, increasing at 0.5°C increments for 5 s each. The qPCR primers a189 and mb661 were used to amplify the *pmoA* gene, with thermocycler settings of 94°C for 4 min and 35 cycles of 94°C for 30 s, 56°C for 30 s, and 72°C for 1 min, followed by the same melt curve described above.

Statistical analysis. All statistical analyses were carried out in R version 3.5.1 (59). PERMANOVA was performed using the adonis() function, Bray-Curtis dissimilarities were calculated with the vegdist() function, and canonical analyses of principal coordinates were performed with the capscale() function from the vegan package (60). Unconstrained principal-coordinate analysis was performed using the pcoa() function in the ape package (61). Likelihood ratio tests and differential abundance analyses were performed using DESeq2 (62). The models used in the likelihood ratio test were the full model, sequencing lane + time point + cultivar, compared to a reduced model, sequencing lane + time point. These models were run on data subsetted by compartment. Hypergeometric tests were performed by taking the list of taxonomies at each taxonomic level from the list of cultivar-sensitive OTUs and comparing them to the list of the same taxonomic rank of all OTUs present within each compartment. Hypergeometric tests were performed with the enricher() function from the package clusterProfiler using default parameters with no upper or lower size cutoff (63). Variance stabilization was performed with the vst() function from DESeq2, which normalizes the variance within each OTU while accounting for library size (62). Clustering was performed on Euclidean distances of Z-score-transformed relative abundances ([value − mean]/standard deviation) using the function hclust from the stats package (59). Clusters were determined using the function tsclust() from the package dtwclust (64). The number of clusters was determined by graphing the mean sum of squares for a number of clusters ranging from 2 to 10 and identifying where the slope leveled out. Linear models and ANOVA were performed using lm() and anova(), respectively, from the stats package (59). qPCR results were analyzed using log-transformed data, and posttransformation normalization was checked using normal Q-Q plots from the stats package. All plots were generated with the ggplot2 package (65). All scripts are posted on GitHub (https://github.com/zliechty/RiceCH4).

Greenhouse experiment setup. The aerenchyma measurement experiment was carried out in a UC Davis greenhouse in the summer of 2018 in a randomized complete block design. Four 23-gallon tubs were arranged in a 2 by 2 layout, with each tub holding 16 plants (8 of each cultivar) in 5.5- × 5.5-in. pots. Plants were sampled monthly, beginning 1 month after germination. At each time point, two plants of each cultivar were sampled.

Pycnometer measurements. The pycnometer measurements followed an established protocol (66). Soil was washed from the roots using tap water. Once all soil was removed, approximately 1 g of root taken from the first 10 cm below the root-shoot junction was sampled. Three independent replicates per plant were sampled. Samples were patted dry with paper towels, weighed, and cut into approximately 1-cm pieces. This was put into a pycnometer and weighed. The pycnometer was then vacuum infiltrated for 5 rounds of 5-min intervals or until bubbles stopped rising upon vacuum initiation, and then they were weighed again. The equation $(P\_vr − P\_r)/(P\_w + R − P\_r)$ was used to calculate airspace, where P_w is the weight of the pycnometer with only water, P_r is the weight of the pycnometer with roots and water, P_vr is the weight of the pycnometer with vacuum-infiltrated roots, and R is the weight of the dry roots. Water was brought to room temperature before beginning measurements. The three replicates per plant were averaged before statistical analysis was performed.

18

Cross-section preparation, imaging, and analysis. Plants were washed in the same fashion as described above in "Pycnometer measurements." A 3-cm section of root was cut with a razor blade and vacuum infiltrated with FAA (50% ethanol 95%, 5% glacial acetic acid, 10% formalin, 35% water) for 10 min. The root sample was then embedded in 5% agarose and flash frozen with liquid nitrogen. The plug was then vacuum infiltrated with FAA for 10 min and left in FAA overnight. The plugs were then rehydrated in a series of 70%, 50%, 30%, and 10% ethanol washes, each lasting 30 min. The plugs were then stored in water until sectioning. Sectioning was performed with a Leica VT1000 vibratome, with sections ranging from 200 to 300 μm. Root sections were then dyed with 0.1% toluidine blue for 30 s and rinsed with water. Images were taken using Zeiss Axioskoop2 plus microscope with an AxioCam HRc camera. Images were analyzed in ImageJ (67) by dividing the area of airspace by the total area of the root section. Multiple sections of each root were taken, analyzed, and then averaged for statistical analysis.

Data availability. The rhizosphere and endosphere reads can be found at the Sequence Read Archive of NCBI under BioProject accession number PRJNA392701. The rhizoplane reads can be found at BioProject accession number PRJNA598892.

SUPPLEMENTAL MATERIAL

Supplemental material is available online only.

FIG S1, PDF file, 0.1 MB.
FIG S2, PDF file, 0.1 MB.
FIG S3, PDF file, 0.1 MB.
FIG S4, PDF file, 0.1 MB.
TABLE S1, DOCX file, 0.1 MB.
TABLE S2, DOCX file, 0.1 MB.
TABLE S3, DOCX file, 0.1 MB.
DATA SET S1, XLSX file, 0.1 MB.
DATA SET S2, XLSX file, 0.1 MB.

REFERENCES

1. Core Writing Team, Pachauri RK, Meyer LA. 2014. Climate change 2014: synthesis report. Contribution of working groups I, II and III to the fifth assessment report of the Intergovernmental Panel on Climate Change. Intergovernmental Panel on Climate Change, Geneva, Switzerland. https://www.ipcc.ch/site/assets/uploads/2018/05/SYR_AR5_FINAL_full _wcover.pdf.
2. Conrad R. 2009. The global methane cycle: recent advances in understanding the microbial processes involved. Environ Microbiol Rep 1:285–292. https://doi.org/10.1111/j.1758-2229.2009.00038.x.
3. Bridgham SD, Cadillo-Quiroz H, Keller JK, Zhuang Q. 2013. Methane emissions from wetlands: biogeochemical, microbial, and modeling perspectives from local to global scales. Glob Chang Biol 19:1325–1346. https://doi.org/10.1111/gcb.12131.
4. Liu Y, Whitman WB. 2008. Metabolic, phylogenetic, and ecological diversity of the methanogenic archaea. Ann N Y Acad Sci 1125:171–189. https://doi.org/10.1196/annals.1419.019.
5. Lu Y, Wassmann R, Neue H-U, Huang C. 2000. Dissolved organic carbon and methane emissions from a rice paddy fertilized with ammonium and nitrate. J Environ Qual 29:1733–1740. https://doi.org/ 10.2134/jeq2000.00472425002900060002x.
6. Watanabe A, Takeda T, Kimura M. 1999. Evaluation of origins of CH_4 carbon emitted from rice paddies. J Geophys Res 104:23623–23629. https://doi.org/10.1029/1999JD900467.
7. Yu KW, Wang ZP, Chen GX. 1997. Nitrous oxide and methane transport through rice plants. Biol Fertil Soils 24:341–343. https://doi.org/10.1007/ s003740050254.
8. Drake HL, Horn MA, Wüst PK. 2009. Intermediary ecosystem metabolism as a main driver of methanogenesis in acidic wetland soil. Environ Microbiol Rep 1:307–318. https://doi.org/10.1111/j.1758-2229.2009.00050.x.
9. Evans PN, Boyd JA, Leu AO, Woodcroft BJ, Parks DH, Hugenholtz P, Tyson GW. 2019. An evolving view of methane metabolism in the Archaea. Nat Rev Microbiol 17:219–232. https://doi.org/10.1038/s41579-018-0136-7.
10. Neue H-U. 1993. Methane emission from rice fields. Bioscience 43: 466–474. https://doi.org/10.2307/1311906.
11. Thauer RK, Kaster A-K, Seedorf H, Buckel W, Hedderich R. 2008. Methanogenic archaea: ecologically relevant differences in energy conservation. Nat Rev Microbiol 6:579–591. https://doi.org/10.1038/nrmicro1931.
12. Su J, Hu C, Yan X, Jin Y, Chen Z, Guan Q, Wang Y, Zhong D, Jansson C, Wang F, Schnürer A, Sun C. 2015. Expression of barley SUSIBA2 transcription factor yields high-starch low-methane rice. Nature 523: 602–606. https://doi.org/10.1038/nature14673.
13. Simmonds MB, Anders M, Adviento-Borbe MA, van Kessel C, McClung A, Linquist BA. 2015. Seasonal methane and nitrous oxide emissions of several rice cultivars in direct-seeded systems. J Environ Qual 44: 103–114. https://doi.org/10.2134/jeq2014.07.0286.
14. Jiang Y, van Groenigen KJ, Huang S, Hungate BA, van Kessel C, Hu S, Zhang J, Wu L, Yan X, Wang L, Chen J, Hang X, Zhang Y, Horwath WR, Ye R, Linquist BA, Song Z, Zheng C, Deng A, Zhang W. 2017. Higher

19

yields and lower methane emissions with new rice cultivars. Glob Chang Biol 23:4728–4738. https://doi.org/10.1111/gcb.13737.

15. Ma K, Qiu Q, Lu Y. 2009. Microbial mechanism for rice variety control on methane emission from rice field soil. Glob Chang Biol 16:3085–3095. https://doi.org/10.1111/j.1365-2486.2009.02145.x.

16. Edwards J, Johnson C, Santos-Medellín C, Lurie E, Podishetty NK, Bhatnagar S, Eisen JA, Sundaresan V. 2015. Structure, variation, and assembly of the root-associated microbiomes of rice. Proc Natl Acad Sci U S A 112:E911–E920. https://doi.org/10.1073/pnas.1414592112.

17. Santos-Medellín C, Edwards J, Liechty Z, Nguyen B, Sundaresan V. 2017. Drought stress results in a compartment-specific restructuring of the rice root-associated microbiomes. mBio 8:e00764-17. https://doi.org/10.1128/mBio.00764-17.

18. Edwards JA, Santos-Medellín CM, Liechty ZS, Nguyen B, Lurie E, Eason S, Phillips G, Sundaresan V. 2018. Compositional shifts in root-associated bacterial and archaeal microbiota track the plant life cycle in field-grown rice. PLoS Biol 16:e2003862. https://doi.org/10.1371/journal.pbio.2003862.

19. Zhang J, Zhang N, Liu YX, Zhang X, Hu B, Qin Y, Xu H, Wang H, Guo X, Qian J, Wang W, Zhang P, Jin T, Chu C, Bai Y. 2018. Root microbiota shift in rice correlates with resident time in the field and developmental stage. Sci China Life Sci 61:613–621. https://doi.org/10.1007/s11427-018-9284-4.

20. Rogers CW, Brye KR, Smartt AD, Norman RJ, Gbur EE, Evans-White MA. 2014. Cultivar and previous crop effects on methane emissions from drill-seeded, delayed-flood rice production on a silt-loam soil. Soil Sci 179:28–36. https://doi.org/10.1097/SS.0000000000000039.

21. Brye KR, Rogers CW, Smartt AD, Norman RJ, Hardke JT, Gbur EE. 2017. Methane emissions as affected by crop rotation and rice cultivar in the Lower Mississippi River Valley, USA. Geoderma Reg 11:8–17. https://doi.org/10.1016/j.geodrs.2017.08.004.

22. Smartt AD, Brye KR, Rogers CW, Norman RJ, Gbur EE, Hardke JT, Roberts TL. 2016. Previous crop and cultivar effects on methane emissions from drill-seeded, delayed-flood rice grown on a clay soil. Appl Environ Soil Sci 2016:9542361. https://doi.org/10.1155/2016/9542361.

23. Zhang J, Liu YX, Zhang N, Hu B, Jin T, Xu H, Qin Y, Yan P, Zhang X, Guo X, Hui J, Cao S, Wang X, Wang C, Wang H, Qu B, Fan G, Yuan L, Garrido-Oter R, Chu C, Bai Y. 2019. NRT1.1B is associated with root microbiota composition and nitrogen use in field-grown rice. Nat Biotechnol 37:676–684. https://doi.org/10.1038/s41587-019-0104-4.

24. He S, Malfatti SA, McFarland JW, Anderson FE, Pati A, Huntemann M, Tremblay J, Glavina del Rio T, Waldrop MP, Windham-Myers L, Tringe SG. 2015. Patterns in wetland microbial community composition and functional gene repertoire associated with methane emissions. mBio 6:e00066-15. https://doi.org/10.1128/mBio.00066-15.

25. Zhang J, Jiao S, Lu Y. 2018. Biogeographic distribution of bacterial, archaeal and methanogenic communities and their associations with methanogenic capacity in Chinese wetlands. Sci Total Environ 622–623: 664–675. https://doi.org/10.1016/j.scitotenv.2017.11.279.

26. Sojka RE. 1988. Measurement of root porosity (volume of root air space). Environ Exp Bot 28:275–280. https://doi.org/10.1016/0098-8472(88)90050-0.

27. Lu Y, Conrad R. 2005. In situ stable isotope probing of methanogenic archaea in the rice rhizosphere. Science 309:1088–1090. https://doi.org/10.1126/science.1113435.

28. Jetten MSM, Stams AJM, Zehnder A. 1992. Methanogenesis from acetate: a comparison of the acetate metabolism in Methanothrix soehngenii and Methanosarcina spp. FEMS Microbiol Lett 88:181–198. https://doi.org/10.1111/j.1574-6968.1992.tb04987.x.

29. Chin KJ, Lukow T, Conrad R. 1999. Effect of temperature on structure and function of the methanogenic archaeal community in an anoxic rice field soil. Appl Environ Microbiol 65:2341–2349. https://doi.org/10.1128/AEM.65.6.2341-2349.1999.

30. Ferry JG. 1993. Fermentation of acetate, p 304–334. In Methanogenesis. Springer US, Boston, MA.

31. Karakashev D, Batstone DJ, Trably E, Angelidaki I. 2006. Acetate oxidation is the dominant methanogenic pathway from acetate in the absence of Methanosaetaceae. Appl Environ Microbiol 72:5138–5141. https://doi.org/10.1128/AEM.00489-06.

32. Morris BEL, Henneberger R, Huber H, Moissl-Eichinger C. 2013. Microbial syntrophy: Interaction for the common good. FEMS Microbiol Rev 37: 384–406. https://doi.org/10.1111/1574-6976.12019.

33. Shiau YJ, Cai Y, Jia Z, Chen CL, Chiu CY. 2018. Phylogenetically distinct methanotrophs modulate methane oxidation in rice paddies across

Taiwan. Soil Biol Biochem 124:59–69. https://doi.org/10.1016/j.soilbio.2018.05.025.

34. Stępniewska Z, Goraj W, Kuźniar A, Łopacka N, Małysza M. 2017. Enrichment culture and identification of endophytic methanotrophs isolated from peatland plants. Folia Microbiol (Praha) 62:381–391. https://doi.org/10.1007/s12223-017-0508-9.

35. Liu P, Pommerenke B, Conrad R. 2018. Identification of Syntrophobacteraceae as major acetate-degrading sulfate reducing bacteria in Italian paddy soil. Environ Microbiol 20:337–354. https://doi.org/10.1111/1462-2920.14001.

36. Liu P, Conrad R. 2017. Syntrophobacteraceae-affiliated species are major propionate-degrading sulfate reducers in paddy soil. Environ Microbiol 19:1669–1686. https://doi.org/10.1111/1462-2920.13698.

37. Sigren LK, Byrd GT, Fisher FM, Sass RL. 1997. Comparison of soil acetate concentrations and methane production, transport, and emission in two rice cultivars. Global Biogeochem Cycles 11:1–14. https://doi.org/10.1029/96GB03040.

38. Huang Y, Sass R, Fisher F. 1997. Methane emission from Texas rice paddy soils. 2. Seasonal contribution of rice biomass production to CH_4 emission. Glob Chang Biol 3:491–500. https://doi.org/10.1046/j.1365-2486.1997.00106.x.

39. Aulakh MS, Wassmann R, Bueno C, Kreuzwieser J, Rennenberg H. 2001. Characterization of root exudates at different growth stages of ten rice (Oryza sativa L.) cultivars. Plant Biol 3:139–148. https://doi.org/10.1055/s-2001-12905.

40. Groot TT, van Bodegom PM, Meijer HAJ, Harren F. 2005. Gas transport through the root–shoot transition zone of rice tillers. Plant Soil 277: 107–116. https://doi.org/10.1007/s11104-005-0435-4.

41. Ragsdale SW, Pierce E. 2008. Acetogenesis and the Wood-Ljungdahl pathway of CO_2 fixation. Biochim Biophys Acta 1784:1873–1898. https://doi.org/10.1016/j.bbapap.2008.08.012.

42. McInerney MJ, Struchtemeyer CG, Sieber J, Mouttaki H, Stams AJM, Schink B, Rohlin L, Gunsalus RP. 2008. Physiology, ecology, phylogeny, and genomics of microorganisms capable of syntrophic metabolism. Ann N Y Acad Sci 1125:58–72. https://doi.org/10.1196/annals.1419.005.

43. Conrad R, Klose M. 1999. Anaerobic conversion of carbon dioxide to methane, acetate and propionate on washed rice roots. FEMS Microbiol Ecol 30:147–155. https://doi.org/10.1111/j.1574-6941.1999.tb00643.x.

44. Schuchmann K, Müller V. 2016. Energetics and application of heterotrophy in acetogenic bacteria. Appl Environ Microbiol 82:4056–4069. https://doi.org/10.1128/AEM.00882-16.

45. Edwards J, Santos-Medellín C, Nguyen B, Kilmer J, Liechty Z, Veliz E, Ni J, Phillips G, Sundaresan V. 2019. Soil domestication by rice cultivation results in plant-soil feedback through shifts in soil microbiota. Genome Biol 20:221. https://doi.org/10.1186/s13059-019-1825-x.

46. Brune A, Ludwig W, Schink B. 2002. Propionivibrio limicola sp. nov., a fermentative bacterium specialized in the degradation of hydroaromatic compounds, reclassification of Propionibacter pelophilus as Propionivibrio pelophilus comb. nov. and amended description of the genus Propionivibrio. Int J Syst Evol Microbiol 52:441–444. https://doi.org/10.1099/00207713-52-2-441.

47. Davydova MN, Sabirova RZ. 2002. Antioxidative enzymes of sulfate-reducing bacterium desulfovibrio desulfuricans: superoxide dismutase and peroxidases. Biochemistry (Mosc) 67:822–825. https://doi.org/10.1023/a:1016313111104.

48. Kirby TW, Lancaster JR, Fridovich I. 1981. Isolation and characterization of the iron-containing superoxide dismutase of Methanobacterium bryantii. Arch Biochem Biophys 210:140–148. https://doi.org/10.1016/0003-9861(81)90174-0.

49. Brioukhanov A, Netrusov A, Sordel M, Thauer RK, Shima S. 2000. Protection of Methanosarcina barkeri against oxidative stress: identification and characterization of an iron superoxide dismutase. Arch Microbiol 174: 213–216. https://doi.org/10.1007/s002030000180.

50. Guyot JP, Brauman A. 1986. Methane production from formate by syntrophic association of Methanobacterium bryantii and Desulfovibrio vulgaris JJ. Appl Environ Microbiol 52:1436–1437. https://doi.org/10.1128/AEM.52.6.1436-1437.1986.

51. Yamada T, Sekiguchi Y, Hanada S, Imachi H, Ohashi A, Harada H, Kamagata Y. 2006. Anaerolinea thermolimosa sp. nov., Levilinea saccharolytica gen. nov., sp. nov. and Leptolinea tardivitalis gen. nov., sp. nov., novel filamentous anaerobes, and description of the new classes Anaerolineae classis nov. and Caldilineae classis nov. in the bacterial phylum Chloroflexi. Int J Syst Evol Microbiol 56:1331–1340. https://doi.org/10.1099/ijs.0.64169-0.

20

52. Grégoire P, Bohli M, Cayol J-L, Joseph M, Guasco S, Dubourg K, Cambar J, Michotey V, Bonin P, Fardeau M-L, Ollivier B. 2011. *Caldilinea tarbellica* sp. nov., a filamentous, thermophilic, anaerobic bacterium isolated from a deep hot aquifer in the Aquitaine Basin. Int J Syst Evol Microbiol 61:1436–1441. https://doi.org/10.1099/ijs.0.025676-0.

53. Xia Y, Wang Y, Wang Y, Chin FYL, Zhang T. 2016. Cellular adhesiveness and cellulolytic capacity in *Anaerolineae* revealed by omics-based genome interpretation. Biotechnol Biofuels 9:111. https://doi.org/10.1186/s13068-016-0524-z.

54. Edwards J, Santos-Medellín C, Sundaresan V. 2018. Extraction and 16S rRNA sequence analysis of microbiomes associated with rice roots. Bio Protoc 8:e2884. https://doi.org/10.21769/BioProtoc.2884.

55. Caporaso JG, Kuczynski J, Stombaugh J, Bittinger K, Bushman FD, Costello EK, Fierer N, Peña AG, Goodrich JK, Gordon JI, Huttley GA, Kelley ST, Knights D, Koenig JE, Ley RE, Lozupone CA, McDonald D, Muegge BD, Pirrung M, Reeder J, Sevinsky JR, Turnbaugh PJ, Walters WA, Widmann J, Yatsunenko T, Zaneveld J, Knight R. 2010. QIIME allows analysis of high-throughput community sequencing data. Nat Methods 7:335–336. https://doi.org/10.1038/nmeth.f.303.

56. Masella AP, Bartram AK, Truszkowski JM, Brown DG, Neufeld JD. 2012. PANDAseq: paired-end assembler for Illumina sequences. BMC Bioinformatics 13:31. https://doi.org/10.1186/1471-2105-13-31.

57. Edgar RC. 2010. Search and clustering orders of magnitude faster than BLAST. Bioinformatics 26:2460–2461. https://doi.org/10.1093/bioinformatics/btq461.

58. DeSantis TZ, Hugenholtz P, Larsen N, Rojas M, Brodie EL, Keller K, Huber T, Dalevi D, Hu P, Andersen GL. 2006. Greengenes, a chimera-checked 16S rRNA gene database and workbench compatible with ARB. Appl Environ Microbiol 72:5069–5072. https://doi.org/10.1128/AEM.03006-05.

59. R Core Team. 2018. R: a language and environment for statistical computing. R Foundation for Statistical Computing, Vienna, Austria. https://www.r-project.org/.

60. Oksanen J, Blanchet FG, Friendly M, Kindt R, Legendre P, McGlinn D, Minchin PR, O'Hara RB, Simpson GL, Solymos P, Stevens MHH, Szoecs E, Wagner H. 2018. vegan: community ecology package. R package version 2.5-2. https://cran.r-project.org/package=vegan.

61. Paradis E, Claude J, Strimmer K. 2004. APE: analyses of phylogenetics and evolution in R language. Bioinformatics 20:289–290. https://doi.org/10.1093/bioinformatics/btg412.

62. Love MI, Huber W, Anders S. 2014. Moderated estimation of fold change and dispersion for RNA-seq data with DESeq2. Genome Biol 15:550. https://doi.org/10.1186/s13059-014-0550-8.

63. Yu G, Wang L-G, Han Y, He Q-Y. 2012. clusterProfiler: an R package for comparing biological themes among gene clusters. Omi A. OMICS 16:284–287. https://doi.org/10.1089/omi.2011.0118.

64. Giorgino T. 2009. Computing and visualizing dynamic time warping alignments in R: the dtw package. J Stat Softw 31:1–24.

65. Wickham H. 2016. ggplot2: elegant graphics for data analysis. Springer-Verlag, New York, NY.

66. Van Noordwijk M, Brouwer G. 1988. Quantification of air-filled root porosity: a comparison of two methods. Plant Soil 111:255–258. https://doi.org/10.1007/BF02139949.

67. Schneider CA, Rasband WS, Eliceiri KW. 2012. NIH Image to ImageJ: 25 years of image analysis. Nat Methods 9:671–675. https://doi.org/10.1038/nmeth.2089.

68. Oren A. 2014. The family *Rhodocyclaceae*, p 975–998. *In* Rosenberg E, DeLong EF, Lory S, Stackebrandt E, Thompson F (ed), The prokaryotes. Springer Berlin Heidelberg, Berlin, Germany.

69. Harwood CS, Canale-Parola E. 1983. *Spirochaeta isovalerica* sp. nov., a marine anaerobe that forms branched-chain fatty acids as fermentation products. Int J Syst Bacteriol 33:573–579. https://doi.org/10.1099/00207713-33-3-573.

70. Stackebrandt E, Schumann P. 2014. The family *Cellulomonadaceae*, p 163–184. *In* Rosenberg E, DeLong EF, Lory S, Stackebrandt E, Thompson F (ed), The prokaryotes. Springer Berlin Heidelberg, Berlin, Germany.

71. Marchandin H, Jumas-Bilak E. 2014. The family *Veillonellaceae*, p 433–453. *In* Rosenberg E, DeLong EF, Lory S, Stackebrandt E, Thompson F (ed), The prokaryotes. Springer Berlin Heidelberg, Berlin, Germany.

72. Kuever J. 2014. The family *Desulfovibrionaceae*, p 107–133. *In* Rosenberg E, DeLong EF, Lory S, Stackebrandt E, Thompson F (ed), The prokaryotes. Springer Berlin Heidelberg, Berlin, Germany.

73. Sun L, Toyonaga M, Ohashi A, Tourlousse DM, Matsuura N, Meng X-Y, Tamaki H, Hanada S, Cruz R, Yamaguchi T, Sekiguchi Y. 2016. *Lentimicrobium saccharophilum* gen. nov., sp. nov., a strictly anaerobic bacterium representing a new family in the phylum *Bacteroidetes*, and proposal of *Lentimicrobiaceae* fam. nov. Int J Syst Evol Microbiol 66:2635–2642. https://doi.org/10.1099/ijsem.0.001103.

74. Narihiro T, Terada T, Ohashi A, Kamagata Y, Nakamura K, Sekiguchi Y. 2012. Quantitative detection of previously characterized syntrophic bacteria in anaerobic wastewater treatment systems by sequence-specific rRNA cleavage method. Water Res 46:2167–2175. https://doi.org/10.1016/j.watres.2012.01.034.

75. Kuever J. 2014. The Family *Syntrophobacteraceae*, p 289–299. *In* Rosenberg E, DeLong EF, Lory S, Stackebrandt E, Thompson F (ed), The prokaryotes. Springer Berlin Heidelberg, Berlin, Germany.

21
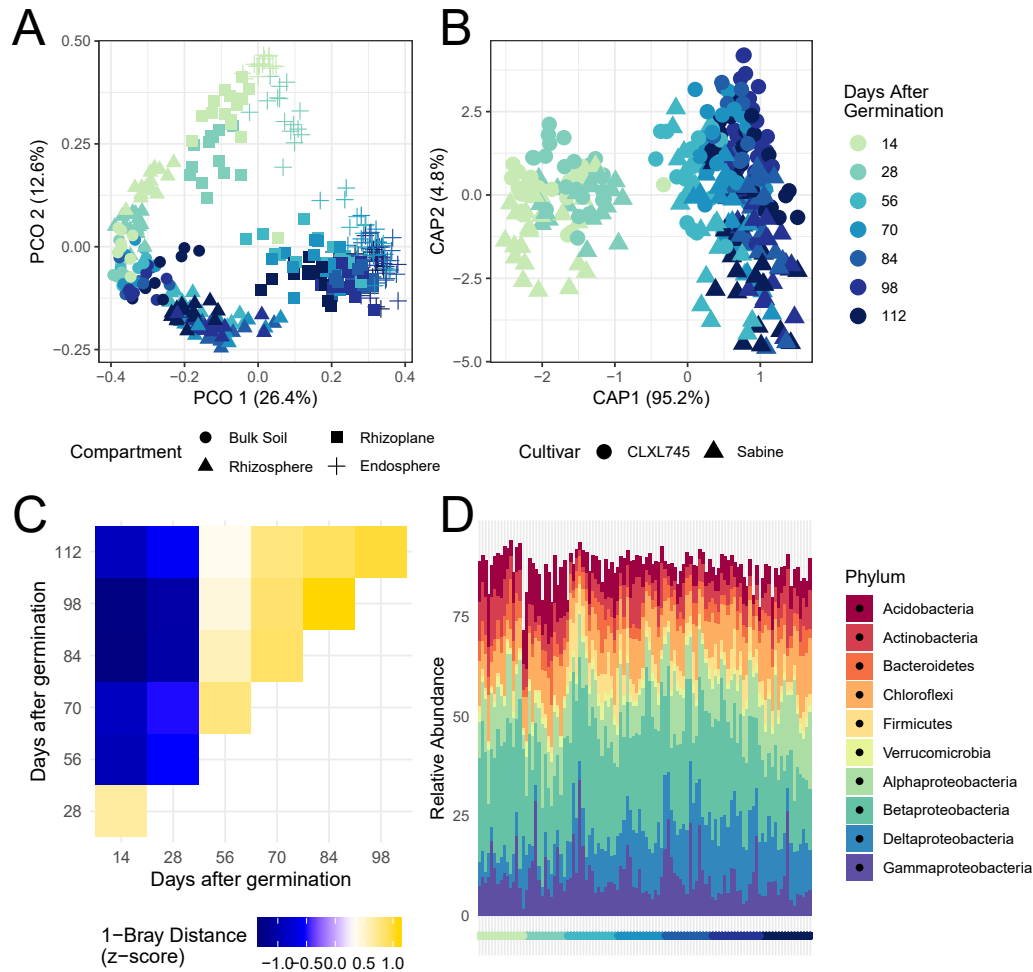
Supplemental Figure 1 Rhizoplane samples follow previously established compartmental and temporal patterns. (A) Principal-coordinate analysis using Bray-Curtis distances. Points are colored by date, whereas shape is determined by compartment. The first two axes are shown. The first axis corresponds to compartment and the second to time. (B) Graphical depiction of CAP described in Fig. 1. The y axis is the same as in Fig. 1A. Here, the first axis is shown to correspond with time. (C) Heat map depicting the pairwise similarity between samples of different time points using the Z-score of 1-Bray dissimilarity. The Bray dissimilarity comparisons for the endosphere and rhizosphere samples can be found in Edwards et al. (18). (D) Bar plots of the 10 most abundant taxa in the rhizoplane. Colored dots underneath bars indicate sample age using the same colors as in panels A and B.
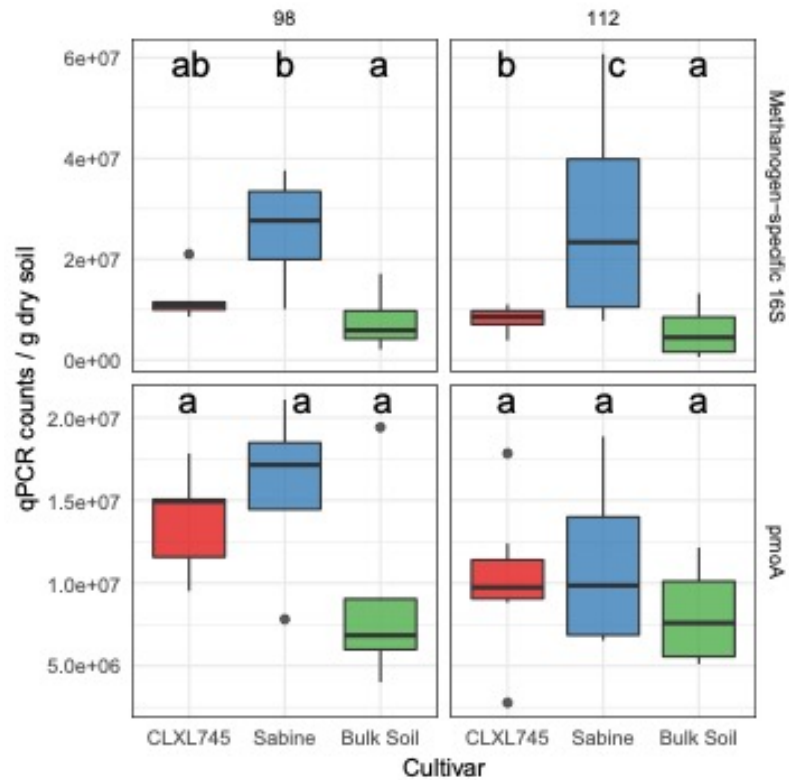
Supplemental Figure 2 Abundances of methanogen-specific 16S rRNA region and the methanotrophic-associated *pmoA* gene in the bulk soils and rhizospheres of Sabine and CLXL745 for the final two time points in counts per gram of dry weight. Letters above boxplots indicate which pairwise comparisons within that group are significant ($P < 0.05$, Tukey adjustment on log-transformed data).
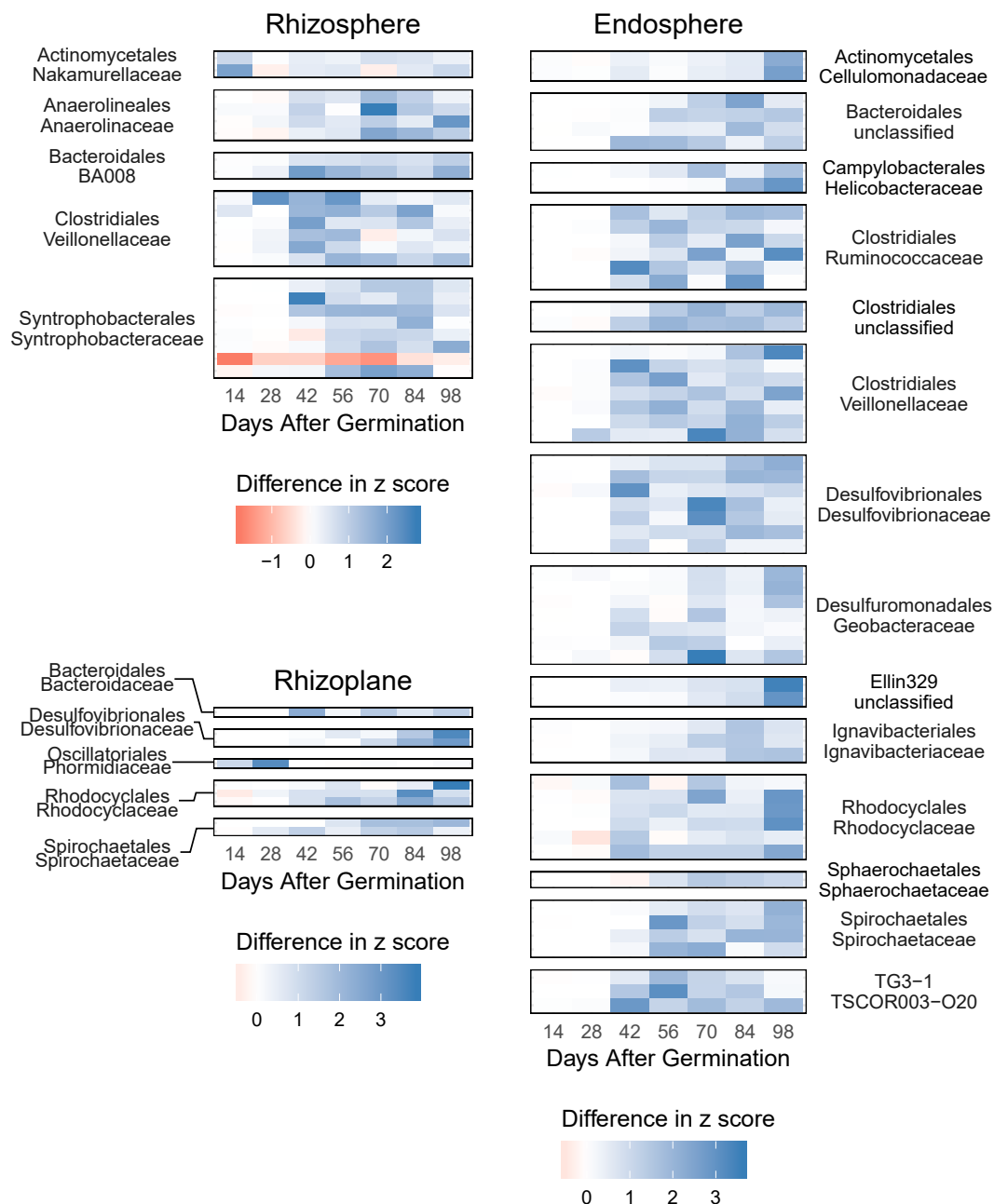
Supplemental Figure 3 Difference in Z-scores of each OTU overrepresented within the list of cultivar-sensitive OTUs ($P < 0.05$). Each column represents one time point, and each row is an individual OTU within the compartment denoted on the right. The Z-score is calculated within the OTU across all time points within both cultivars. The difference was calculated by subtracting the Z-score of CLXL745 from Sabine, meaning positive numbers (blue) are enriched in Sabine over CLXL745, and negative numbers (red) are enriched in CLXL745. White indicates no difference in Z-score.

24
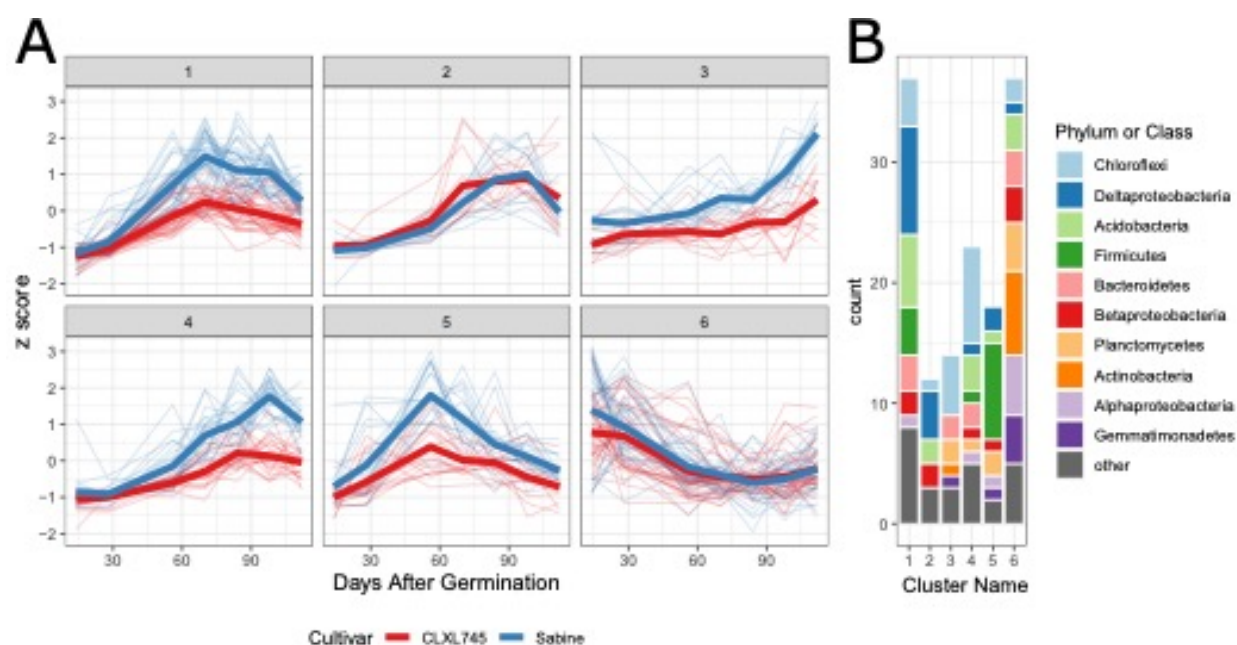
Supplemental Figure 4 Clustering analysis of the cultivar-sensitive rhizosphere OTUs. (A) The trend in Z-scores of OTUs within each cluster. The thick lines are the average trend of the cluster, and the faint lines are the seasonal trend of each individual OTU. Both methanogens are contained in cluster 2. (B) Composition of each cluster, with color indicating the phylum to which the OTUs in each cluster belong.

25

A

	Df	SumsOfSqs	MeanSqs	F.Model	R2	Pr(>F)	
Compartment	2	15.142	7.5709	57.684	0.21931	0.001	***
Plot	1	0.38	0.3798	2.894	0.0055	0.004	**
Days	1	9.687	9.6871	73.808	0.14031	0.001	***
Cultivar	1	0.474	0.4745	3.615	0.00687	0.003	**
Days:Cultivar	1	0.303	0.3029	2.308	0.00439	0.018	*
Compartment:Days	2	1.977	0.9887	7.533	0.02864	0.001	***
Compartment:Cultivar	2	0.26	0.1298	0.989	0.00376	0.417	
Residuals	311	40.818	0.1312		0.59122		
Total	321	69.041		1			

B

	Df	SumsOfSqs	MeanSqs	F.Model	R2	Pr(>F)	
Library	1	0.1807	0.18066	1.933	0.01437	0.045	*
Plot	1	0.1578	0.15784	1.6889	0.01256	0.082	.
Days	1	2.6921	2.69214	28.8047	0.21415	0.001	***
Cultivar	1	0.1875	0.18745	2.0057	0.01491	0.04	*
Days:Cultivar	1	0.1002	0.10023	1.0724	0.00797	0.284	
Residuals	99	9.2527	0.09346		0.73603		
Total	104	12.571		1			

C

	Df	SumsOfSqs	MeanSqs	F.Model	R2	Pr(>F)	
Plot	1	0.2625	0.2625	1.6905	0.01313	0.048	*
Days	1	3.5609	3.5609	22.931	0.17807	0.001	***
Cultivar	1	0.2605	0.2605	1.6773	0.01302	0.045	*
Days:Cultivar	1	0.2298	0.2298	1.4801	0.01149	0.093	.
Residuals	101	15.6839	0.1553		0.78429		
Total	105	19.9976		1			

D

	Df	SumsOfSqs	MeanSqs	F.Model	R2	Pr(>F)	
Library	1	0.1777	0.1777	1.237	0.00833	0.193	
Plot	1	0.1965	0.1965	1.368	0.00921	0.149	
Days	1	5.3979	5.3979	37.576	0.25306	0.001	***
Cultivar	1	0.2834	0.2834	1.973	0.01329	0.041	*
Days:Cultivar	1	0.1915	0.1915	1.333	0.00898	0.158	
Residuals	105	15.0836	0.1437		0.70713		
Total	110	21.3307		1			

E

	Df	SumsOfSqs	MeanSqs	F.Model	R2	Pr(>F)	
Days	1	0.4442	0.44423	3.5364	0.06396	0.001	***
Cultivar	1	0.1296	0.12959	1.0316	0.01866	0.392	
Days:Cultivar	1	0.0907	0.09072	0.7222	0.01306	0.81	
Residuals	50	6.2809	0.12562		0.90432		
Total	53	6.9454		1			

F

	Df	Sum Sq	Mean Sq	F value	Pr(>F)	
Timepoint	6	34.39	5.73	3.645	0.001644	**
Cultivar	1	348.62	348.62	221.7074	< 2.2e-16	***
Timepoint:Cultivar	6	65.4	10.9	6.9323	6.35E-07	***
Residuals	308	484.31	1.57			

Supplemental Table 1 (A) PERMANOVA testing the effects of compartment, plot, days, cultivar, days by cultivar, compartment by days, and compartment by cultivar on Bray-Curtis distances. Bulk soil samples were removed prior to analysis. (B to D) PERMANOVA testing the effects of lane, plot, days, cultivar, and cultivar by days of interaction with the rhizosphere (B), rhizoplane (C), and endosphere (D) Bray-Curtis distances. Plot refers to the plots containing one cultivar or the other; cultivars were grown exclusively in four plots each, and therefore this factor is nested within the cultivar term. Lane refers to the library in which the samples were sequenced. The rhizosphere, endosphere, and bulk soil samples were spread out across 4 libraries, so this term is included in the ANOVA, whereas the rhizoplane samples were all sequenced in the same library. This setup causes compartment to be nested in lane, meaning it cannot be included in Table S1A. (E) PERMANOVA testing the effects of time and cultivar (here meaning plots growing one cultivar or the other) and their interaction on bulk soil Bray-Curtis distances. (F) ANOVA testing the effects of cultivar, time, and their interaction on Bray-Curtis distances that have compartment partialled out in the CAP analysis.

Compartment	trait	term	sumsq	meansq	statistic	p.value	p.adjusted
Rhizosphere	chemoheterotrophy	Cultivar	25740.82983	25740.82983	1.216132805	0.273028846	0.344878542
Rhizosphere	dark_hydrogen_oxidation	Cultivar	1571.945049	1571.945049	8.168011739	0.005284406	0.01409175
Rhizosphere	fermentation	Cultivar	2331.558965	2331.558965	2.96139415	0.088672838	0.15201058
Rhizosphere	iron_respiration	Cultivar	794.9878708	794.9878708	1.296221112	0.257893073	0.343857431
Rhizosphere	methanogenesis	Cultivar	499.6093564	499.6093564	21.71614785	1.08E-05	0.000129196
Rhizosphere	methanotrophy	Cultivar	16.01623472	16.01623472	0.403047243	0.527112722	0.60241454
Rhizosphere	reductive_acetogenesis	Cultivar	358.6525583	358.6525583	8.80592199	0.003836153	0.011508458
Rhizosphere	sulfate_respiration	Cultivar	5413.451985	5413.451985	2.291834162	0.133521753	0.213634805
Endosphere	chemoheterotrophy	Cultivar	159061.7169	159061.7169	10.18190418	0.001911297	0.009463255
Endosphere	dark_hydrogen_oxidation	Cultivar	1125.698579	1125.698579	6.144526592	0.014908187	0.032526954
Endosphere	fermentation	Cultivar	22125.76477	22125.76477	22.28281154	7.92E-06	0.000129196
Endosphere	iron_respiration	Cultivar	6198.683996	6198.683996	10.11866449	0.001971512	0.009463255
Endosphere	methanogenesis	Cultivar	96.46063826	96.46063826	6.929120846	0.009867786	0.023682686
Endosphere	methanotrophy	Cultivar	189.5657967	189.5657967	1.803694407	0.182400546	0.273600819
Endosphere	reductive_acetogenesis	Cultivar	1201.651256	1201.651256	16.09269109	0.000118675	0.000949403
Endosphere	sulfate_respiration	Cultivar	30736.24631	30736.24631	8.927810598	0.003557407	0.011508458
Rhizoplane	chemoheterotrophy	Cultivar	703.2039912	703.2039912	0.05948514	0.807854619	0.807854619
Rhizoplane	dark_hydrogen_oxidation	Cultivar	186.1880534	186.1880534	1.532597089	0.218873034	0.308997225
Rhizoplane	fermentation	Cultivar	2796.218024	2796.218024	5.26361027	0.02405128	0.048102561
Rhizoplane	iron_respiration	Cultivar	98.30765908	98.30765908	0.259044991	6.12E-01	0.665550326
Rhizoplane	methanogenesis	Cultivar	52.52191331	52.52191331	4.919533607	0.029016258	0.053568476
Rhizoplane	methanotrophy	Cultivar	16.48617431	16.48617431	0.223083262	0.637819062	0.665550326
Rhizoplane	reductive_acetogenesis	Cultivar	612.1502755	612.1502755	9.109539826	0.003289417	0.011508458
Rhizoplane	sulfate_respiration	Cultivar	1451.093773	1451.093773	0.706644687	0.402739422	0.483287306

Supplemental Table 2 ANOVA testing the effect of each trait assigned by FAPROTAX to the overrepresented cultivar-sensitive OTUs within each compartment. ANOVA was run on each trait individually, and then the cultivar term was extracted and corrected for multiple testing using the Benjamini-Hochberg method.

A

	Df	Sum Sq	Mean Sq	F value	Pr(>F)
Timepoint	3	0.044291	0.014764	5.0349	0.02217
Cultivar	1	0.000494	0.000494	0.1685	0.6901
Timepoint:Cultivar	3	0.012924	0.004308	1.4692	0.28139
Residuals	10	0.029322	0.002932		

B

	Df	Sum Sq	Mean Sq	F value	Pr(>F)
Timepoint	3	2784.36	928.12	31.2651	6.25E-12
Cultivar	1	445.14	445.14	14.9954	0.000289
Timepoint:Cultivar	3	17.18	5.73	0.1929	0.900793
Residuals	55	1632.7	29.69		

C

Timepoint	contrast	estimate	SE	df	t.ratio	p.value
1	CLXL745-Sabine	-4.099476	2.724221	55	-1.505	0.1381
2	CLXL745-Sabine	-4.708275	2.724221	55	-1.728	0.0895
3	CLXL745-Sabine	-5.642603	2.819837	55	-2.001	0.0503
4	CLXL745-Sabine	-6.847717	2.724221	55	-2.514	0.0149

Supplemental Table 3 (A) ANOVA testing the effects of time, cultivar, and their interaction on section measurements. (B) ANOVA testing the effects of time, cultivar, and their interaction on pycnometer measurements. (C) Contrasts between CLXL745 and Sabine at each of the four time points.

Chapter 2

Prolonged drought imparts lasting compositional changes to the rice root microbiome

Christian Santos-Medellín[1,4,*], Zachary Liechty[1,*], Joseph Edwards[1,5], Bao Nguyen[1,6], Bihua Huang[2], Bart C. Weimer [2] and Venkatesan Sundaresan [1,3]

[1]Department of Plant Biology, University of California, Davis, Davis, CA, USA. [2]Department of Population Health and Reproduction, 100K Pathogen Genome Project, University of California, Davis, Davis, CA, USA. [3]Department of Plant Sciences, University of California, Davis, Davis, CA, USA. [4]Present address: Department of Plant Pathology, University of California, Davis, Davis, CA, USA. [5]Present address: Department of Integrative Biology, University of Texas, Austin, TX, USA. [6]Present address: Microbiology and Environmental Toxicology Department, University of California, Santa Cruz, Santa Cruz, CA, USA.

[*]These authors contributed equally: Christian Santos-Medellín, Zachary Liechty.

Abstract

Microbial symbioses can mitigate drought stress in crops but harnessing these beneficial interactions will require an in-depth understanding of root microbiome responses to drought cycles. Here, by detailed temporal characterization of root-associated microbiomes of rice plants during drought stress and recovery, we find that endosphere communities remained compositionally altered after rewatering, with prolonged droughts leading to decreased resilience. Several endospheric Actinobacteria were significantly enriched during drought and for weeks after rewatering. Notably, the most abundant endosphere taxon during this period was a *Streptomyces*, and a corresponding isolate promoted root growth. Additionally, drought stress disrupted the temporal dynamics of late-colonizing microorganisms, permanently altering the normal successional trends of root microbiota. These findings reveal that severe drought results in enduring impacts on rice root microbiomes, including enrichment of taxonomic groups that could shape the recovery response of the host, and have implications relevant to drought protection strategies using root microbiota.

Author Contributions

This study was co-lead between CS-M and ZL. CS-M was responsible for the setup, sampling, and 16S profiling and analysis of the greenhouse. ZL was responsible for identification of OTU 1037355 in other datasets, selection of microbial isolates of interest, the semi-sterile experiment, phenotypic and 16S profiling of the semi-sterile experiment, and genome sequencing of SLBN-177. CS-M, ZL, and VS conceptualized the experiments. JE and BN aided in carrying out experiments. BH and BW generated the SLBN-177 genome sequence.

Check for updates

Prolonged drought imparts lasting compositional changes to the rice root microbiome

Christian Santos-Medellín[1,4,7], Zachary Liechty[1,7], Joseph Edwards[1,5], Bao Nguyen[1,6], Bihua Huang[2], Bart C. Weimer [2] and Venkatesan Sundaresan [1,3 ✉]

Microbial symbioses can mitigate drought stress in crops but harnessing these beneficial interactions will require an in-depth understanding of root microbiome responses to drought cycles. Here, by detailed temporal characterization of root-associated microbiomes of rice plants during drought stress and recovery, we find that endosphere communities remained compositionally altered after rewatering, with prolonged droughts leading to decreased resilience. Several endospheric Actinobacteria were significantly enriched during drought and for weeks after rewatering. Notably, the most abundant endosphere taxon during this period was a *Streptomyces*, and a corresponding isolate promoted root growth. Additionally, drought stress disrupted the temporal dynamics of late-colonizing microorganisms, permanently altering the normal successional trends of root microbiota. These findings reveal that severe drought results in enduring impacts on rice root microbiomes, including enrichment of taxonomic groups that could shape the recovery response of the host, and have implications relevant to drought protection strategies using root microbiota.

rought is the largest contributor to world-wide crop loss[1]. With an average of 25% yield reduction under drought[2], rice is particularly susceptible to this abiotic stress, due in part to its semi-aquatic growth habit and its small root system[3]. Rice responds to drought episodes through a slew of molecular, physiological and morphological changes aimed to mitigate stress and facilitate recovery after rewatering[4]. Plant–microbe symbioses can further boost stress resistance by enhancing the plant response to environmental perturbations[5]. As such, the harnessing of plant–microbe interactions has emerged as a complementary approach to reduce crop losses associated with drought[6] and understanding the ecological principles governing root microbiome assembly under environmental stressors has become a research priority[7].

Drought triggers a compartment-specific restructuring of the rice root microbiota, with endosphere communities displaying a more pronounced response than rhizosphere communities[8]. This compositional shift is characterized by a prominent increase of a diverse group of monoderm bacteria, including Actinobacteria, Chloroflexi and aerobic Firmicutes. Such taxonomic signatures are consistent across multiple rice cultivars and soil types. Similar trends have been independently observed in a wide variety of plant species, across cereals and dicots[9,10], indicating that monoderm enrichment is a phylogenetically conserved response in plants under drought stress. While these cross-sectional studies have shed light on the compositional changes that root-associated microbiomes undergo during drought, the temporal dynamics on rewatering are less understood. This recovery period is particularly relevant as both plants and microbes undergo quick physiological changes that can reshape the underlying network of biotic interactions[6]. Furthermore, evaluating the resilience of root communities (that is, their rate of recovery after a disturbance) can help us determine the permanence of drought-mediated alterations.

In irrigated rice, root communities display a highly conserved temporal development characterized by a rapid turnover during the early vegetative stages followed by a relative stabilization as the host transitions into flowering[11,12]. These community dynamics are driven by a phylogenetically diverse group of microbial taxa that experience consistent longitudinal shifts across multiple geographic regions and growing seasons[11]. Previously, we showed that drought-stressed rice root communities are developmentally paused compared to well-watered communities[11], and similar trends were observed in sorghum[13]. Assessing the impact of this effect on the recovery period can reveal the extent to which drought disrupts the temporally coordinated interplay between host and root microorganisms. In sorghum, the drought-mediated enrichment of monoderm bacteria was reported to rapidly return to predrought levels on rewatering[13], suggesting that the impact might be short lived.

As drought episodes become longer and more frequent[1], it will be important to gain detailed knowledge of the consequences of extended drought on plant-associated microbiomes, especially in drought-sensitive crops. As highlighted in a recent review, there is a 'need for improved mechanistic understanding of the complex feedbacks between plants and microbes during, and particularly after, drought'[6]. Here, we conducted a detailed temporal profiling of the rhizosphere and endosphere communities of rice plants grown under a range of drought-stress durations to investigate the following questions: (1) how does drought duration affect the recovery of root communities and how does this response vary across compartments, (2) what is the range of temporal dynamics displayed by drought-responsive microorganisms and (3) does the drought-mediated delay in microbiome development persist on recovery? We found that extended drought produces lasting changes to root microbiota composition, manifested by phyla-dependent patterns of enrichment and depletion, especially involving persistent

[1]Department of Plant Biology, University of California, Davis, Davis, CA, USA. [2]Department of Population Health and Reproduction, 100K Pathogen Genome Project, University of California, Davis, Davis, CA, USA. [3]Department of Plant Sciences, University of California, Davis, Davis, CA, USA. [4]Present address: Department of Plant Pathology, University of California, Davis, Davis, CA, USA. [5]Present address: Department of Integrative Biology, University of Texas, Austin, TX, USA. [6]Present address: Microbiology and Environmental Toxicology Department, University of California, Santa Cruz, Santa Cruz, CA, USA. [7]These authors contributed equally: Christian Santos-Medellín, Zachary Liechty. ✉e-mail: sundar@ucdavis.edu

enrichment of specific taxa, of which the most abundant was found to be putatively beneficial by isolation and further characterization.

Results

Experimental design. To characterize the effect of drought on the temporal progressions of root-associated communities, we exposed rice plants (*Oryza sativa* ssp. *japonica* variety M-206), grown in agricultural soil under controlled greenhouse conditions, to one of three increasingly longer drought-stress (DS) periods: DS1 (11 days), DS2 (21 days) and DS3 (33 days). DS2 corresponds to the duration of drought stress used in a previous study that identified clear compositional shifts in the root microbiomes of drought-stressed rice plants grown under similar conditions[8], and the duration of DS1 and DS3 were chosen to further explore the effects of mild and severe drought relative to this baseline. Given that microbiome succession is highly dynamic during the vegetative growth phase of rice[11], all drought treatments were initiated at 41 days after transplantation, before plants transitioned to the reproductive stage and microbiome composition stabilized. All plants experiencing drought treatments survived and eventually entered the reproductive phase (Supplementary Fig. 1). As a control treatment (water control, WC), we kept an additional set of rice plants under well-watered conditions throughout the whole experiment. For each of the four watering regimes (WC, DS1, DS2 and DS3), plants were destructively sampled roughly every 10 days for a total of 13 collection time points spanning 136 days. This collection scheme covered the complete life cycle of rice and allowed us to track microbiome succession before, during and after drought (Fig. 1a). For each plant sampled, we profiled the bacterial and archaeal diversity associated with the rhizospheric and endospheric communities via high-throughput amplicon sequencing of the V4 region of the 16S ribosomal RNA gene. After filtering organellar sequences and removing operational taxonomic units (OTUs) not present in at least 5% of all samples, we identified 4,135 OTUs (mean sequencing depth = 20,740 reads).

Beta-diversity patterns reveal root compartment differences in drought recovery. Root compartment was the main driver of microbiome composition as evidenced by a clear separation between rhizosphere and endsophere communities across the first axis of an unconstrained principal coordinates analysis (PCoA) performed on weighted UniFrac distances (Extended Data Fig. 1a). Moreover, a permutational multivariate analysis of variance (PerMANOVA) indicated that root compartment explained most of the variation in the whole dataset ($F_{1,400} = 1070.36$, $R^2 = 0.628$, $P < 0.001$). Therefore, to better explore the impact of drought treatment, collection time, and their interaction on each compartment, we ran a PerMANOVA on rhizosphere and endosphere samples independently. In both cases, all main and interaction effects were significant (Table 1).

We then explored the longitudinal trends of beta diversity captured by the first axis of independent PCoAs performed on each compartment (Fig. 1c,d and Extended Data Fig. 1c–f). In both rhizosphere and endosphere communities, PCo1 tracked the compositional development that root communities underwent during the life cycle of rice plants as evidenced by the progressive transition of early to late time points along the axis. Additionally, PCo1 displayed drought-mediated shifts in community composition throughout time: while all watering regimes followed similar trajectories before drought onset (41-day-old mark), drought-treated plants started diverging from well-watered communities as soon as irrigation was suspended. The separation between control and stressed communities increased for as long as drought conditions were kept, with 31-day drought-stressed communities (DS3) showing the largest deviation from well-watered samples. Finally, drought treatments presented differential recovery dynamics on rewatering: while both DS1 and DS2 samples recovered relatively quickly, DS3 communities remained significantly altered after drought stress was ceased

($P_{FDR} < 0.05$, asterisks in Fig. 1c,d, Supplementary Table 1). This significant deviation from controlled communities was sustained for 50 days in the endosphere whereas it only lasted for 20 days in the rhizosphere, suggesting potential differences in community resilience across compartments. In contrast, drought treatments had only a minor impact on the alpha diversity of root communities (Supplementary Fig. 2 and Supplementary Table 2).

Beta-diversity patterns in rhizosphere and endosphere microbiomes diverged from the temporal trends displayed by the water content in our samples. In particular, soil percentage moisture was significantly reduced for all drought treatments during the stress period but immediately returned to control levels after irrigation was resumed (Fig. 1b). Thus, despite soil moisture being fully restored, prolonged drought hindered the ability of root communities to quickly recover.

Drought-responsive taxa follow distinct longitudinal trends within and between compartments. To identify taxa affected by watering regime throughout time, we fitted negative binomial models to the abundances of individual OTUs and ran pairwise Wald tests contrasting well-watered controls against each drought-stess treatment (DS1, DS2 and DS3) in each compartment at each collection time point. We found a total of 214 rhizospheric OTUs and 221 endospheric OTUs affected by treatment in at least one comparison (Fig. 2a and Supplementary Table 3, $P_{FDR} < 0.05$). The temporal distribution of significant effects among these differentially abundant OTUs followed distinct patterns in each compartment: in the rhizosphere, significance was mostly observed during the drought period; in the endosphere, it widely extended to the recovery phase of the experiment, especially for treatment DS3.

While this approach detected clear ecological signals driven by drought stress (for example, the number of differentially abundant OTUs was proportional to duration of stress), it also identified OTUs affected by other, potentially stochastic, processes. For example, multiple OTUs were found to be significantly affected by watering treatment in the collection time points preceding drought onset, when conditions were identical across treatments (Fig. 2a). This effect was more pronounced in the endosphere communities, which exhibited greater within-compartment variation than rhizosphere communities (Extended Data Fig. 1b). Thus, to identify coherent patterns of drought response in the set of differentially abundant OTUs, we performed hierarchical clustering on the $\log_2$ fold changes computed across all comparisons (Supplementary Table 4 and Extended Data Fig. 2). This method distinguished three rhizospheric and two endospheric modules displaying clear longitudinal trends across drought treatments (Fig. 2b).

One rhizospheric module consisted of 100 OTUs whose relative abundances increased under drought stress. Such enrichment was proportional to the duration of stress and was mostly constrained to the span of suspended irrigation in each treatment. The OTUs exhibiting this transient enrichment belonged mainly to the phyla Actinobacteria, Gemmatimonadetes and Chloroflexi. In contrast, the other two rhizospheric modules showed clear signatures of depleted abundance under drought conditions, although each with unique recovery dynamics: while 64 OTUs were transiently depleted, that is their relative abundances were quickly restored after irrigation was resumed, 26 OTUs were persistently depleted, that is their relative abundances remained decreased weeks after stress was ceased. This latter pattern was particularly conspicuous in rhizospheres of plants that underwent 31 days of drought (DS3). While both depletion modules were enriched in OTUs classified as Acidobacteria, Betaproteobacteria and Deltaproteobacteria, each one featured a unique pattern at a lower taxonomic resolution (Extended Data Fig. 3). On one hand, most transiently depleted Betaproteobacteria belonged to order MND1, whereas almost all persistently depleted were Rhodocyclales. On the other hand, Deltaproteobacteria

classified as Myxococcales and Desulfuromonadales were prominent in the transient and persistent modules, respectively.

Out of the two endospheric modules, one encompassed 21 OTUs enriched under drought while the other one contained 64 OTUs depleted under drought. In both cases, these shifts in abundances persisted after drought stress was suspended, albeit to different extents for each module. For OTUs positively impacted by drought, the increase in relative abundances persisted, depending on the specific treatment, from 10 to 20 days after irrigation was resumed. More than 80% of OTUs in this semipersistently enriched module belonged to the phylum Actinobacteria. In contrast, for OTUs negatively affected by drought, depleted abundance relative to well-watered controls was observed throughout the whole recovery phase. Moreover, similar to the results observed in the rhizosphere, several persistently depleted OTUs were classified as Myxococcales and Rhodocyclales (Extended Data Fig. 3). Together, these results indicate that phylogenetically distinct groupings of bacterial taxa follow diverse trajectories throughout drought stress and recovery in root-associated compartments.

A highly occurring *Streptomyces* becomes the most abundant taxon in endosphere communities during and after drought. Given the strong taxonomic signature displayed by the set of semipersistently drought-enriched OTUs (Fig. 2b), we further explored the compositional trends of each individual Actinobacteria within this module. In particular, we calculated the abundance-occupancy curves of rhizosphere and endosphere communities, and located each OTU along these spectra (Fig. 3a). Overall, semipersistently enriched Actinobacteria were among the most highly abundant and occurring members of root-associated communities, especially in the endosphere. One *Streptomyces* taxon, OTU 1037355, was notably predominant: not only was it detected in all collected samples, but also its mean relative abundance was greater than that of 99 and 97% of all OTUs in the endosphere and rhizosphere communities, respectively. Furthermore, analysing its temporal dynamics across treatments, we found that OTU 1037355 became the most abundant taxon in endosphere communities by the end of the DS2 and DS3 drought periods, reaching a mean relative abundance of 13.5% (Fig. 3b). Additionally, OTU 1037355 remained the most abundant taxon in the endosphere during the early stages of recovery. In rhizosphere communities, the drought-mediated enrichment of OTU 1037355 was less prominent as it only reached a maximum relative abundance of 1.3% in drought-stressed samples. Moreover, even though the abundance of this OTU increased during the drought period,

it immediately declined after irrigation was resumed. Thus, despite being significantly affected by drought in both communities, OTU 1037355 exhibited compartment-specific recovery trends.
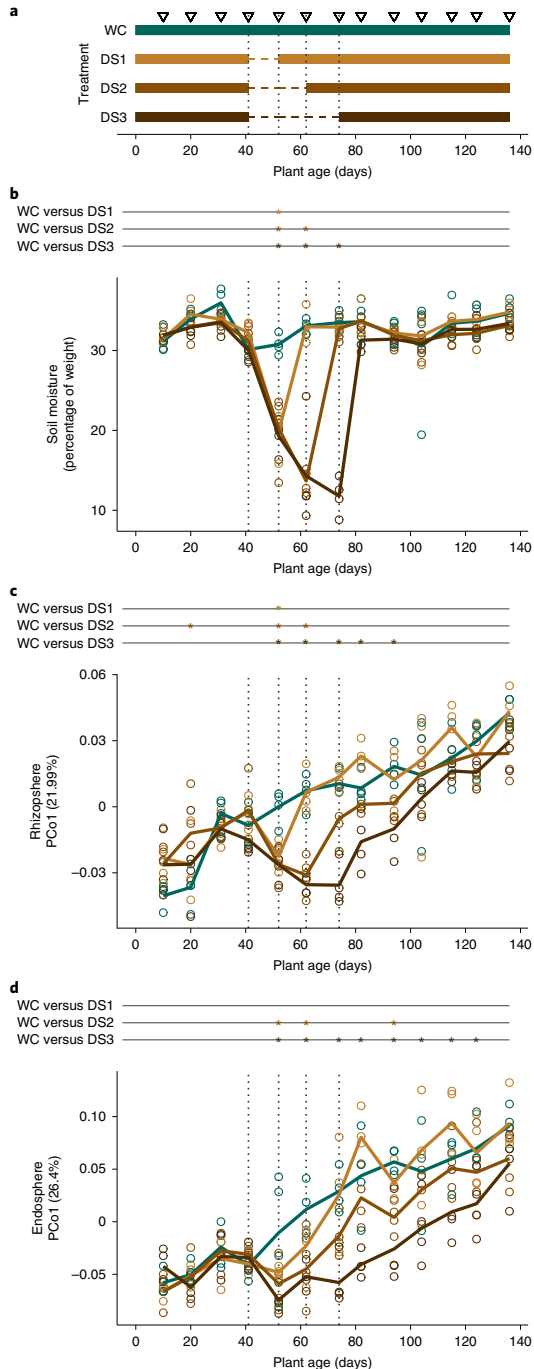

Fig. 1 | Compositional dynamics of rhizosphere and endosphere communities before, during and after drought. a, Timeline of the watering regimes followed by control (WC) and drought-stressed (DS1, DS2 and DS3) plants. Horizontal lines represent the watering status during the experiment: solid segments indicate periods of constant irrigation while dotted segments indicate periods of suspended irrigation. Upside-down triangles mark each of 13 collection time points spanning the complete life cycle of rice plants. **b**, Soil percentage moisture as measured by gravimetric water content **c,d**, Beta-diversity patterns in the rhizosphere (**c**) and endosphere (**d**) communities. In both cases, the *y* axis displays the position of each sample across the first principal coordinate (PCo) from a weighted UniFrac PCo analysis and the *x* axis displays the age of the plant at the moment of sample collection. The trend lines in **b**, **c** and **d** represent the mean values for each treatment throughout the experiment. Asterisks on top indicate a significant difference ($P_{FDR} < 0.05$ where FDR is false discovery rate) between the control and each of the drought treatments at a specific time point. Statistical significance was determined by ANOVA and pairwise contrasts (two-sided) corrected with the Benjamini–Hochberg procedure. Supplementary Table 1 contains the effect sizes, standard errors and *P* values for all pairwise contrasts performed for **b**, **c** and **d**.

Table 1 | Influence of experimental factors and their interaction on the beta diversities of rhizosphere and endosphere communities

Rhizosphere			Endosphere		
Time	Treatment	Time × Treatment	Time	Treatment	Time × Treatment
$F_{12,156} = 7.397$	$F_{3,156} = 4.806$	$F_{36,156} = 1.532$	$F_{12,156} = 8.132$	$F_{3,156} = 6.273$	$F_{36,156} = 1.258$
$R^2 = 0.283$	$R^2 = 0.046$	$R^2 = 0.176$	$R^2 = 0.307$	$R^2 = 0.059$	$R^2 = 0.143$
$P = 0.001$	$P = 0.001$	$P = 0.001$	$P = 0.001$	$P = 0.001$	$P = 0.006$

We then assessed if the pattern of sustained enrichment displayed by OTU 1037355 was a reproducible feature of endosphere communities by analysing its longitudinal dynamics in an independent drought experiment performed on the same rice cultivar grown in the same agricultural soil. Briefly, 1-month-old plants were drought stressed for 21 days and allowed to recover for 7 days (Methods). Samples were collected each week to track the drought-mediated temporal shifts and postdisturbance trends. The microbial profiles confirmed that this OTU was significantly enriched during and after the imposition of drought conditions (Extended Data Fig. 4). This shift was even more conspicuous as the mean relative abundance of OTU 1037355 reached up to 24.0% of the total community in drought-stressed samples.

The high occupancy displayed by OTU 1037355 in both drought-stressed and well-irrigated plants suggests a strong association of this taxon with rice plants. To evaluate the presence of this OTU in the root-associated communities of a diverse panel of rice cultivars grown in a set of compositionally distinct soils, we re-analysed rhizosphere and endosphere profiles derived from two previously published studies: a cross-sectional experiment assessing the effects of drought on rice microbiomes across three distinct California soils (including the soil used in this experiment)[8], and a time series characterizing the microbial dynamics of rice plants grown in Arkansas[11,14] (see Methods for a detailed description of the datasets). In all cases, we found that OTU 1037355 displayed high occupancies in both rhizosphere and endosphere communities, suggesting that this taxon is a core member of the rice root microbiome (Extended Data Fig. 5a). The ubiquitous presence of this taxon in the Arkansas samples also demonstrates that the consistent interaction with this OTU throughout the plant life cycle is not limited to the soil source used in this experiment. In addition, on comparing the relative abundances of OTU 1037355 in drought-stressed and well-watered plants, we confirmed that the drought-mediated enrichment of this taxon was conserved across the different California soils tested in the study (Extended Data Fig. 5b).

A *Streptomyces* isolate classified as OTU 1037355 is a root growth-promoting bacteria. To assess if this highly occurring *Streptomyces* taxon was part of the readily culturable fraction of the root microbiota, we screened a set of bacterial isolates previously collected from rice-associated rhizosphere and endosphere communities (Methods) and found nine isolates classified as OTU 1037355. We then compared these isolates against the most prevalent sequence variant that mapped to OTU 1037355 in our longitudinal drought experiment; this sequence variant comprised 63.4% of all sequences mapping to that OTU (Supplementary Fig. 3a). Five of the isolates differed by a single nucleotide, and one isolate, SLBN-177, was additionally derived from the same soil source as the longitudinal drought experiment. The full 16S rRNA gene of SLBN-177 was sequenced and compared against the NCBI 16S rRNA gene database to further refine its taxonomic classification. We found that SLBN-177 shared 100% similarity with sequences from *Streptomyces pratensis*, *Streptomyces anulatus* and *Streptomyces praecox* (*S. praecox* has been proposed as a synonym of *S. anulatus*[15]).

Due to the sequence similarity and source of isolate, we further investigated the effects of SLBN-177 on rice growth phenotypes. First, seeds were inoculated with one of three microbial treatments: SLBN-177, SLBN-111 or a mock control. SLBN-111 is an Actinobacteria isolate from the genus *Microbacterium* and its associated OTU, 1108350, was found in low abundance in both the rhizosphere and endosphere communities (Supplementary Fig. 3b). Unlike many other Actinobacteria taxa, OTU 1108350 was not significantly altered by drought in any compartment. Due to the weak association of OTU 1108350 with the plant and its stability under drought, SLBN-111 was selected to distinguish the effects of SLBN-177 on rice seedlings from a general response caused by the introduction of a foreign microorganism at high abundance. Inoculated seeds were grown for 10 days in an axenic closed system, followed by a 14-day period of non-sterile drought stress in an open system (with WC plants still fully watered), followed by 7 days of recovery. Plants were then harvested, and root and leaf growth parameters were measured (Fig. 4a and Supplementary Fig. 4). A principal component analysis revealed that both watering and microbial treatments influenced the phenotypes of rice plants (Fig. 4b). Watering treatment was the driving factor separating samples along the first axis while microbial treatment distinguished samples along the second axis. SLBN-177-inoculated plants clustered separately from mock- and SLBN-111-inoculated plants. Furthermore, root length was the main variable distinguishing microbial treatments (Fig. 4b and Supplementary Table 5). Notably, contrasts demonstrated that roots of SLBN-177-treated plants were significantly longer than mock- and SLBN-111-treated plants in both well-watered and drought conditions (Fig. 4c and Supplementary Table 6). Microbial treatments did not significantly affect any other measured trait; however, all phenotypic measurements were significantly reduced by drought (Extended Data Fig. 6a and Supplementary Table 5).

To explore potential mechanisms responsible for the root elongation, the genome of SLBN-177 was sequenced, assembled and annotated. The assembly yielded 7.78 megabases of sequence and 6,975 putative coding sequences. Mapping genes to Kyoto Encyclopedia of Genes and Genomes (KEGG) pathways identified genes involved in the production of indole-3-acetic acid (IAA) through the indole-3-acetamide pathway, including *iaaM* (a tryptophan 2-monooxygenase) and *amiA2* (a putative amidase). The *iaaM* gene shared 93, 88.9 and 88.5% amino acid similarity with homologues from *S.* sp. ADI96-02, *S. coelicolor* and *S. scabiei*, respectively, of which the last two have previously been implicated in IAA biosynthesis[16,17] (Extended Data Fig. 6b). Additionally, we identified gene clusters potentially involved in the biosynthesis of siderophores (83% similarity to known desferroxamin B/E gene clusters; 90% similarity to coelichelin) and antimicrobials (65% similarity to carbapenem MM4550) (Supplementary Table 7). While the presence of these genes alone does not implicate them in host-associated responses to SLBN-177, they are potential targets for further study.

To confirm that SLBN-177 colonized the roots of rice plants, we performed 16S rRNA gene profiling on the endospheres of a subset of samples and compared the relative abundance of microbial reads to organellar reads. The mean relative abundance of OTU 1037355 on
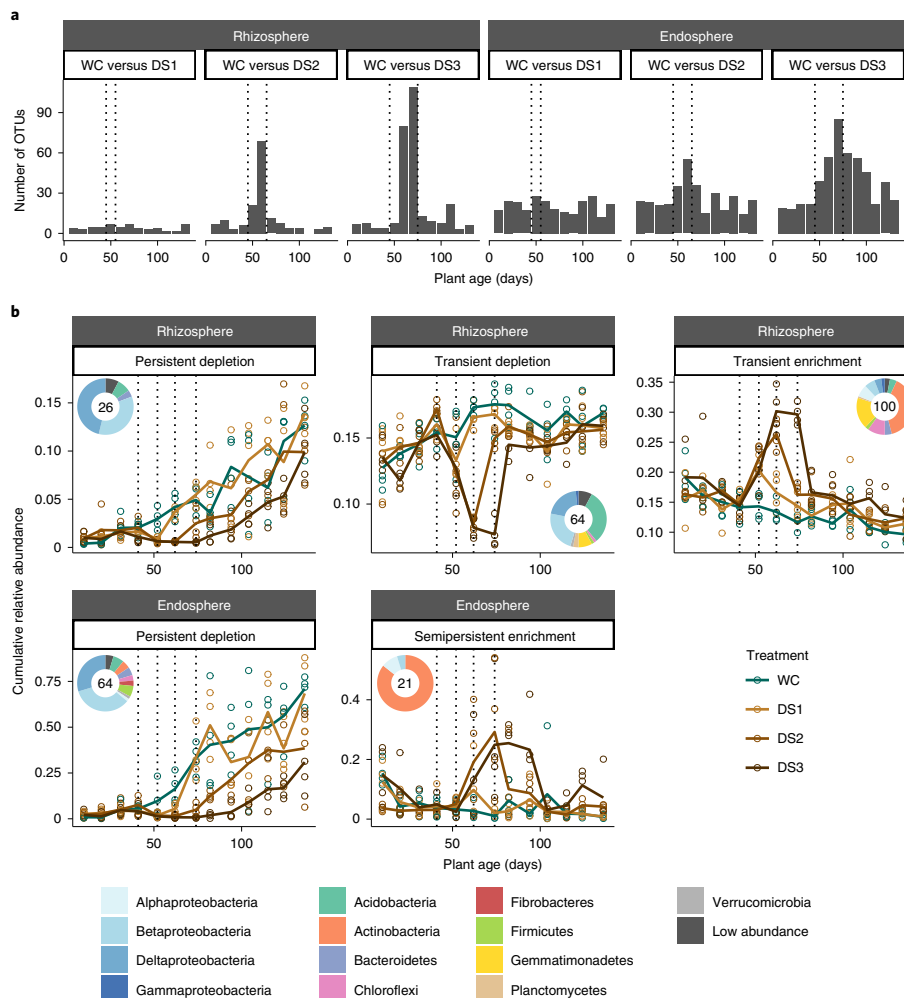
Fig. 2 | Drought-responsive OTUs show distinct longitudinal trends within and between compartments. a, Number of differentially abundant OTUs ($P_{FDR} < 0.05$) detected between well-watered controls and each of the drought treatments at each time point. Statistical significance was determined by negative binomial generalized linear models and pairwise Wald tests (two-sided) corrected with the Benjamini–Hochberg procedure. Supplementary Table 3 contains the effect sizes, standard errors and P values for all significant pairwise contrasts. **b**, Longitudinal shifts in the cumulative relative abundances of rhizosphere and endosphere drought-responsive modules detected through hierarchical clustering. The complete set of detected clusters is provided in Extended Data Fig. 2. Trend lines represent the mean values for each treatment throughout the experiment and inset donut plots display the size (number of OTUs) and taxonomic composition of each module. In all panels, the vertical dotted lines delimit the periods of suspended irrigation for each of the drought treatments.

SLBN-177-treated plants reached 5.7 and 30.7% in well-watered and drought-recovered samples, respectively, suggesting the enrichment of SLBN-177 persists in the recovery phase, as observed in OTU 1037355 in the previously described experiments (Extended Data Fig. 6c). In contrast, OTU 1108350 was barely detected in SLBN-111-treated samples, reaching a maximum relative abundance of 0.001%. Two drought-recovered control plants also had notable relative abundances of OTU 1037355, which could be a consequence of the open system portion of the experiment or carry over as seed endophytes not eliminated by surface sterilization, as has recently been reported in rice[18].

Regardless of the cause, the relative abundances of OTU 1037355 in these plants were much lower than drought-recovered plants inoculated with SLBN-177 (Extended Data Fig. 6c). Collectively, these results indicate that OTU 1037355 is a plant-growth promoting *Streptomyces* that is a key contributor to the compositional dynamics of endosphere communities during drought and recovery.

Drought permanently alters root-associated microbiome development. Relative abundances of root-associated taxa follow reproducible longitudinal trends that can be used to track root
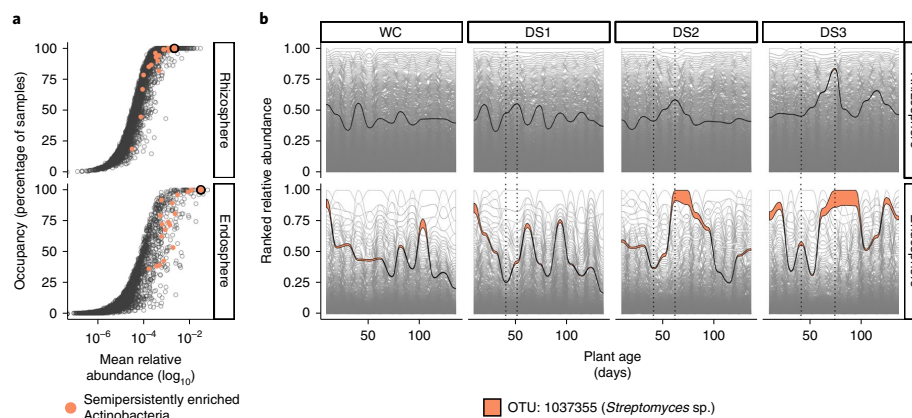
Fig. 3 | A drought-enriched OTU becomes the most abundant member of the endosphere communities. a, Occupancy–abundance curves for the rhizosphere and endosphere communities. The *x* axis displays the log-transformed mean relative abundance of each OTU while the *y* axis displays the percentage of samples in which each OTU was detected. Actinobacteria OTUs detected as semipersistently enriched in the endosphere (Fig. 2b) are coloured in orange and OTU 1037355 is further highlighted by a black outline. **b**, Ranked relative abundances of individual community members throughout time. Each ribbon represents a single OTU in the community: for each time point, width indicates its relative abundance while the position across the *y* axis indicates its rank within the community. The most abundant member of the semipersistent enrichment module, *Streptomyces* sp. (OTU ID 1037355), is highlighted. In all panels, the vertical dotted lines delimit the periods of suspended irrigation in each of the drought treatments.

microbiome maturation throughout time by training random forests models[11]. Using this approach on field-grown samples, we have previously shown that drought-stressed plants host a developmentally immature microbiota[11]. However, whether microbiome immaturity persists on rewatering is currently unknown. To explore this possibility, we used samples from well-watered plants to train separate full random forest models for each compartment by regressing OTU relative abundances as a function of host chronological age. For each compartment, we ranked each OTU on the basis of age-predicting importance and selected the top 65 (a threshold identified through cross-validation, Extended Data Fig. 7a) to generate sparse random forest models (Supplementary Table 8). Similar to the age-discriminant taxa detected in our previous field study[11], these top OTUs could be classified as early, late or complex root colonizers on the basis of their relative abundance patterns through time: early colonizers displayed initial high abundances that progressively declined, late colonizers exhibited initial low abundances that progressively increased and complex colonizers comprised OTUs that did not fit either of these two trends (Extended Data Fig. 7c and Supplementary Table 8). Among the set of early endosphere colonizers, most were classified as Chloroflexi and Betaproteobacteria (mainly Burkholderiales), whereas the set of early rhizosphere colonizers were more phylogenetically diverse. In contrast, both compartments had a clear enrichment of Deltaproteobacteria (mainly Myxococcales) and Betaproteobacteria (mainly Rhodocyclales) in the set of late colonizers (Extended Data Fig. 8).

The 65-taxon sparse models explained the 89.06 and 90.08% of variance related to plant age in the rhizosphere and endosphere communities, respectively. Furthermore, these models accurately predicted plant age on a validation set of well-watered samples, indicating that this approach was able to capture the consistent taxonomic shifts observed during normal root microbiome succession. We then applied the sparse random forest models to each of three drought regimes to assess the effect of drought on microbiome succession. We observed a clear deviation from the baseline development established by well-watered controls (Fig. 5a). To further measure this divergence, we calculated the relative microbiome

maturity of each sample as the difference between the predicted microbiome age and the baseline microbiome age of well-watered plants collected at the same chronological age (Fig. 5b and Supplementary Table 9). The results showed that, before drought onset, all watering regimes tracked normal microbiome development. However, microbiome progression was interrupted during drought and relative microbiome maturity became increasingly delayed. Furthermore, the extent of this microbiome immaturity was proportional to the duration of stress, with DS3 communities showing the highest departure from baseline development. For DS2 and DS3 samples, this microbiome immaturity persisted throughout the rest of the life cycle, even after irrigation was resumed. This pattern coincided with a delay in flowering displayed by drought-stressed plants, with DS2 and DS3 samples reaching developmental stages later than WC plants (Extended Data Fig. 9).

To understand the compositional changes driving the drought-mediated delay in root microbiome development, we analysed the abundance patterns of age-discriminant taxa across watering treatments. In both compartments, we observed a clear shift in the transition of dominance between early and late colonizers (Fig. 5c). In the rhizosphere, this transition was detected at the roughly 50- and 90-day-old marks in WC and DS3 plants, respectively; in the endosphere, the transition was detected at approximately the 70 and 120-day-old marks in WC and DS3 plants, respectively. This temporal shift in root microbiome assembly was mostly linked to a delay in the onset of late colonizers as evidenced by a persistent decrease in their relative abundances on drought stress. Additionally, there was a considerable overlap between the set of late colonizers and the differentially abundant OTUs assigned to the persistently depleted modules detected in the rhizosphere and endosphere communities (Extended Data Fig. 7b). Overall, these results indicate that drought stress permanently delayed microbiome development by affecting the recruitment of late colonizers.

Discussion

Drought-induced changes to the microbiome persist into the recovery period. Here we provide a detailed characterization of
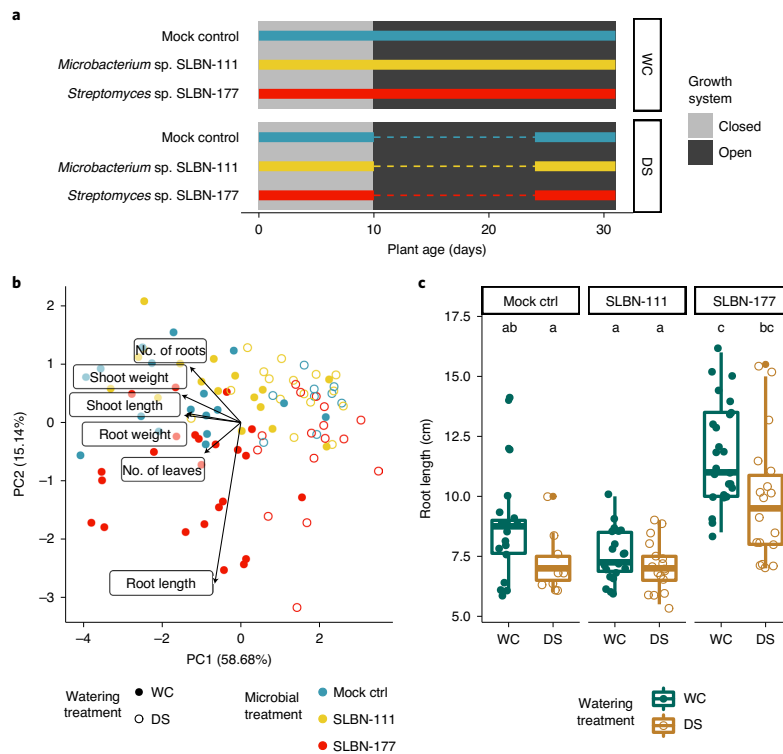
Fig. 4 | *Streptomyces* sp. SLBN-177 significantly increases root length under controlled conditions. a, Timeline of the watering regimes followed by control (WC) and drought-stressed plants. Horizontal lines represent the watering status during the experiment: solid segments indicate periods of constant irrigation while dotted segments indicate periods of suspended irrigation. Colours indicate the microbial treatment applied at the beginning of the experiment. The background colours indicate the periods during which the plant-growth system was closed (that is, axenic) or open. **b**, Principal component analysis of plant phenotypes. Points represent individual plants harvested at the end of the experiment and vectors indicate the contribution of each of the measured variables. The microbial treatment and watering regime received by each plant are indicated by colour and shape, respectively. **c**, Distribution of root lengths across microbial treatments and watering regimes. Boxes display the median and interquartile range, and data points further than 1.5× the interquartile range from box hinges are plotted as outliers. Letters at the top indicate significantly different groupings (adjusted $P < 0.05$). Statistical significance was determined by ANOVA and a Games–Howell test (two-sided). Supplementary Table 6 contains the effect sizes, standard errors and P values for all pairwise contrasts.

the drought-mediated changes and postdisturbance dynamics of root microbiomes through the life cycle of rice plants (*Oryza sativa* ssp. *japonica* cv. M-206). We show that both the magnitude of compositional changes undergone during drought and the capacity to fully recover on rewatering are significantly affected by the duration of drought stress experienced by the host and its associated bacterial and archaeal communities. In particular, we show that prolonged drought led to a severe microbiome restructuring that persisted even after irrigation was re-established, a trend that was more pronounced in the endosphere than in the rhizosphere. Previous cross-sectional studies performed on rice[8] and other plant species[10] have shown that, relative to the rhizosphere, endosphere communities are more strongly impacted by drought. This differential response has been attributed to a closer interaction of endosphere microorganisms with their host[10]. Similarly, the delay in endosphere recovery observed in this study might stem from the long-term effects induced by drought episodes at the whole plant level. Alternatively, differences in microbiome resilience between compartments could stem from the range of microbe–microbe

interactions supported by rhizosphere and endosphere communities. For example, a recent study in soil communities linked network topological properties such as high network connectivity and low modularity to decreased bacterial community stability under drought[19].

Hierarchical clustering of differentially abundant OTUs further revealed modules of drought-responsive taxa that followed distinct longitudinal shifts within and between compartments (Fig. 2b) Such patterns might stem from differences in the life strategies of these taxa. For instance, copiotrophs could recover more quickly than oligotrophs as they exhibit higher growth rates and lower resource use efficiency[20]. Moreover, the presence or absence of relevant functional traits could also impact recovery rate. Rewetting of dry soils, for example, releases specific forms of carbon and nitrogen to the environment[21], and the ability to metabolize these liberated resources could facilitate a quick recovery. In contrast, the reoxygenation of soils during drought could inhibit the growth and activity of the anaerobic microorganisms that colonize rice roots later in the season[14,22,23]. Several taxa persistently depleted
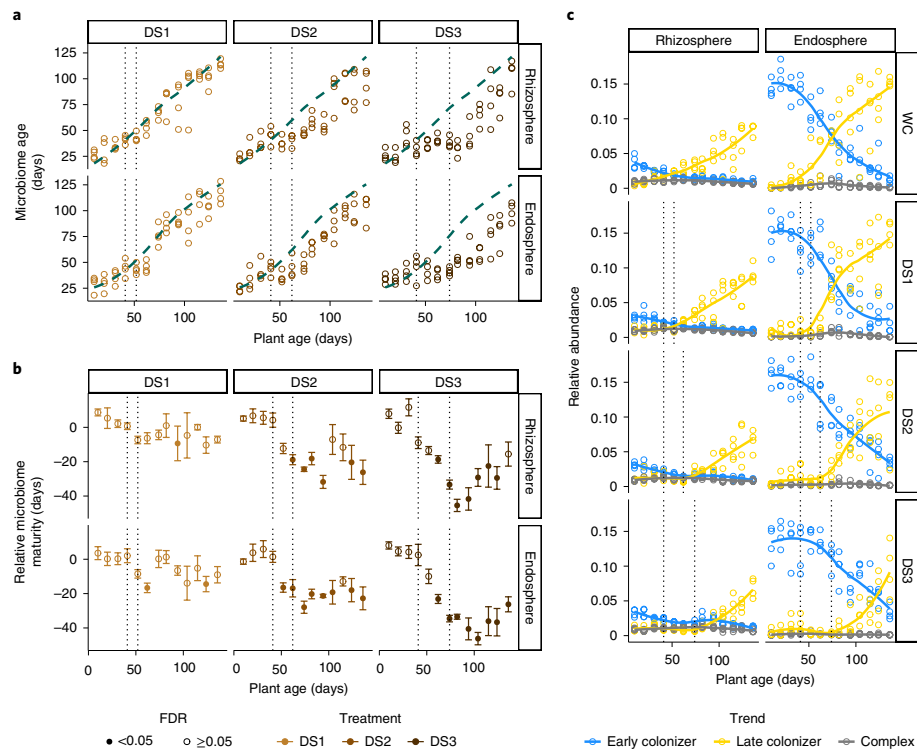
Fig. 5 | Persistent immaturity of root microbiomes in drought-stressed plants. a, Microbiome age predictions of rhizosphere and endosphere communities across drought-stress treatments (DS1, DS2 and DS3). The dashed curve represents the baseline microbiome development under well-irrigated conditions and was calculated by fitting a loess curve between the predicted microbiome age and the chronological plant age in the control (WC) test set. **b**, Relative microbiome maturity measured as the difference between the predicted microbiome age and the interpolated value of the loess curve at each sampling time point. Points indicate mean microbiome maturity and error bars indicate the standard deviation ($n = 4$ for each treatment and collection time point combination). Solid points denote a significant difference between the predicted ages of control and drought-treated plants ($P_{FDR} < 0.05$). Statistical significance was determined by ANOVA and pairwise contrasts (two-sided) corrected with the Benjamini–Hochberg procedure. Supplementary Table 9 contains the effect sizes, standard errors and P values for all pairwise contrasts performed. **c**, Longitudinal shifts in the aggregated relative abundances of the early, late and complex colonizers used in the random forest models.

by drought included members of *Desulfovibrio*, *Geobacter* and *Anaeromyxobacter*, known anaerobic genera[24–27] that could have been negatively affected by drought-induced reoxygenation.

Additionally, plant–microbe interactions could impact the responses of rhizosphere and endosphere microorganisms during and after drought. Root exudation is a temporally dynamic process that can promote or inhibit the growth of particular microbial taxa[28]. It has been shown that drought and rewetting can modify exudate composition[29], which in turn could alter the activity of microorganisms at the root–soil interface[30]. A metabolomic profile of drought-stressed rice roots has shown an increased abundance of uridine and raffinose, as well as numerous unidentified metabolites during drought stress[31], which could alter host–microbe interactions in the endosphere. Drought can also potentially reshape microbiome composition through altering the growth and architectural properties of roots[32]. Finally, as evidenced by the delayed flowering observed across drought-stressed plants in our study (Extended Data Fig. 9a), rice can respond to drought by pausing its transition from vegetative to reproductive growth[33] This developmental arrest could impact root microbiome assembly processes

that rely on temporally staged host-mediated signalling. Using a random forest approach, we found that the temporal progressions of rhizosphere and endosphere communities were also interrupted during prolonged drought stress (Fig. 5). While drought-induced delays in microbiome development have been reported by us and others[11,13], our postdisturbance sampling scheme allowed us to further evaluate if this drought-induced microbiome immaturity persisted after irrigation was resumed. We found that root communities remained underdeveloped throughout the whole recovery period due to a delay in the arrival of late root colonizers, many of which were part of the OTUs identified as persistently depleted in our differential abundance analysis. Late-colonizing taxa have been recently shown to follow reproducible temporal abundance patterns in the rhizosphere and endosphere communities of different rice genotypes grown across geographically distant areas and over multiple growing seasons[11]. This high degree of conservation suggests that plant selectivity might play a key role in the late-stage assembly dynamics of root microbiomes, further suggesting that the drought-induced delay of late colonizers observed in our study might be linked to host-mediated processes.

A defining characteristic of drought recovery dynamics is persistent enrichment of Actinobacteria. The drought-mediated enrichment of Actinobacteria in root-associated microbiomes, a pattern broadly shared across a wide diversity of plants[8–10], has been shown to correspond to an increase in the absolute abundance of members of this phylum[13,34]. Here, we have found that several Actinobacteria remained enriched in endosphere communities after rewatering, for up to 3 weeks before declining, a distinct recovery trend that was both compartment-specific and dependent on the degree of drought stress. Among these taxa, *Streptomyces* OTU 1037355 reached relative abundances as high as 24% of the total community (Fig. 3b and Extended Data Fig. 4b), becoming the most abundant member in the endosphere during drought and persisting through recovery. Our findings contrast with the rapid resilience recently reported for the root microbiomes of sorghum, in which the relative abundances of Actinobacteria quickly returned to well-watered levels within a week of concluding an 8-week period of drought[13]. Sorghum is naturally drought tolerant, so the conflicting results of the root microbiomes might reflect differential responses of the host to drought treatments and recovery. Drought-induced molecular changes that persist into recovery have been observed in both rice and sorghum[35,36], and investigating how these persistent changes alter root and exudate chemistry and subsequently interface with the microbiome could further our understanding of these contrasting results. Alternatively, the differences in microbiome recovery observed between rice and sorghum could be independent of the host and caused by differences in soil properties and/or starting microbial community.

An interesting facet of OTU 1037355 was its ubiquitous presence across all drought-stressed and well-watered plants profiled in this study, which indicates that this taxon is part of the core root microbiome of rice. Core microorganisms have been proposed to establish closer associations with their hosts that can result in mutualistic interactions[37], a trait that could be exploited to develop probiotic approaches to improve the performance of agroecosystems[38]. However, limitations in the experimental design (in this instance, samples originating from a single soil source and a single genotype) can erroneously inflate the occurrence of a microorganism in host-associated communities[39]. By analysing previously published datasets, we identified that OTU 1037355 also displayed high occupancies in rhizosphere and endosphere communities from plants grown in multiple California and Arkansas soils (Extended Data Fig. 5a). These samples encompassed multiple rice genotypes, further suggesting that the close association between OTU 1037355 and its host is preserved across a diverse panel of rice cultivars. Furthermore, OTU 1037355 was found to be impacted by drought in the roots of plants grown in other California soils, indicating that its response during drought is conserved across different microbiome backgrounds. While the recovery dynamics of OTU 1037355 are only known for the particular soil and cultivar combination used in this study, the presence and enrichment observed across multiple soils and cultivars (Extended Data Fig. 5) suggest these interactions might potentially be broadly applicable to rice plants across different soil types. Expanding the characterization of recovery dynamics to a broader range of rice cultivars, other host plants and soils will be needed to evaluate the influence of host genotype and soil source on root microbiome resilience.

Root colonization by SLBN-177, an isolate corresponding to the most abundant drought-enriched OTU (OTU 1037355), significantly increased root length in both well-watered and drought-stressed rice seedlings. This pattern contrasts with that displayed by a sorghum-associated *Streptomyces* recently found to exclusively promote root growth under drought[13], suggesting that SLBN-177 is a general root growth-promoting strain whose effects on the host could be amplified under drought due to its increased relative abundance rather than a mechanism directly triggered by

drought. Thus, the root growth promotion by SLBN-177 can potentially persist into the postdrought period during which it remains enriched. In a previous study, drought-mediated root elongation was associated with a more robust response by rice plants to subsequent drought events[40]. Specifically, root growth initiated in the recovery period allowed rice roots to penetrate hardpan soil, allowing greater access to water on recurrent droughts[40]. Furthermore, a recent study found a positive correlation between drought tolerance and the relative abundance of endospheric *Streptomyces* across a diversity of angiosperms[10], indicating that the potential beneficial role of Actinobacteria enrichment in root microbiomes might be more general. Many of the other Actinobacteria genera persistently enriched under drought, including *Actinoplanes*, *Catellatospora*, *Dactylosporangium*, *Pseudonocardia* and *Amycolaptopsis*, have been previously associated with plant-growth promotion[41], and are therefore potential targets for future studies.

The mechanism by which root elongation occurs is currently unknown, but the genome sequence provides candidate targets for future studies. The SLBN-177 genome contains putative auxin biosynthesis genes, a phytohormone previously demonstrated to be produced by microbes and benefit plants under drought stress[16,42]. Further research is necessary to determine whether these genes are involved with root growth promotion between SLBN-177 and the host, or whether root growth promotion is triggered by other molecular mechanisms acting through other uncharacterized genes in the genome. Furthermore, while root growth promotion was an observed phenotype here, it is possibly not the exclusive interaction occurring between SLBN-177 and the host. For example, the genome of SLBN-177 also contained gene clusters involved in the synthesis of antibiotics, which could inhibit the activity of opportunistic pathogens; and siderophores, which could provide iron to the host as well as trigger induced systemic resistance[43–45].

As extreme climate events become more prevalent, crops will probably experience multiple periods of intermittent drought within a growing season[46] and the ability to quickly recover and prepare for future drought events could be vital for survival. Plants are able to prepare for these future drought events through the development of a 'stress memory,' a series of morphological, molecular and physiological modifications that plants undergo during an initial drought episode that prime a more robust response to subsequent drought events[47,48]. As an extended root phenotype[49], rhizosphere and endosphere communities might also contribute to this stress memory by preserving aspects of their compositional response to drought on rewatering. Our results suggest that a 'memory' of drought is retained in the endospheric root microbiome through the patterns of overall diversity, underdevelopment of late communities and differences in abundances of key taxa, such that plants that have undergone drought stress are distinguishable by microbiome compositions from those that have not. These findings also have implications for strategies to harness microbial communities to confer drought tolerance in field crops. For example, as drought-responsive microorganisms can display compartment-specific recovery trends, identifying taxa that are effective at colonizing the endosphere might be important for sustained protection. Furthermore, in conditions where intermittent drought events are frequent, it would be preferable to select candidates for beneficial taxa from the subset of taxa that persist within the root beyond the drought period and avoid those that rapidly disappear at the end of the drought event.

Methods

Experimental design. All data presented in this study were gathered from two controlled greenhouse experiments and one controlled growth chamber experiment performed at the University of California-Davis. The main study was carried out in the winter/spring of 2018, the complementary study was a small pilot experiment carried out in the summer of 2017 and the growth chamber experiment was carried out in the winter of 2019.

Main experiment. To account for potential thermal gradients previously associated with evaporative cooling systems[50], we defined four experimental blocks covering the area between the cooling pad and the extracting fans installed in our greenhouse. Each block consisted of five plastic containers, each holding 16 potted plants. Watering treatments were assigned to individual plastic containers following the arrangement displayed in Supplementary Fig. 5: each drought treatment (DS1, DS2, DS3) was assigned to four plastic containers while the well-watered control treatment (WC) was assigned to eight plastic containers. The additional WC replicates were used exclusively to train the random forests models. Ten days after seedling transplantation, samples were collected roughly every 10 days (Fig. 1a) for a total of 13 collection time points spanning 136 d. This design resulted in four biological replicates per treatment and collection time point combination.

Complementary experiment. Fifty potted plants were randomly assigned to one of two watering regimes: DS or WC. Samples were collected at the 28-, 350-, 42-, 49- and 56-d marks, encompassing one predrought, three drought and one postdrought time points. This design resulted in five biological replicates per treatment and collection time point combination.

Semisterile phenotyping experiment. One hundred and fifty-six seeds were inoculated with SLBN-177, SLBN-111 or a mock treatment in closed, sterile 75-ml culture tubes with an initial total of 28 WC and 24 DS replicates for each isolate treatment. After 10 d, a 2-week period of drought stress was initiated followed by a week of recovery, at which point the plants were harvested.

Plant growth. Oryza sativa subsp. *japonica* cv. M-206, the most commonly grown rice cultivar in California, was used for all experiments described in this study. Dehulled seeds were treated with a 50% commercial bleach solution (Clorox, final concentration of NaOCl 3.7%) for 5 min followed by five washes with sterile water. Surface-sterilized seeds were plated on Murashige and Skoog agar, and germinated in a growth chamber for 7 d. Individual seedlings were then transplanted to pots holding agricultural soil collected from a rice field in Arbuckle, California (39°0'42.235"N, 121°55'19.632"W). This field had a history of 8 years of rice monoculture before sampling, and chemical analysis on this soil had previously been performed[51] (Supplementary Table 10).

Watering regimes. During non-drought periods, deionized water was added directly to the plastic containers holding the individual potted plants to keep the soil under submergence. Given that the amount of water needed varied throughout the life cycle of rice plants, irrigation was performed ad libitum every other day. Drought was initiated by draining all water from the plastic containers and allowing soils to dry. In the main experiment, DS1, DS2 and DS3 drought treatments started 41 d after transplantation and lasted for 11, 21 and 33 d, respectively (Fig. 1a). In the complementary study, drought started 28 d after transplantation and lasted for 21 d. Similar to the approach used in our previous drought study[8], once plants started exhibiting drought stress symptoms (leaf curling and senescence), enough deionized water (roughly 250 ml) was added to each tub to ensure plants remained alive but under stress (as evidenced by the wilting displayed by plants receiving drought treatments, Supplementary Fig. 1). At the end of the drought period, water was added to the plastic containers to recover the plants.

Gravimetric water content measurements. For each pot collected, soil samples were harvested and placed in 15-ml Falcon tubes. After recording the initial weight, samples were allowed to dry inside a 42 °C oven for 4 months to ensure equal drying across samples collected at different time points. The dry weight of the samples was recorded and the percentage of moisture was calculated.

Isolation of microbes. Bacterial colonies were isolated from rhizosphere and endosphere communities of rice plants derived from a previous study[8]. Briefly, rice plants were grown in three different agricultural soils (including the one used in this experiment) under controlled greenhouse conditions. One-month-old plants were drought stressed for 3 weeks and root systems were harvested. Isolates were then collected by plating both rhizosphere soil and ground root tissue resuspended in sterile PBS on Actinomycete Isolation Agar (Himedia).

Semisterile phenotyping experiment. Glass culture tubes (75 ml) filled with 15 g of wetted calcined clay were autoclaved twice for 1 h with 24 h between autoclave cycles. Dehulled rice seeds were sterilized with a 15-min bleach treatment (3.7% NaOCl), followed by a 5-min ethanol treatment (70% EtOH), followed by five washes with sterile water. Isolates SLBN-177 and SLBN-111 were grown in Luria-Bertani liquid media and diluted in half-strength Murashige and Skoog media with no added sugar to an optical density (OD_{600}) of 0.01. Individual surface-sterilized seeds were placed in each tube and treated with 10 ml of sterile or inoculated Murashige and Skoog medium. Tubes were placed in four trays with seven tubes designated for the WC treatment and six tubes designated for the drought treatment. Plants were grown in sterile conditions for 10 d. After this period, the culture tube lids were removed and drought-treated plants were

allowed to dry out for 14 d, while WC plants were irrigated periodically with sterile water (2–3 d to maintain a water level approximately even with the height of the clay, approximately 2–4 ml per tube). After the drought period, all plants were well watered for a 7-d recovery period. Plants were then harvested, and growth phenotypes (shoot and root length and fresh weight, as well as the number of leaves and roots) measured. Additionally, sections of the roots were washed with sterile water and flash frozen for 16S rRNA gene amplicon sequencing. Tubes with non-germinating seeds or early seedling death (plants that never grew larger than 5 cm) were excluded from the analysis. This resulted in a final replication of 25 and 18 for SLBN-177-treated plants, 20 and 17 for SLBN-111-treated plants, and 18 and nine for control plants for watered and drought conditions, respectively.

Microbiome sample collection, processing and DNA extraction. Root sample collection, compartment processing and DNA extraction were performed as previously described[52]. Briefly, we scooped whole plants outside the pots and shook them vigorously to remove all the soil not firmly attached to the roots. We then collected the 5 cm of root tissue immediately below the shoot–root junction in a 50-ml Falcon tube filled with 15 ml of sterile PBS. Rhizosphere samples were collected by vortexing the roots and collecting 500 μl of the resulting soil suspension in PowerBead tubes (Mo Bio Laboratories). Endosphere samples were collected by washing the roots in fresh PBS to further discard any remaining soil and sonicating them three times (50 to 60 Hz for 30 s). Sonicated roots were placed in PowerBead tubes and homogenized by intense agitation for 1 min (Mini Beadbeater. BioSpec Products). DNA extractions were performed immediately after compartment separation, following the PowerSoil DNA isolation kit (Mo Bio Laboratories) protocol. No negative controls were included during DNA extractions, although the same kit reagents were used when processing samples collected at the same time point. As such, we do not expect microbial contamination to confound comparisons between drought-treated and control samples within individual time points.

16S rRNA gene amplicon library preparation. Library construction followed a previously described dual-indexing strategy[52,53]. For 16S rRNA gene libraries, the V4 region was amplified using the universal primers 515F (GTGCCAGCMGCCGCGGTAA) and 806R (GGACTACHVGGGTWTCTAAT)[53]. No measures were taken to minimize amplification of host chloroplast and mitochondria sequences. Amplification was carried out with the following touchdown PCR program: a first phase consisting of 95 °C for 5 min, followed by seven cycles of 95 °C for 45 s, 65 °C for 1 min (decreasing at 2 °C per cycle) and 72 °C for 90 s, with a second phase consisting of 30 cycles of 95 °C for 45 s, 50 °C for 30 s and 72 °C for 90 s, followed by a final extension at 72 °C for 10 min. All PCR amplifications were performed using the HotStar HiFidelity polymerase kit (Qiagen). After running a 1% agarose gel to verify proper amplification, libraries were cleaned with AmPure XP magnetic beads (Beckman Coulter, Inc.), quantified (Qubit double-stranded DNA HS assay kit, Thermo Fisher Scientific) and pooled in equimolar concentrations. Pooled libraries were then concentrated, gel purified (nucleoscopic gel and PCR cleanup kit, Macherey-Nagel), quality checked (BioAnalyzer HS DNA kit, Agilent Technologies) and submitted for 2- by 250-bp Miseq sequencing (Illumina).

16S rRNA gene amplicon sequence processing. Sequence processing followed a similar workflow as the one implemented in previous studies characterizing the root communities or rice plants[8,11,14]. Briefly, the paired-end reads were demultiplexed with custom scripts (https://github.com/bulksoil/BananaStand) and assembled into single sequences with PANDAseq[54]. Chimeric sequences were then detected and discarded with usearch61 (ref. [55]). OTU clustering at 97% identity was performed with the QIIME[56] implementation of UCLUST[55], using a close reference strategy against the 13_8 release of the Greengenes 16S rRNA gene sequence database[57]. OTUs classified as mitochondria and chloroplast were discarded from the OTU table (except in the semisterile phenotyping experiment), and non-prevalent OTUs (defined as OTUs not present in at least 5% of our samples) were filtered out. On removal of reads classified as mitochondria or chloroplast, 38.3% of endosphere reads and 99.2% of rhizosphere reads were kept. On removal of non-prevalent OTUs, 38.1% of endosphere reads and 98.5% of rhizosphere reads remained. Thus, prevalence filtering removed less than 1% of reads classified as microbial

Reanalysis of published datasets. Data from Santos-Medellin et al.[8] and Liechty et al.[14] (from the same experiment as Edwards et al.[11]) were processed independently as described above, up until clustering. The first dataset included rhizosphere and endosphere profiles derived from four rice cultivars (*Oryza glaberrima* TOg7102 and CG14, and *Oryza sativa* ssp. *indica* IR20 and ssp. *japonica* M-206) grown in agricultural soils from Arbuckle, Biggs and Davis, California. Samples from this study encompassed well-watered and drought-stressed plants collected at the end of a 21-day drought treatment. The second dataset consisted of rhizosphere and endosphere profiles associated with two rice cultivars (*Oryza sativa* Sabine and the commercial cultivar CLXL745) grown in an agricultural field in Arkansas. Samples from this study spanned eight time points collected every 2 weeks throughout the life cycle of rice plants. Processed sequences from all

41

studies (including the ones derived from this work) were concatenated and OTU clustering was performed following the same parameters as described above.

Genome sequencing. SLBN-177 was grown in liquid Luria-Bertani for 24 h and DNA was extracted with a Qiagen Blood and Tissue kit. DNA sequencing was done in the laboratory of B. Weimer (UC Davis) as part of the 100K Pathogen Genome Project[58] as previously described[59]. Approximately 600 ng of purified genomic DNA was used to construct a sequencing library using the KAPA HyperPlus library preparation kit (Roche Diagnostics). Library size distribution verification was done on Caliper LabChip GX (Perkin Elmer) and library quantification was done with the KAPA Library Quantification Kit (Roche Diagnostics). Pooled libraries were sequenced on the Illumina HiSeq X Ten using a PE150 protocol. Reads were trimmed with Trimmomatic[60], assembled with SPAdes[61] and annotated with prokka[62], all with default settings. Contigs shorter than 1,000 bp or with an average coverage less than 20× were excluded. KEGG Ontology terms were extracted from the prokka output using the script Prokka2KEGG (https://github.com/SilentGene/Bio-py/tree/master/prokka2kegg). Secondary metabolite biosynthesis gene clusters were identified using antiSMASH[63].

Statistical analyses. All analyses were conducted in the R Environment v.3.5.1 (ref. [64]). For beta-diversity analyses, we used phyloseq[65] to calculate weighted UniFrac distances[66] on OTU counts normalized via variance-stabilizing transformation[67,68] using the prebuilt '97_otu.tree' phylogeny included in the Greengenes database[57]. We carried out unconstrained principal coordinate analysis using the pcoa() function from the ape package[69]. PerMANOVA analyses were performed with the adonis() function implemented in the vegan package[70]. For all PerMANOVA tests, permutations were constrained to each experimental block (Supplementary Fig. 5), using the strata argument. For alpha-diversity analyses, we used vegan to calculate the Shannon index on OTU counts normalized via variance-stabilizing transformation. All plots were generated with ggplot2 (ref. [71]).

Linear mixed models. Linear mixed models were implemented with the lmerTest package[72] to assess the effect of the experimental factors on percentage of soil moisture, community composition (as captured by the first principal coordinate) and microbiome age. In all models, watering treatment, collection time point and their interaction were treated as fixed effects, while experimental blocks (Supplementary Fig. 5) were treated as random effects. Within each time point, pairwise contrasts comparing individual drought treatments (DS1, DS2 and DS3) against WCs were performed using the emmeans package[73]. False discovery rate (Benjamini–Hochberg procedure) was used to correct for multiple testings. Similarly, in the semisterile experiment, watering treatment and isolate inoculation were treated as fixed effects and 'tray' was treated as a random effect. Games–Howell P value adjustment was used to determine post hoc contrast significance using the rstatix package[74]. Compact letter display was determined with the multcompLetters() function from the multcompView package[75].

Differential abundance testing. The DESeq2 package[67,68] was used to implement negative binomial generalized models to test the effect of experimental factors on the abundance of individual OTUs. The models included watering treatment, collection time point and their interaction as fixed effects. Within each time point, pairwise Wald tests were performed to compare individual drought treatments (DS1, DS2 and DS3) against WCs. For each contrast, effect size shrinkage was performed using the lfcShrink() function. To account for multiple testings within and across contrasts, all comparisons performed within each compartment were pooled together before using false discovery rate (Benjamini–Hochberg procedure) to adjust P values. Groups of differentially abundant OTUs with similar drought responses were identified by performing hierarchical clustering (Ward's algorithm) on shrunken log fold changes with the hclust() function[64]. Finally, an additional taxonomic classification was performed by recovering the representative sequences of each differentially abundant OTU and comparing their V4 region against the SILVA database (132 release)[76] via the UCLUST taxonomy assigner[55]. These alternative taxonomic assignments are provided in Supplementary Table 4 as a complement to the Greengenes-based classification used for all the analyses in this study.

Random forest models. The randomForest package[77] was used to develop random forest models for each compartment following an approach previously used to characterize the age of rice plants as a function of root-associated microbiome composition[11]. Briefly, a training dataset consisting of 52 rhizosphere and 52 endosphere profiles derived from an additional batch of well-watered plants (WC_TRN in Supplementary Fig. 5) was used to generate full random forest models by regressing the relative abundances of individual OTUs against the chronologic age of rice plants. To estimate the optimal number of age-discriminant OTUs needed to perform accurate predictions, we first used the importance() function to rank individual OTUs on the basis of their contribution to the accuracy of the models. We then used the rfcv() function to perform a tenfold cross-validation that evaluated model performance as a function of the number of top-age-discriminant OTUs included in the model. This approach revealed that optimal performance was achieved when models included the top 65 age-discriminant OTUs (Extended

Data Fig. 7a). Therefore, the top 65 OTUs identified in each compartment were used to train compartment-specific sparse models that were then applied to a validating dataset encompassing the rest of well-watered WC samples not used to train the models. Finally, these sparse models were applied to DS samples to estimate the microbiome ages before, during and after drought.

To calculate the relative microbiome maturity of drought-stressed plants, we adapted an approach previously used to study the effect of malnourishment on gut microbiome succession of infants during early development[78]. First, for each compartment, we used the validating dataset of WC plants to fit a loess curve between host chronological age and the microbiome age predicted by our sparse models (Extended Data Fig. 10a). These curves served as baselines of microbiome development during the life cycle of well-watered rice plants. Relative microbiome maturity was then estimated by calculating the difference between the predicted microbiome age of each drought-stressed plant and the baseline microbiome age of well-watered plants of the same chronological age (Extended Data Fig. 10b,c).

Reporting Summary. Further information on research design is available in the Nature Research Reporting Summary linked to this article.

Data availability

Raw reads have been deposited in the Sequene Read Archive under BioProject PRJNA551661. The SLBN-177 sequence has been deposited within the 100K Project BioProject PRJNA743693 with accession number SRR15049341. The Greengenes database (v.13_8) can be downloaded from http://qiime.org/home_static/dataFiles.html. The SILVA database (v.132) can be downloaded from https://www.arb-silva.de/download/archive/qiime/.

Code availability

All scripts and intermediate files are available in GitHub (https://github.com/cmsantosm/RiceDroughtRecovery).

References

1. Lesk, C., Rowhani, P. & Ramankutty, N. Influence of extreme weather disasters on global crop production. *Nature* **529**, 84–87 (2016).
2. Zhang, J. et al. Effect of drought on agronomic traits of rice and wheat: a meta-analysis. *Int. J. Environ. Res. Public Health* **15**, 839 (2018).
3. Hirasawa, T., in *Genetic Improvement of Rice for Water-Limited Environments* (eds Ito, O, O'Toole, J. C. & Hardy, B.) 89–98 (International Rice Research Institute, 1999).
4. Pandey, V. & Shukla, A. Acclimation and tolerance strategies of rice under drought stress. *Rice Sci.* **22**, 147–161 (2015).
5. Compant, S., van der Heijden, M. G. A. & Sessitsch, A. Climate change effects on beneficial plant-microorganism interactions. *FEMS Microbiol. Ecol.* **73**, 197–214 (2010).
6. de Vries, F. T., Griffiths, R. I., Knight, C. G., Nicolitch, O. & Williams, A. Harnessing rhizosphere microbiomes for drought-resilient crop production. *Science* **368**, 270–274 (2020).
7. Busby, P. E. et al. Research priorities for harnessing plant microbiomes in sustainable agriculture. *PLoS Biol.* **15**, e2001793 (2017).
8. Santos-Medellín, C., Edwards, J., Liechty, Z., Nguyen, B. & Sundaresan, V. Drought stress results in a compartment-specific restructuring of the rice root-associated microbiomes. *mBio* **8**, e00764-17 (2017).
9. Naylor, D., DeGraaf, S., Purdom, E. & Coleman-Derr, D. Drought and host selection influence bacterial community dynamics in the grass root microbiome. *ISME J.* https://doi.org/10.1038/ismej.2017.118 (2017).
10. Fitzpatrick, C. R. et al. Assembly and ecological function of the root microbiome across angiosperm plant species. *Proc. Natl Acad. Sci. USA* https://doi.org/10.1073/pnas.1717617115 (2018).
11. Edwards, J. A. et al. Compositional shifts in root-associated bacterial and archaeal microbiota track the plant life cycle in field-grown rice. *PLoS Biol.* **16**, e2003862 (2018).
12. Zhang, J. et al. Root microbiota shift in rice correlates with resident time in the field and developmental stage. *Sci. China Life Sci.* **61**, 613–621 (2018).
13. Xu, L. et al. Drought delays development of the sorghum root microbiome and enriches for monoderm bacteria. *Proc. Natl Acad. Sci. USA* **115**, E4284–E4293 (2018).
14. Liechty, Z. et al. Comparative analysis of root microbiomes of rice cultivars with high and low methane emissions reveals differences in abundance of methanogenic archaea and putative upstream fermenters. *mSystems* **5**, e00897-19 (2020).
15. Rong, X. & Huang, Y. Taxonomic evaluation of the *Streptomyces griseus* clade using multilocus sequence analysis and DNA–DNA hybridization, with proposal to combine 29 species and three subspecies as 11 genomic species. *Int. J. Syst. Evol. Microbiol.* **60**, 696–703 (2010).

16. Lin, L. & Xu, X. Indole-3-acetic acid production by endophytic *Streptomyces* sp. En-1 isolated from medicinal plants. *Curr. Microbiol.* **67**, 209–217 (2013).

17. Legault, G. S., Lerat, S., Nicolas, P. & Beaulieu, C. Tryptophan regulates thaxtomin A and indole-3-acetic acid production in Streptomyces scabiei and modifies its interactions with radish seedlings. *Phytopathology* **101**, 1045–1051 (2011).

18. Guo, J. et al. Seed-borne, endospheric and rhizospheric core microbiota as predictor for plant functional traits across rice cultivars are dominated by deterministic processes. *New Phytol.* https://doi.org/10.1111/nph.17297 (2021).

19. de Vries, F. T. et al. Soil bacterial networks are less stable under drought than fungal networks. *Nat. Commun.* **9**, 3033 (2018).

20. de Vries, F. T. & Shade, A. Controls on soil microbial community stability under climate change. *Front. Microbiol.* **4**, 265 (2013).

21. Borken, W. & Matzner, E. Reappraisal of drying and wetting effects on C and N mineralization and fluxes in soils. *Glob. Change Biol.* **15**, 808–824 (2009).

22. Lueders, T. & Friedrich, M. W. Effects of amendment with ferrihydrite and gypsum on the structure and activity of methanogenic populations in rice field soil. *Appl. Environ. Microbiol.* **68**, 2484–2494 (2002).

23. Linquist, B. A. et al. Reducing greenhouse gas emissions, water use, and grain arsenic levels in rice systems. *Glob. Change Biol.* **21**, 407–417 (2015).

24. Speirs, L. B. M., Rice, D. T. F., Petrovski, S. & Seviour, R. J. The phylogeny, biodiversity, and ecology of the chloroflexi in activated sludge. *Front. Microbiol.* **10**, 2015 (2019).

25. Thomas, S. H. et al. The mosaic genome of *Anaeromyxobacter dehalogenans* strain 2CP-C suggests an aerobic common ancestor to the delta-proteobacteria. *PLoS ONE* **3**, e2103 (2008).

26. Yang, T. H., Coppi, M. V., Lovley, D. R. & Sun, J. Metabolic response of *Geobacter sulfurreducens* towards electron donor/acceptor variation. *Microb. Cell Fact.* **9**, 90 (2010).

27. Keller, K. L. & Wall, J. D. Genetics and molecular biology of the electron flow for sulfate respiration in desulfovibrio. *Front. Microbiol.* **2**, 135 (2011).

28. Zhalnina, K. et al. Dynamic root exudate chemistry and microbial substrate preferences drive patterns in rhizosphere microbial community assembly. *Nat. Microbiol.* https://doi.org/10.1038/s41564-018-0129-3 (2018).

29. Williams, A. & de Vries, F. T. Plant root exudation under drought: implications for ecosystem functioning. *New Phytol.* **225**, 1899–1905 (2020).

30. Vries, F. T. et al. Changes in root-exudate-induced respiration reveal a novel mechanism through which drought affects ecosystem carbon cycling. *New Phytol.* **224**, 132–145 (2019).

31. Casartelli, A. et al. Exploring traditional aus-type rice for metabolites conferring drought tolerance. *Rice* **11**, 9 (2018).

32. Pérez-Jaramillo, J. E. et al. Linking rhizosphere microbiome composition of wild and domesticated *Phaseolus vulgaris* to genotypic and root phenotypic traits. *ISME J.* https://doi.org/10.1038/ismej.2017.85 (2017).

33. Kang, D.-J. & Futakuchi, K. Effect of moderate drought-stress on flowering time of interspecific hybrid progenies (*Oryza sativa* L. × *Oryza glaberrima* Steud.). *J. Crop Sci. Biotechnol.* **22**, 75–81 (2019).

34. Guo, X. et al. Host-associated quantitative abundance profiling reveals the microbial load variation of root microbiome. *Plant Commun.* **1**, 100003 (2020).

35. Varoquaux, N. et al. Transcriptomic analysis of field-droughted sorghum from seedling to maturity reveals biotic and metabolic responses. *Proc. Natl Acad. Sci. USA* https://doi.org/10.1073/pnas.1907500116 (2019).

36. Li, P. et al. Physiological and transcriptome analyses reveal short-term responses and formation of memory under drought stress in rice. *Front. Genet.* **10**, 55 (2019).

37. Vandenkoornhuyse, P., Quaiser, A., Duhamel, M., Le Van, A. & Dufresne, A. The importance of the microbiome of the plant holobiont. *New Phytol.* **206**, 1196–1206 (2015).

38. Toju, H. et al. Core microbiomes for sustainable agroecosystems. *Nat. Plants* **4**, 247–257 (2018).

39. Shade, A. & Stopnisek, N. Abundance-occupancy distributions to prioritize plant core microbiome membership. *Curr. Opin. Microbiol.* **49**, 50–58 (2019).

40. Suralta, R. R. et al. Plasticity in nodal root elongation through the hardpan triggered by rewatering during soil moisture fluctuation stress in rice. *Sci. Rep.* **8**, 4341 (2018).

41. Hamedi, J. & Mohammadipanah, F. Biotechnological application and taxonomical distribution of plant growth promoting actinobacteria. *J. Ind. Microbiol. Biotechnol.* **42**, 157–171 (2015).

42. Vurukonda, S. S. K. P., Vardharajula, S., Shrivastava, M. & SkZ, A. Enhancement of drought stress tolerance in crops by plant growth promoting rhizobacteria. *Microbiol. Res.* **184**, 13–24 (2015).

43. Aznar, A. & Dellagi, A. New insights into the role of siderophores as triggers of plant immunity: what can we learn from animals? *J. Exp. Bot.* **66**, 3001–3010 (2015).

44. Viaene, T., Langendries, S., Beirinckx, S., Maes, M. & Goormachtig, S. Streptomyces as a plant's best friend? *FEMS Microbiol. Ecol.* https://doi.org/10.1093/femsec/fiw119 (2016).

45. Meena, K. K. et al. Abiotic stress responses and microbe-mediated mitigation in plants: the omics strategies. *Front. Plant Sci.* **8**, 172 (2017).

46. Mukamuhirwa, A. et al. Effect of intermittent drought on grain yield and quality of rice (*Oryza sativa* L.) grown in Rwanda. *J. Agro Crop Sci.* **206**, 252–262 (2020).

47. Fleta-Soriano, E. & Munné-Bosch, S. Stress memory and the inevitable effects of drought: a physiological perspective. *Front. Plant Sci.* **7**, 143 (2016).

48. Ding, Y., Fromm, M. & Avramova, Z. Multiple exposures to drought 'train' transcriptional responses in *Arabidopsis*. *Nat. Commun.* **3**, 740 (2012).

49. de la Fuente Cantó, C. et al. An extended root phenotype: the rhizosphere, its formation and impacts on plant fitness. *Plant J.* **103**, 951–964 (2020).

50. Kittas, C., Bartzanas, T. & Jaffrin, A. Temperature gradients in a partially shaded large greenhouse equipped with evaporative cooling pads. *Biosyst. Eng.* **85**, 87–94 (2003).

51. Edwards, J. et al. Soil domestication by rice cultivation results in plant–soil feedback through shifts in soil microbiota. *Genome Biol.* **20**, 221 (2019).

52. Edwards, J., Santos-Medellín, C. & Sundaresan, V. Extraction and 16S rRNA sequence analysis of microbiomes associated with rice roots. *Bio. Protoc.* **8**, e2884 (2018).

53. Caporaso, J. G. et al. Global patterns of 16S rRNA diversity at a depth of millions of sequences per sample. *Proc. Natl Acad. Sci. USA* **108**, 4516–4522 (2011).

54. Masella, A. P., Bartram, A. K., Truszkowski, J. M., Brown, D. G. & Neufeld, J. D. PANDAseq: paired-end assembler for illumina sequences. *BMC Bioinform.* **13**, 31 (2012).

55. Edgar, R. C. Search and clustering orders of magnitude faster than BLAST. *Bioinformatics* **26**, 2460–2461 (2010).

56. Caporaso, J. G. et al. QIIME allows analysis of high-throughput community sequencing data. *Nat. Methods* **7**, 335–336 (2010).

57. DeSantis, T. Z. et al. Greengenes, a chimera-checked 16S rRNA gene database and workbench compatible with ARB. *Appl. Environ. Microbiol.* **72**, 5069–5072 (2006).

58. Weimer, B. C. 100K Pathogen Genome Project. *Genome Announc.* **5**, e00594-17 (2017).

59. Kong, N. et al. Draft genome sequences of 1,183 Salmonella strains from the 100K Pathogen Genome Project. *Genome Announc.* **5**, e00518–17 (2017).

60. Bolger, A. M., Lohse, M. & Usadel, B. Trimmomatic: a flexible trimmer for Illumina sequence data. *Bioinformatics* **30**, 2114–2120 (2014).

61. Bankevich, A. et al. SPAdes: a new genome assembly algorithm and its applications to single-cell sequencing. *J. Comput. Biol.* **19**, 455–477 (2012).

62. Seemann, T. Prokka: rapid prokaryotic genome annotation. *Bioinformatics* **30**, 2068–2069 (2014).

63. Medema, M. H. et al. antiSMASH: rapid identification, annotation and analysis of secondary metabolite biosynthesis gene clusters in bacterial and fungal genome sequences. *Nucleic Acids Res.* **39**, W339–W346 (2011).

64. R Core Team. *R: A Language and Environment for Statistical Computing* (R Foundation for Statistical Computing, 2018); https://www.R-project.org/

65. McMurdie, P. J. & Holmes, S. phyloseq: an R package for reproducible interactive analysis and graphics of microbiome census data. *PLoS ONE* **8**, e61217 (2013).

66. Lozupone, C. & Knight, R. UniFrac: a new phylogenetic method for comparing microbial communities. *Appl. Environ. Microbiol.* **71**, 8228–8235 (2005).

67. Love, M. I., Huber, W. & Anders, S. Moderated estimation of fold change and dispersion for RNA-seq data with DESeq2. *Genome Biol.* **15**, 550 (2014).

68. McMurdie, P. J. & Holmes, S. Waste not, want not: why rarefying microbiome data is inadmissible. *PLoS Comput. Biol.* **10**, e1003531 (2014).

69. Paradis, E., Claude, J. & Strimmer, K. APE: analyses of phylogenetics and evolution in R language. *Bioinformatics* **20**, 289–290 (2004).

70. Oksanen, J. et al. vegan: Community Ecology Package (2018).

71. Wickham, H. *ggplot2: Elegant Graphics for Data Analysis* (Springer-Verlag, 2016).

72. Kuznetsova, A., Brockhoff, P. B. & Christensen, R. H. B. lmerTest package: tests in linear mixed effects models. *J. Stat. Softw.* **82**, 13 (2017).

73. Lenth, R., Singmann, H., Love, J., Buerkner, P. & Herve, M. Emmeans: estimated marginal means, aka least-squares means. R package v.1, 3 (R Foundation for Statistical Computing, 2018).

74. Kassambara, A. Rstatix: pipe-friendly framework for basic statistical tests. R package v.0.6.0 (R Foundation for Statistical Computing, 2020).

75. Graves, S., Piepho, H.-P., Selzer, L. & Dorai-Raj, S. multcompView: visualizations of paired comparisons. R package v.0.1-7 (R Foundation for Statistical Computing, 2015).

76. Quast, C. et al. The SILVA ribosomal RNA gene database project: improved data processing and web-based tools. *Nucleic Acids Res.* **41**, D590–D596 (2013).

77. Liaw, A. & Wiener, M. Classification and regression by randomForest. *R. News* **2**, 18–22 (2002).

78. Subramanian, S. et al. Persistent gut microbiota immaturity in malnourished Bangladeshi children. *Nature* **510**, 417–421 (2014).

43

Author contributions

C.S.-M., Z.L. and V.S. conceptualized the study. C.S.M., Z.L., J.E. and B.N. performed the experiments. B.H. and B.C.W. generated the SLBN-177 genome sequence and reviewed the paper. C.S.-M. and Z.L. analysed the data. C.S.-M., Z.L., J.E. and V.S. wrote the paper.

Competing interests

The authors declare no competing interests.

Additional information

Extended data is available for this paper at https://doi.org/10.1038/s41477-021-00967-1.

Supplementary information The online version contains supplementary material available at https://doi.org/10.1038/s41477-021-00967-1.

Correspondence and requests for materials should be addressed to V.S.

Peer review information *Nature Plants* thanks Alex Williams, Maggie Wagner and the other, anonymous, reviewer(s) for their contribution to the peer review of this work.

Reprints and permissions information is available at www.nature.com/reprints.

Publisher's note Springer Nature remains neutral with regard to jurisdictional claims in published maps and institutional affiliations.
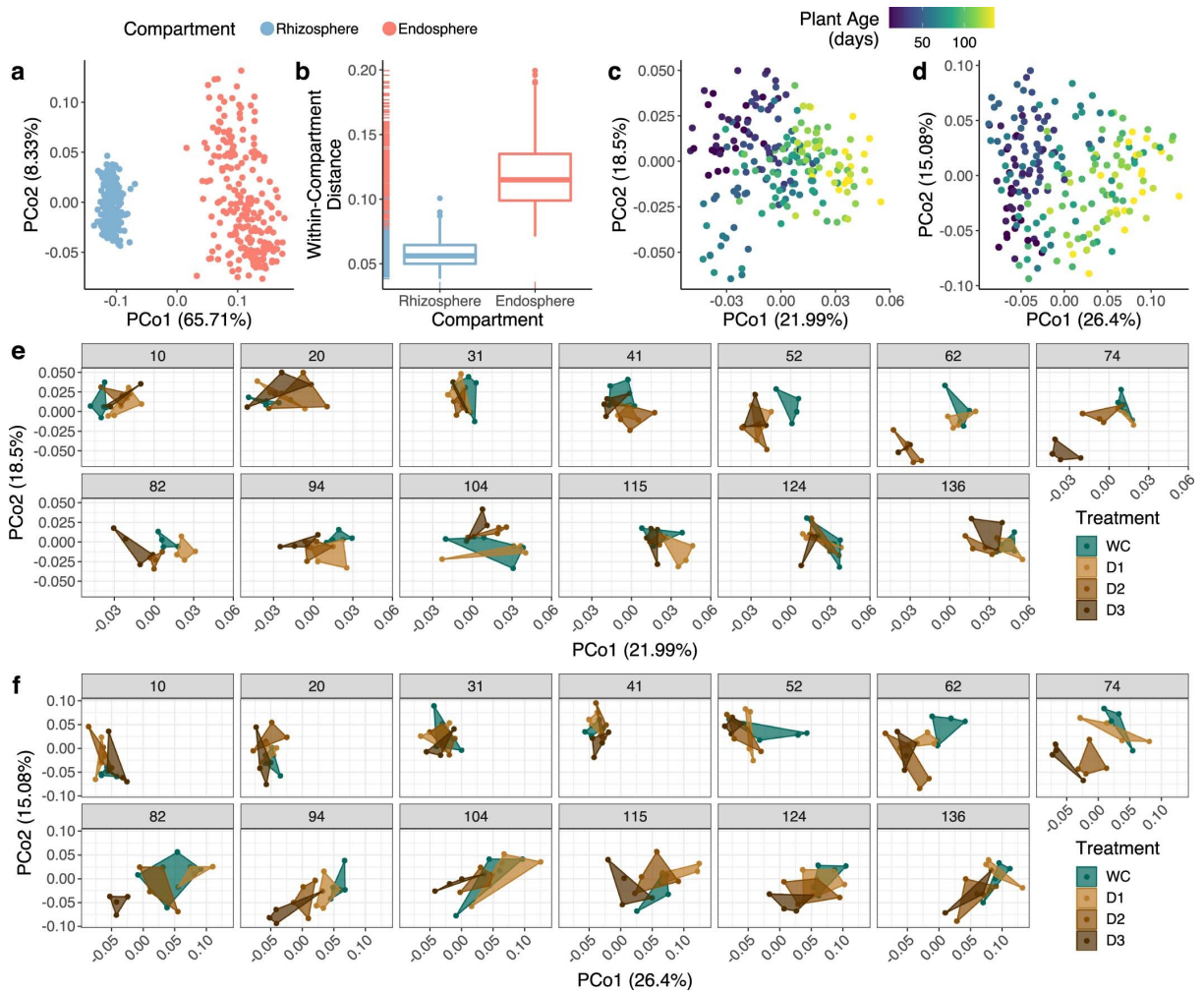
Extended Data Figure 1 Compartments harbor compositionally distinct microbial communities. **a**, Principal coordinates analysis (PCoA) performed on weighted UniFrac distances across the whole dataset. Colours indicate compartment. **b**, Distribution of rhizosphere and endosphere within-group distances, that is distances between samples within each treatment and time point combination. The large variation displayed by endospheres in panels **a** and **b** is, in part, a result of the strong effect that drought treatments had on this compartment. **c-f**, PCoA performed on the rhizosphere (**c** & **e**) and endosphere (**d** & **f**) subsets. In panels **c** and **d**, colours indicate plant age. In panels **e** and **f**, data points are faceted by plant age and coloured by drought treatment.
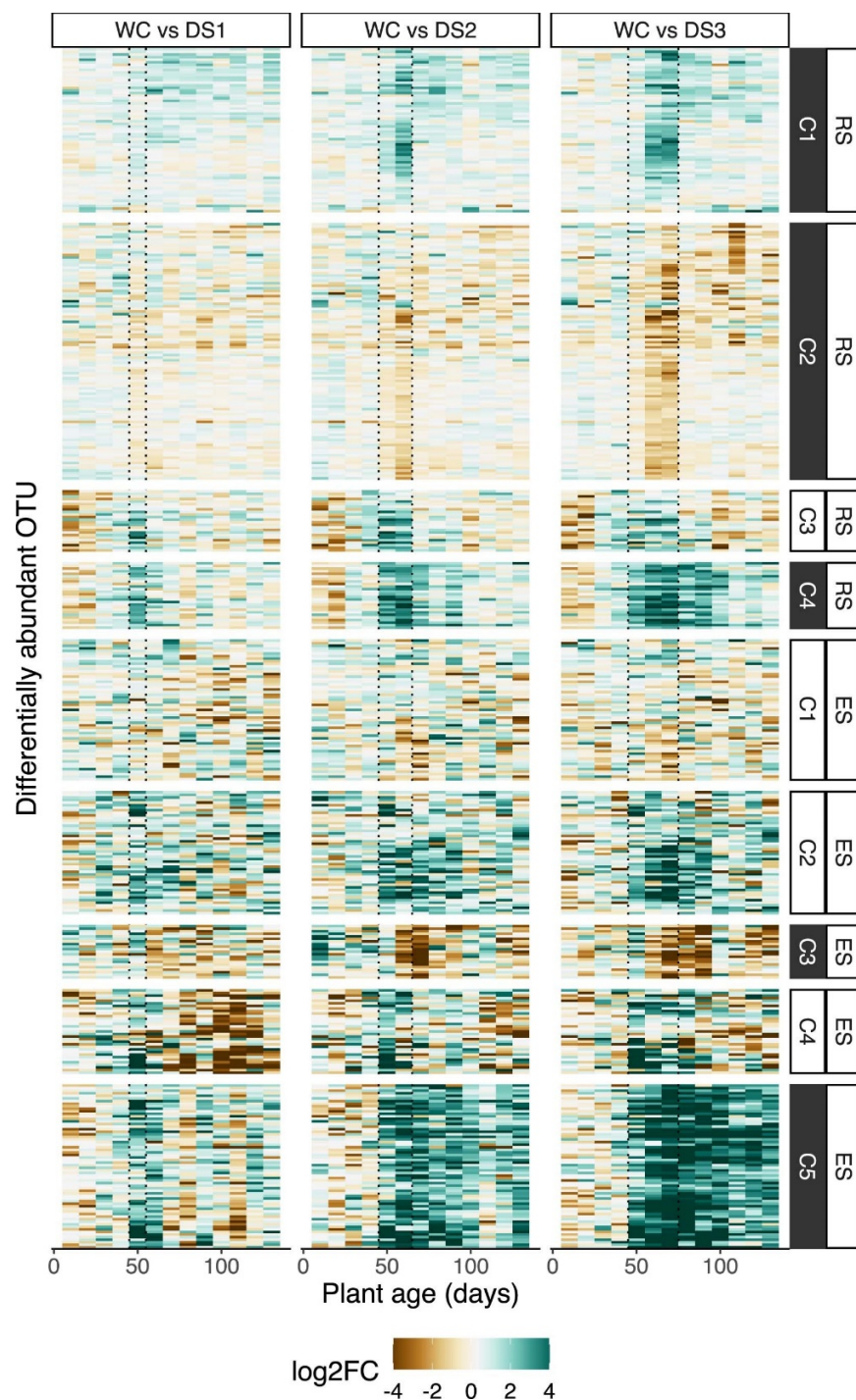
Extended Data Figure 2 Complete set of drought-responsive OTUs. Heatmap displaying the log2 fold-changes between water controls and drought treatments: depletion under drought tends towards green while enrichment under drought tends toward brown. Each row represents a differentially abundant OTU detected as significant (Wald test, FDR < 0.05) in at least one pairwise comparison. Horizontal facets indicate each of the modules detected through hierarchical clustering in the rhizosphere (RS) and endosphere (ES). Clusters shown in Fig. 2b are highlighted in black. Vertical dotted lines delimit the periods of suspended irrigation for each of the drought treatments.

Taxonomy	Rhizosphere			Endosphere	
	Persistent depletion	Transient depletion	Transient enrichment	Persistent depletion	Semipersistent enrichment
Spirochaetes / Spirochaetes / Spirochaetales				2	
Proteobacteria / Gammaproteobacteria / Xanthomonadales			2		
Proteobacteria / Deltaproteobacteria / Myxococcales	5	12	4	14	
Proteobacteria / Deltaproteobacteria / Desulfuromonadales	6			3	
Proteobacteria / Deltaproteobacteria / Desulfovibrionales				2	
Proteobacteria / Betaproteobacteria / Rhodocyclales	7			19	
Proteobacteria / Betaproteobacteria / MND1		6			
Proteobacteria / Betaproteobacteria / Burkholderiales		5	6	3	
Proteobacteria / Alphaproteobacteria / Rhodospirillales			3		
Proteobacteria / Alphaproteobacteria / Rhizobiales			4		
Nitrospirae / Nitrospira / Nitrospirales		3			
Gemmatimonadetes / Gemmatimonadetes / unclassified			4		
Gemmatimonadetes / Gemmatimonadetes / Gemmatimonadales			12		
Gemmatimonadetes / Gemm-1 / unclassified		4			
Firmicutes / Clostridia / Clostridiales				3	
Firmicutes / Bacilli / Bacillales			2		
Fibrobacteres / TG3 / TG3-1				2	
Chloroflexi / Chloroflexi / [Roseiflexales]			5		
Bacteroidetes / Bacteroidia / Bacteroidales				3	
Bacteroidetes / [Saprospirae] / [Saprospirales]			4		
Armatimonadetes / Chthonomonadetes / SJA-22			2		
Actinobacteria / Thermoleophilia / Solirubrobacterales			11		
Actinobacteria / Thermoleophilia / Gaiellales			5		
Actinobacteria / Actinobacteria / Actinomycetales			22	3	18
Acidobacteria / iii1-8 / DS-18			2		
Acidobacteria / Holophagae / Holophagales				2	
Acidobacteria / Acidobacteriia / Acidobacteriales		8			
Acidobacteria / Acidobacteria-6 / iii1-15		10			
Acidobacteria / Acidobacteria-6 / CCU21				2	

Trend

Extended Data Figure 3 Modules of drought responsive OTUs exhibit a strong taxonomic signature. Classification of the differentially abundant OTUs in each of the distinct drought modules detected through hierarchical clustering. Each tile indicates the number of classified OTUs in a particular module, while the colour represents membership to a specific Phylum / Proteobacteria class. Orders with only one representative have been excluded to ease visualization.

47
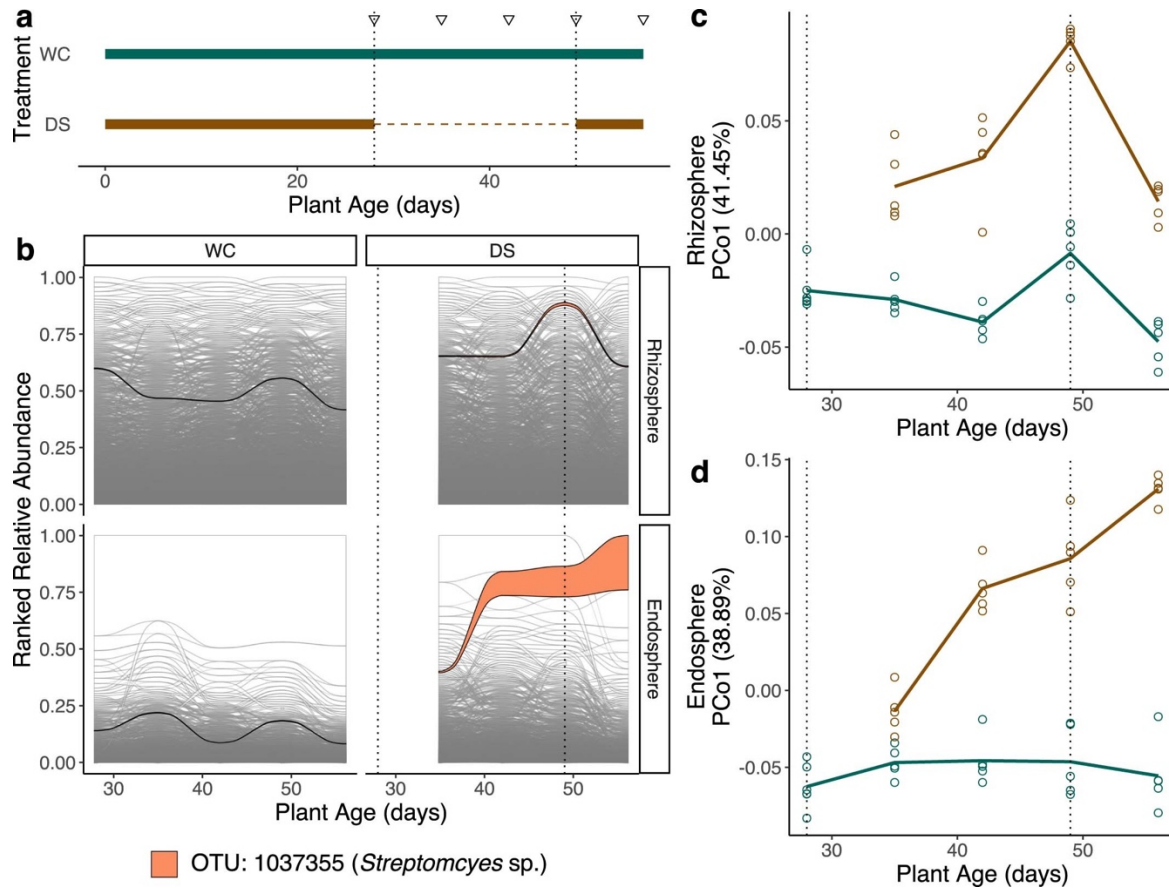
Extended Data Figure 4 OTU 1037355 displays reproducible trends in an independent experiment. a, Timeline of the watering regimes followed by control (WC) and drought-stressed (DS) plants. Horizontal lines represent the watering status during the experiment: solid segments indicate periods of constant irrigation while dotted segments indicate periods of suspended irrigation. Upside down triangles mark each of 5 collection time points. **b**, Ranked relative abundances of individual community members throughout time. Each ribbon represents a single OTU in the community: for each time point, width indicates its relative abundance while the position across the *y* axis indicates its rank within the community. The most abundant member of the semipersistent enrichment module, Streptomyces sp. (OTU ID: 1037355), is highlighted. In all panels, the vertical dotted lines delimit the periods of suspended irrigation in each of the drought treatments. **c,d**, Beta-diversity patterns in the rhizosphere (**c**) and endosphere (**d**) communities. In both cases, the *y* axis displays the position of each sample across the first principal coordinate (PCo) from a weighted UniFrac PCo analysis and the *x* axis displays the age of the plant at the moment of sample collection. In all panels, the vertical dotted lines delimit the periods of suspended irrigation for the drought treatment.
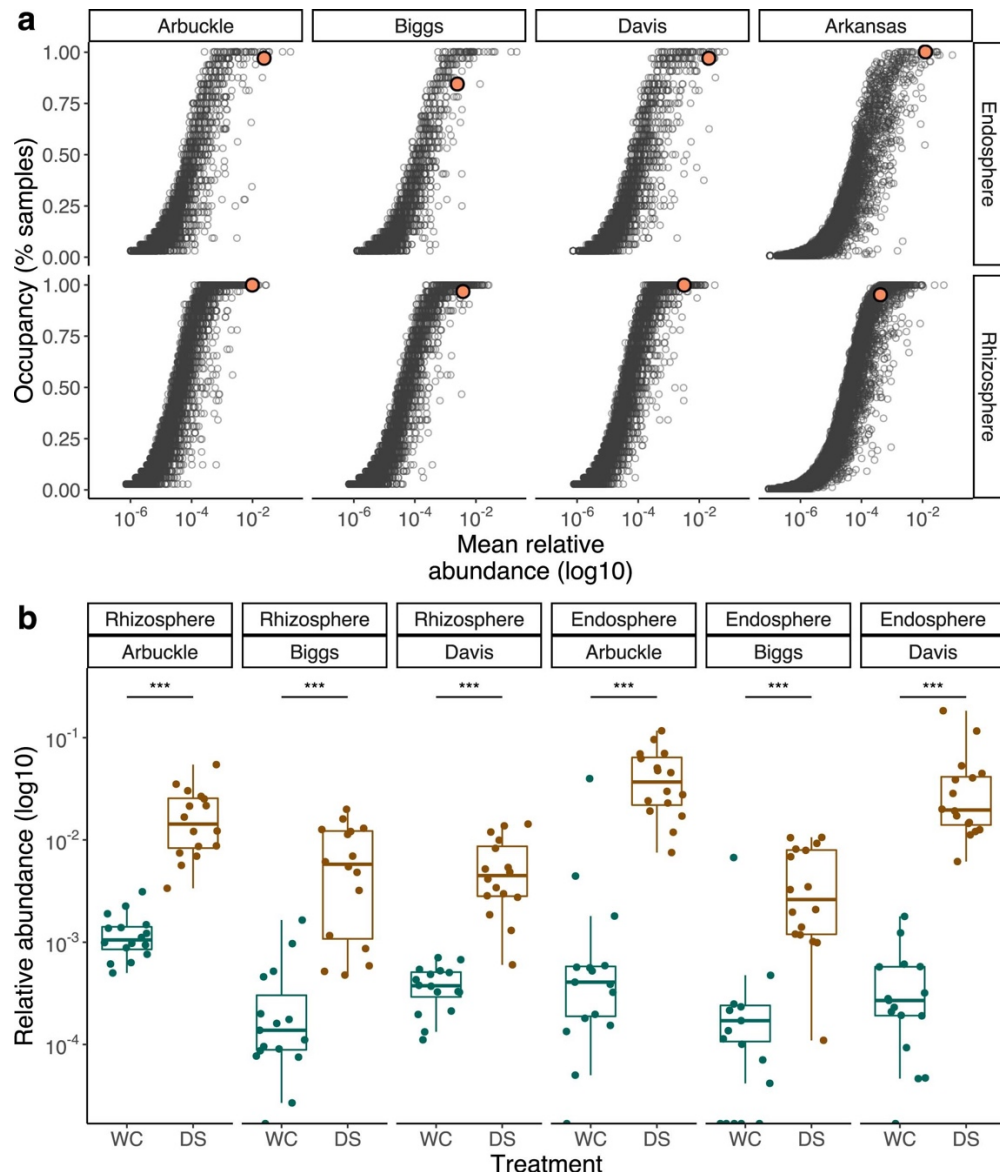
Extended Data Figure 5 OTU 1037355 is highly occurring and displays a significant drought enrichment across compositionally distinct soils. a, Occupancy-abundance curves for rhizosphere and endosphere communities of rice plants grown in three California soils (Arbuckle, Biggs, and Davis), and one Arkansas field. The *x* axis displays the log-transformed mean relative abundance of each OTU while the *y* axis displays the percent of samples in which each OTU was detected. OTU 1037355 is highlighted in orange. **b**, Relative abundance of OTU 1037355 in rhizosphere and endosphere communities of 49-day-old rice plants grown under well irrigated (WC) or drought-stressed (DS) conditions. Asterisks on top indicate a significant difference ($P_{FDR} < 0.001$) between WC and DS treatments. Statistical significance was determined by negative binomial generalized linear models and pairwise Wald tests (two-sided) corrected with the Benjamini-Hochberg procedure.
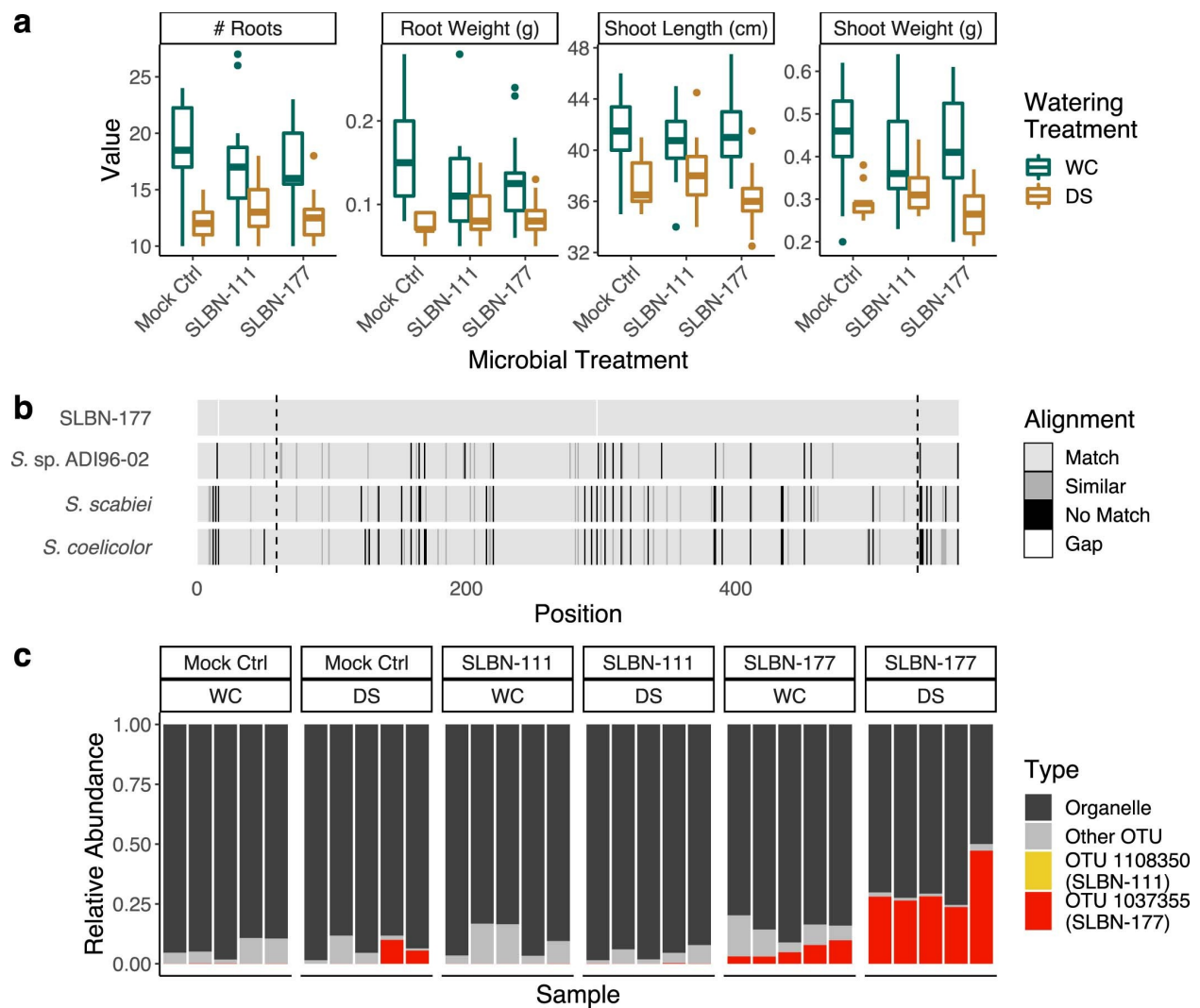
Extended Data Figure 6 Other phenotypic traits were not impacted by Streptomyces sp. SLBN-177. a, Distribution of measured plant phenotypes (number of roots, root weight, shoot weight, and shoot length) across microbial treatments and watering regimes. **b**, Protein alignment of putative *iaaM* genes from SLBN-177, *S. coelicolor*, *S. scabiei*, and *S.* sp ADI96-02 (refs. [16,17]). Black lines indicate an amino acid mismatch with a negative score on the BLOSUM62 matrix, and dark grey bars represent a mismatch with a positive score. The vertical black dashed lines indicate the bounds of the amino oxidase functional domain. **c**, Relative abundances of inoculated isolates in the endospheres of rice plants. Reads identified as mitochondria or chloroplast (collapsed as organellar reads and represented in black) were not discarded in order to measure the degree of colonization. Reads classified as OTUs other than 1037355 (SLBN-177) and 1108350 (SLBN-111) were collapsed and are represented in gray.
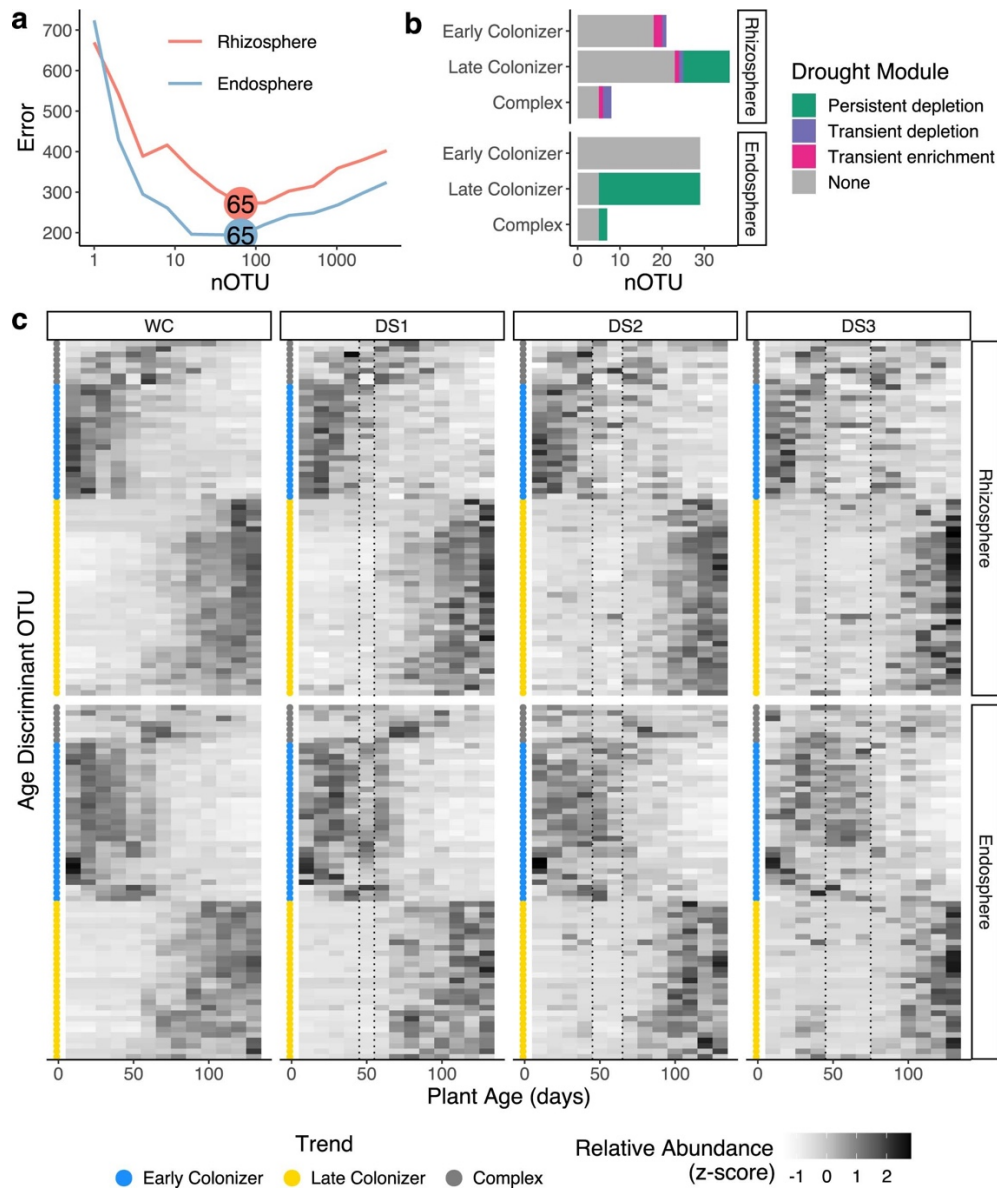
Extended Data Figure 7 Random forests can identify age discriminant OTUs. a, Cross validation error as a function of the number of OTUs used in each model. For both compartments, the lowest error was detected when using the 65 most important taxa. **b**, Overlap between the age-discriminant OTUs and the drought-responsive OTUs detected in each module (Fig. 2b). **c**, Hierarchical clustering of the relative abundances of the age-discriminant OTUs. The heatmap displays the z-transformed mean relative abundances of each OTU across drought treatments and time points. The colours at the left end of each vertical facet indicate the longitudinal trends exhibited by each taxa. In all panels, the vertical dotted lines delimit the periods of suspended irrigation for the drought treatment.
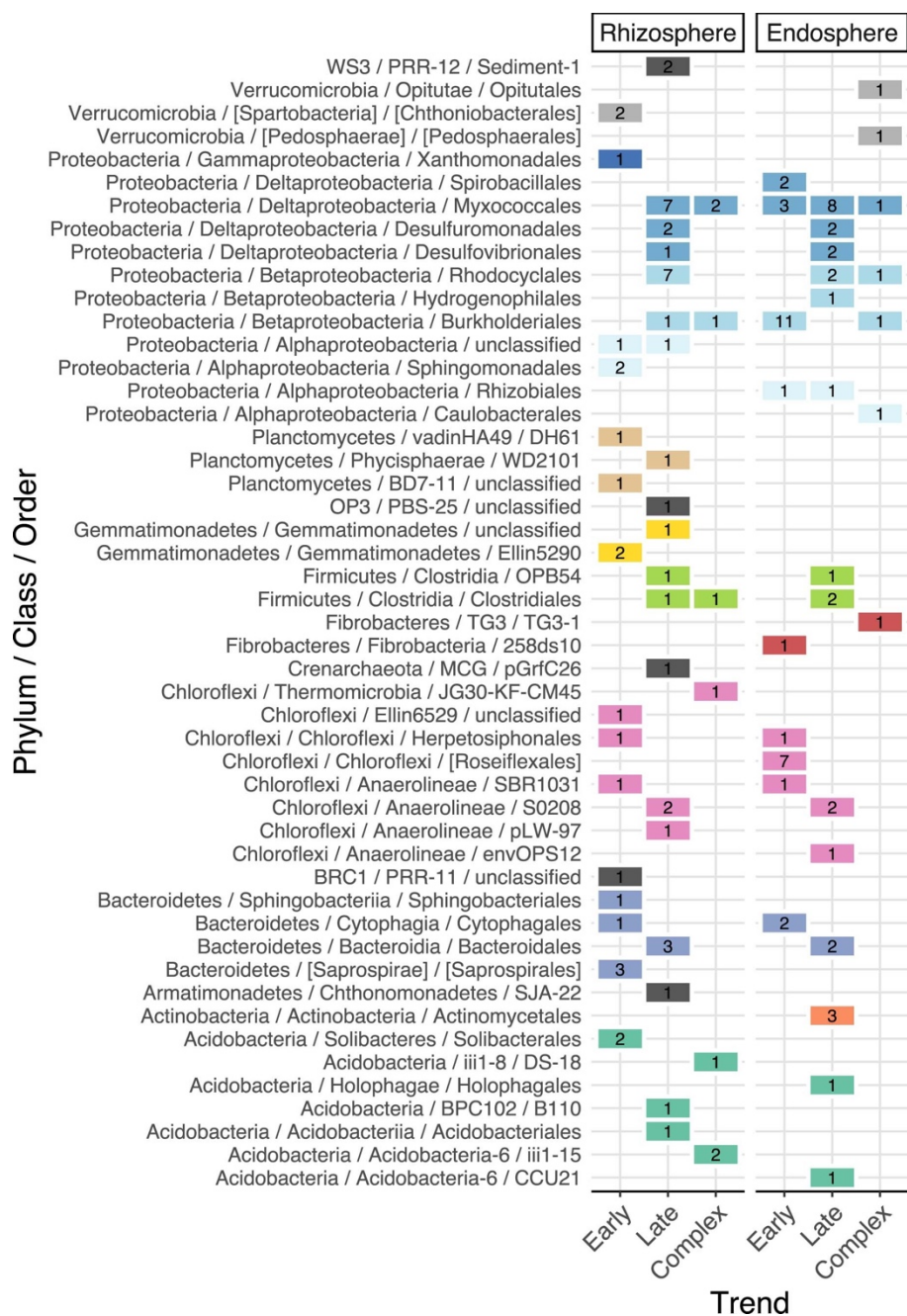
Extended Data Figure 8 Taxonomic classification of the age-discriminant OTUs in each of the longitudinal trends. Each tile indicates the number of classified OTUs in a particular module, while the colour represents membership to a specific Phylum / Proteobacteria class.
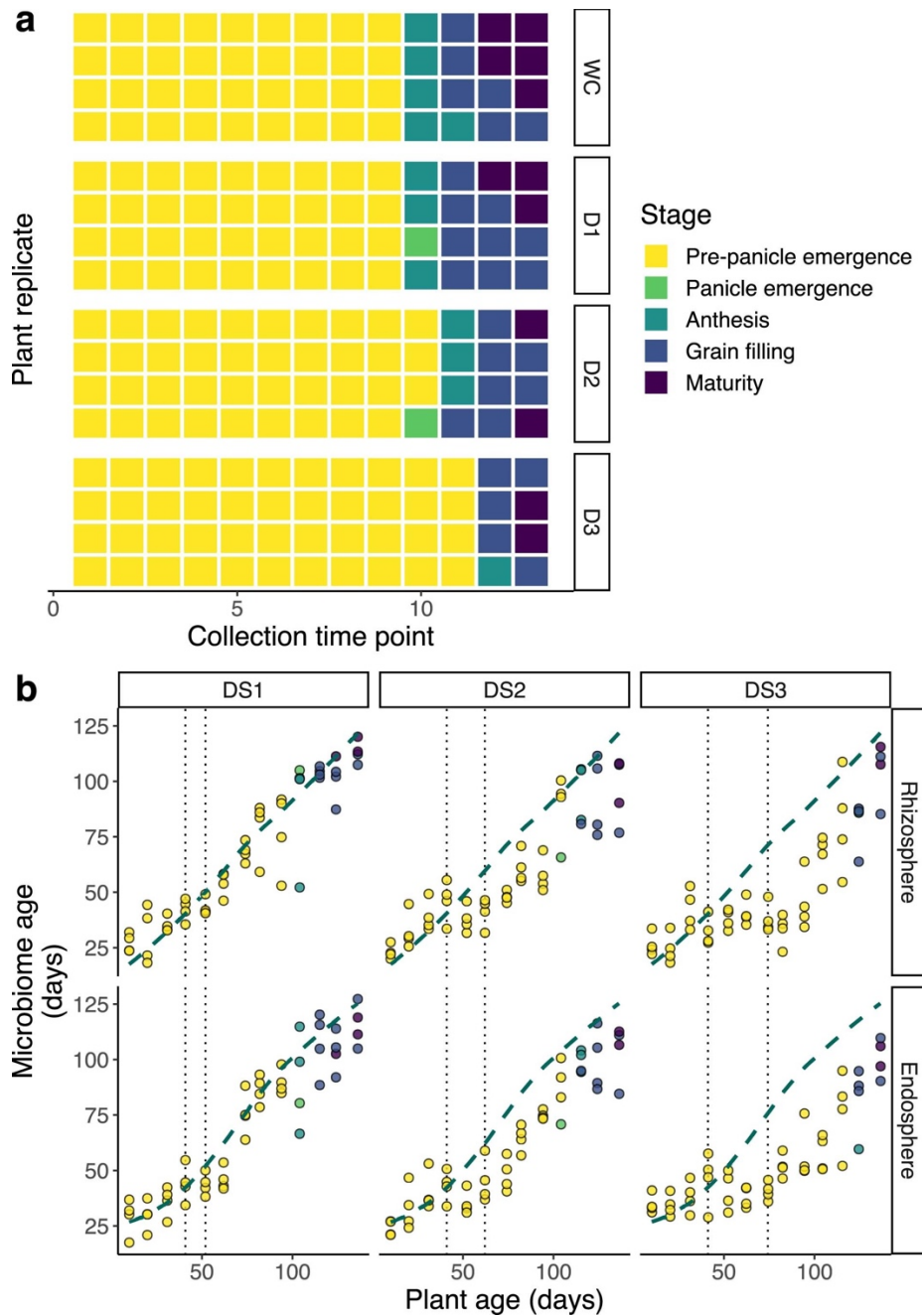
Extended Data Figure 9 Drought stress delayed transition to flowering. a, Developmental growth stages of well-watered and drought-stressed rice plants through the experiment. Photos of each sample were taken at each time point and defined as either pre-panicle emergence (no portion of the panicle visible), panicle emergence (panicle partially emerged from flag leaf), anthesis (panicle fully emerged and anthers visible), grain filling (panicles bent over instead of standing upright), or maturity (flower colour appears yellow). **b**, Developmental growth stage and microbiome age predictions of rhizosphere and endosphere communities across drought treatments (D1, D2, and D3). The dashed curve represents the baseline microbiome development under well-irrigated conditions and was calculated by fitting a loess curve between the predicted microbiome age and the chronological plant age in the control (WC) test set.
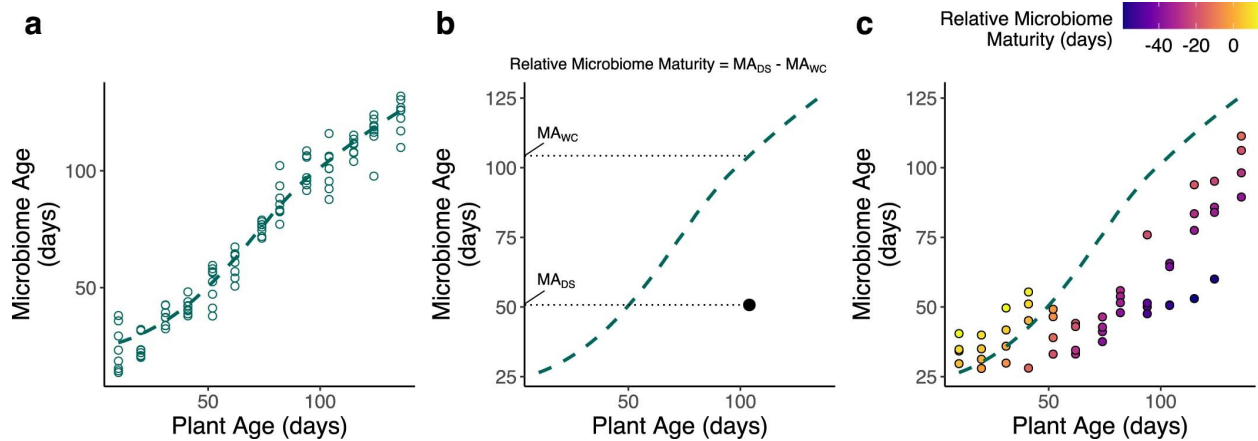
Extended Data Figure 10 Calculation of relative microbiome maturity of drought-stressed samples. a, After applying the sparse random forest models to the validating set of well-watered plants, a loess curve (dashed green line) was fit between host chronological age (*x* axis) and microbiome predicted age (*y* axis). **b**, Using the fitted loess curve as a baseline of microbiome development, relative microbiome maturity was estimated by calculating the difference between the predicted microbiome age of an individual sample and the corresponding baseline microbiome age of well-watered plants. **c**, Using the approach described in B, relative microbiome maturity was calculated for all drought-stressed samples.
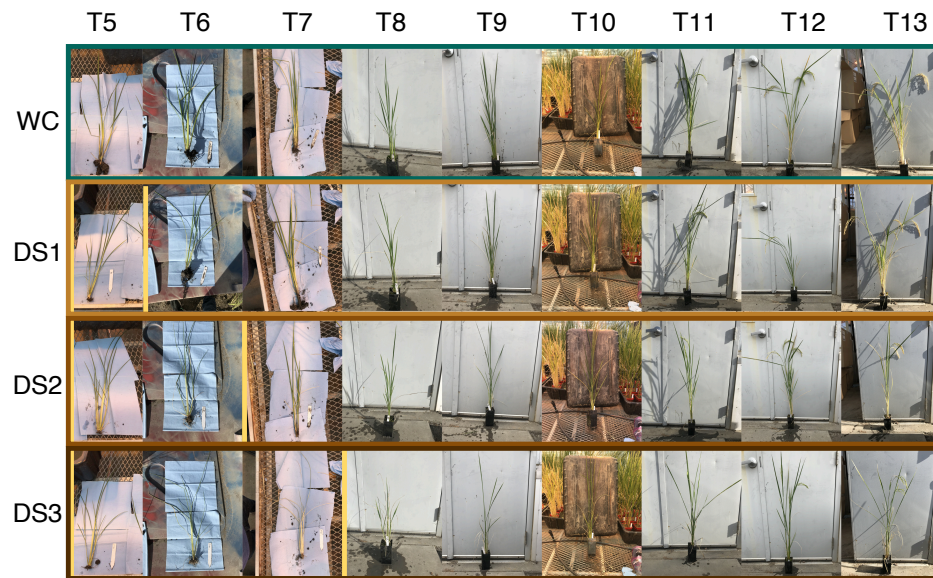
Supplementary Figure 1.
Plant status throughout the experiment. Representative set of plants across all watering treatments during and after drought. Yellow vertical lines indicate the drought period for each treatment. In all cases, drought-stressed plants survived and resumed their development during recovery.
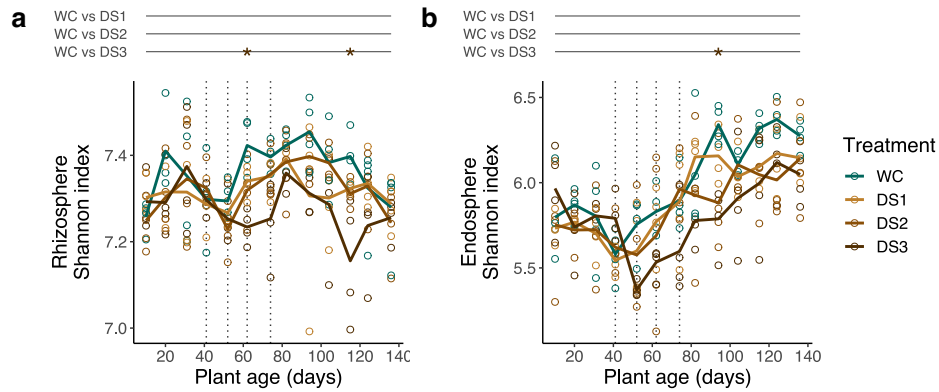
Supplementary Figure 2.
Alpha diversity trends across treatments. Alpha diversity trends the rhizosphere **(a)** and endosphere **(b)** communities. In both cases, the y-axis displays the Shannon index of each sample and the x-axis displays the age of the plant at the moment of sample collection. Trend lines represent the mean values for each treatment throughout the experiment. Asterisks on top indicate a significant difference ($P_{FDR} < 0.05$, Benjamini-Hochberg correction) between the control and each of the drought treatments at a specific time point. Statistical significance was determined by ANOVA and pairwise contrasts (two-sided) corrected with the Benjamini-Hochberg procedure. Supplementary Table 2 contains the effect sizes, standard errors, and P-values for all pairwise contrasts.
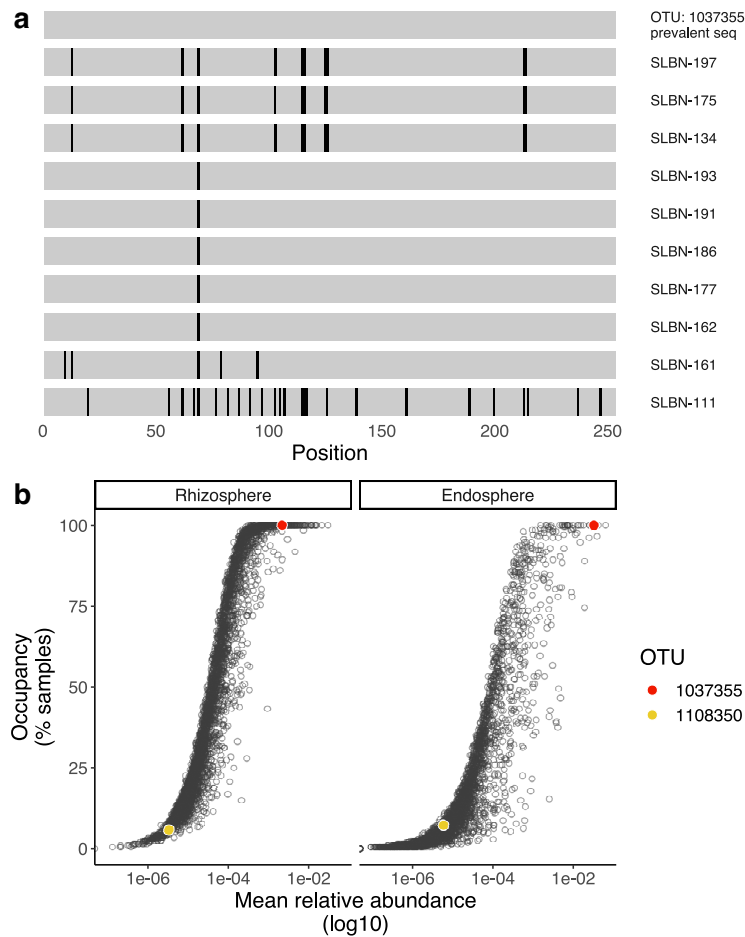
Supplementary Figure 3.
***Streptomyces* sp. SLBN-177 clusters with OTU 1037355**. **(a)** Sequence similarity along the V4 region of the 16S rRNA gene. The upper band represents the most abundant sequence of OTU 1037355 detected in the main drought experiment while the rest of the bands represent individual isolates collected from rice roots. Black lines indicate single nucleotide polymorphisms relative to OTU 1037355. All isolates highlighted in red cluster with OTU 1037355 at a 97% identity, while the isolate highlighted in yellow clusters with OTU 1108350. **(b)** Occupancy-abundance curves for the rhizosphere and endosphere communities. The x-axis displays the log-transformed mean relative abundance of each OTU while the y-axis displays the percent of samples in which each OTU was detected. OTU 1037355 and 1108350 are highlighted.

57
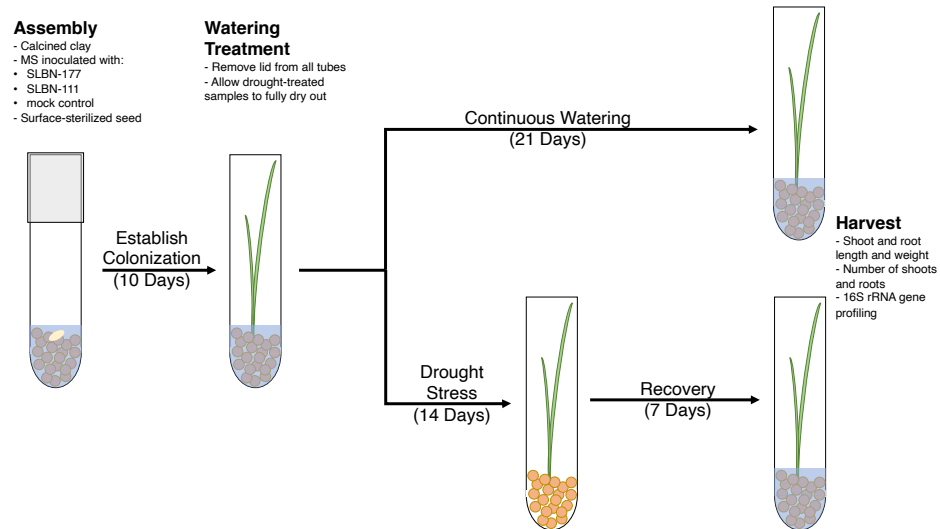
Supplementary Figure 4.
Experimental setup for the phenotyping experiment. Calcined clay, inoculum, and a surface sterilized seed were placed in 75 ml glass culture tubes, and were grown axenically for 10 days, followed by growth in an open system under drought or well-watered conditions. This diagram corresponds to the timeline in Figure 4a and depicts an example tube under each condition at each stage of the experiment.
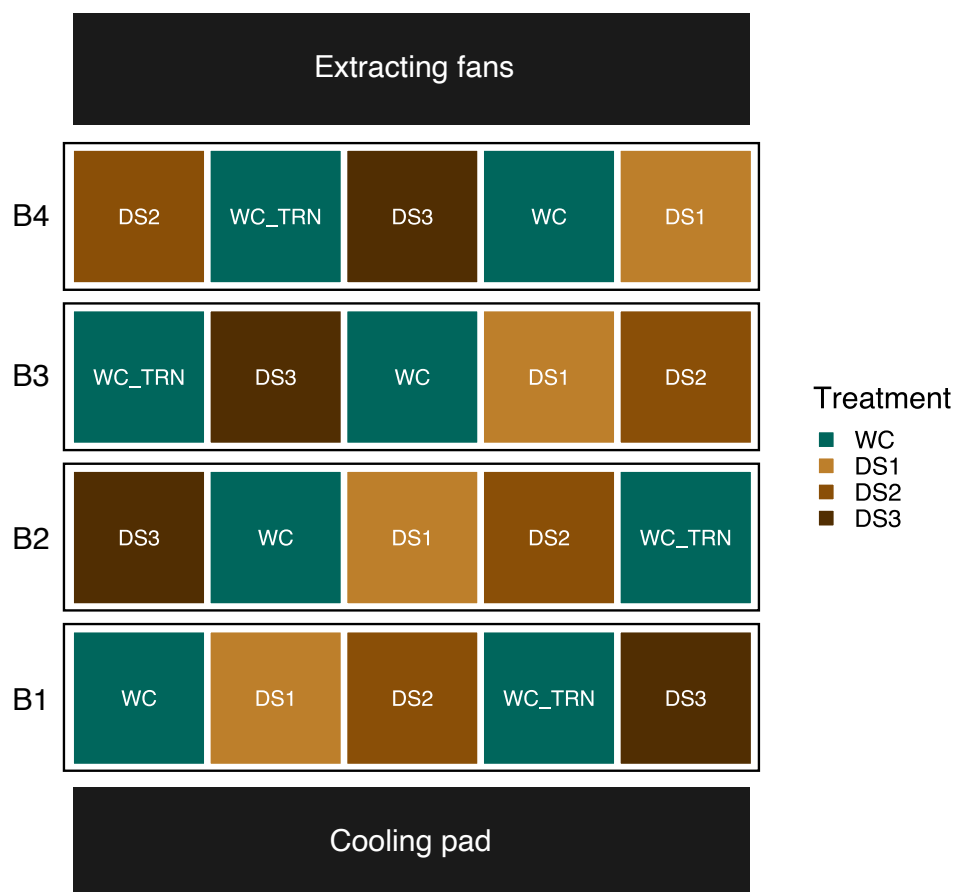
Supplementary Figure 5.
Experimental design for the main drought experiment. Spatial distribution of experimental treatments in the main greenhouse experiment. Watering treatments were assigned to plastic containers (colored boxes), each holding 16 individual potted plants. WC_TRN refers to the well-watered samples that were used to train the random forest models. Black outlines delineate 4 experimental blocks spanning the area between the cooling pad and extracting fans installed in the greenhouse.

Chapter 3

Genome-resolved metagenomics reveals metabolic responses of the rice microbiome to nitrogen fertilizer

Zachary Liechty[1], Ryan Melnyk[1,2], Christian Santos-Medellín[1,3], Esteban Veliz[1], and Venkatesan Sundaresan[1,4]

[1]Department of Plant Biology, University of California, Davis, Davis, CA, USA.
[2]Pivot Bio, Berkely, CA, USA.
[3]Department of Plant Sciences, University of California, Davis, Davis, CA, USA.
[4]Department of Plant Pathology, University of California, Davis, Davis, CA, USA.

Abstract

Nitrogen is a limiting nutrient in rice paddy soil and optimizing fertilizer use is necessary to avoid waste and environmental harm. A key factor in understanding the nitrogen cycle is the microbiome, which can nitrify, denitrify, and fix nitrogen from the environment, thus altering the available forms of nitrogen for the plant. Nitrogen fertilizer in rice paddies can lead to the emission of the greenhouse gasses nitrous oxide and methane. Many studies have investigated the effects of nitrogen on methane emissions, though the results are often conflicting: some studies demonstrate an increase in methane emissions with the addition of fertilizer while others demonstrate a decrease. One possible explanation for these various results is that soils from different geographic locations harbor unique microbial communities, and the addition of nitrogen could affect these communities and functions in a soil-dependent fashion. The unique impacts on different taxa or functions could then subsequently impact the syntrophic relationships with and production of precursor molecules for methanogenesis. To investigate this possibility, we grew rice in three different soils originating from different rice paddies across northern California and

tested the effect of urea fertilizer on the root associated microbiomes. We identified both shared and soil-specific responses among the fertilizer-affected taxa. We further profiled the shifting abundances of microbial functions in the rhizosphere samples of a single soil through shotgun metagenomics and found that the high nitrogen treatment samples had a greater abundance of genes associated with methanogenesis pathways, fermentation pathways that produce methanogenic precursor molecules, and phenolic degradation pathways that produce the precursor molecules for the fermentation pathways. These results shed light on how urea fertilizer affects nitrogen and carbon cycling in rice-associated microbiomes.

Author Contributions

This study was conceptualized by ZL, RM, and VS. RM setup the experiment, and ZL harvested samples and took phenotypic measurements with the assistance of CS-M and EV. ZL extracted DNA, sequenced the 16S region, and analyzed the data. ZL and CS-M processed reads and assembled the metagenome into contigs, and ZL was responsible for binning contigs into MAGs, and all downstream analysis.

Introduction

Rice is a staple crop for over half of the world population[1], and optimizing yields is necessary to meet future demands[2]. Nitrogen is often the most limiting nutrient in rice paddy soil[3], and the addition of nitrogen fertilizer robustly increases yield[4]. However, optimizing nitrogen use is necessary, as overfertilization is ecologically harmful. Over fertilization in rice paddies can lead to pollution of nearby bodies of water through runoff and leaching[5–7], and nitrification of fertilizer leads to the production of nitrous oxide, a potent greenhouse gas with 273 times the global warming potential of carbon dioxide[8]. Over fertilization leads to exponential growth in the rate of nitrous oxide emissions[2], demonstrating the importance of optimizing fertilizer application. Understanding the factors affecting the assimilation of

nitrogen fertilizer by rice is necessary in order to increase yields while mitigating the environmental costs of the application of nitrogen fertilizer. The assimilation of nitrogen in rice is mediated by root-associated microbes as they can nitrify, denitrify, and fix nitrogen, altering the availability of nitrogen for the host[3,9], so it is necessary to understand how microbes are affecting and influenced by nitrogen fertilization in order to optimize fertilizer use.

Nitrogen application can also directly or indirectly affect the rate of emissions of another microbially-produced greenhouse gas, methane. Methane has a global warming potential 27 times higher than carbon dioxide[8], and is produced to a higher degree than nitrous oxide in rice paddies[10]. Methanogenic archaea produce methane from carbon sources originating from the rice plant[11]. Up to 60% of the methane produced by methanogens can also be oxidized by methanotrophs[12]. Methane emissions can be directly impacted by nitrogen fertilizers by either positively stimulating the activity of methanotrophs, or negatively by causing competition between methane and ammonia as substrates for methane monooxygenase, the key enzyme in methane oxidation[13,14]. Fertilizer can indirectly affect methane emissions by increasing root exudation in rice, thus providing a greater carbon pool available to methanogens[15]. Increased fertilization is associated with more methane originating from carbon from the plant rather than soil organic matter, further demonstrating the link between nitrogen fertilizer, exudation, and methane[16]. Many studies have investigated the overall effect of fertilizer on methane emissions, and have found conflicting results, with some studies showing a positive correlation, and others a negative correlation between application rate and methane emissions[17], demonstrating that a variety of factors likely contribute to this relationship.

One factor that could affect the differences in observed methane emissions and nitrogen cycling processes is variation in the initial microbial community structure. Studies of rice associated microbiomes have demonstrated that the soil source is a major factor in determining community composition[18–21]. These studies have shown that soil communities can respond to stimuli in a soil specific manner[19] and that differences in soil communities can also affect plant phenotypes[20]. Further consideration must also be given to the spatial aspect of the microbiome, as community functions likely vary significantly between

62

the semi-anaerobic rhizosphere (soil directly surrounding the root) and the aerobic endosphere (root interior). In this study, we fertilized rice plants grown in three agricultural soils with three different treatments of urea to determine to what degree responses of rhizosphere and endosphere communities were soil specific or universal. We further profile the full metagenome of rhizosphere samples from one of the soils through genome-resolved metagenomics to determine microbial functions affected by nitrogen fertilizer. Our results demonstrate that responses to urea are largely soil-specific, though general trends are identified in the Gammaproteobacteria and Actinobacteria. Furthermore, we find that the addition of nitrogen increased the abundances of pathways and genes associated with aromatic compound degradation, fermentation, and methanogenesis. These results further elucidate how urea fertilizer affects the interactions of the microbiome and its host.

Results

Experimental Design and Treatment effects on plant phenotype

To characterize the effects of urea fertilizer on the rice microbiome, we grew rice (*Oryza sativa* subsp. *japonica* cv. *Kitaake*) in 3 different California paddy soils originating from Arbuckle, Biggs, and Davis, California in a greenhouse, and exposed them to one of three nitrogen treatments: no added urea (no N), low addition of urea (low N) and a high addition of urea (high N) applied before transplanting seedlings (see methods). The "no N" plants began to show signs of nitrogen stress (reduced growth and yellow-colored leaves) after 36 days post transplantation, and samples were harvested after 50 days post transplantation. For each plant, we profiled the endosphere and rhizosphere associated bacterial and archaeal communities through high-throughput amplicon sequencing of the V4 region of the 16S ribosomal RNA gene. Amplicon sequence variants (ASVs) corresponding to plant organellar reads, as well as ASVs not present in more than 5% of samples were removed, resulting in 2221 ASVs, with a mean sequencing depth of 21,335 reads.

The height, shoot weight, number of tillers, and leaf color were measured in all plants before sampling the microbiome. ANOVA demonstrated that the height, weight, number of tillers, and some color aspects (the R and G values of the RGB color spectrum, as well as lightness and hue) were affected by the nitrogen treatment (Figure 1, Figure S1, Table S1). Investigating the contrasts demonstrated that the number of tillers and weight increased in both nitrogen treatments across all soils, and the height increased in both treatments in the Biggs and Arbuckle samples and in the high N treatment in the Davis samples (Table S2). The R and G components of the RGB color value were similarly decreased in both treatments in Arbuckle and Biggs, and in the high N treatment in Davis (Table S2). A greater value of both R and G is indicative of more yellow coloring, which is indicative of nitrogen stress[22]. The hue was significantly increased in the Biggs samples with added nitrogen, further indicating a shift from yellow to green colors, and lightness was reduced in all comparisons to the high N treatment (Table S2).

Figure 1
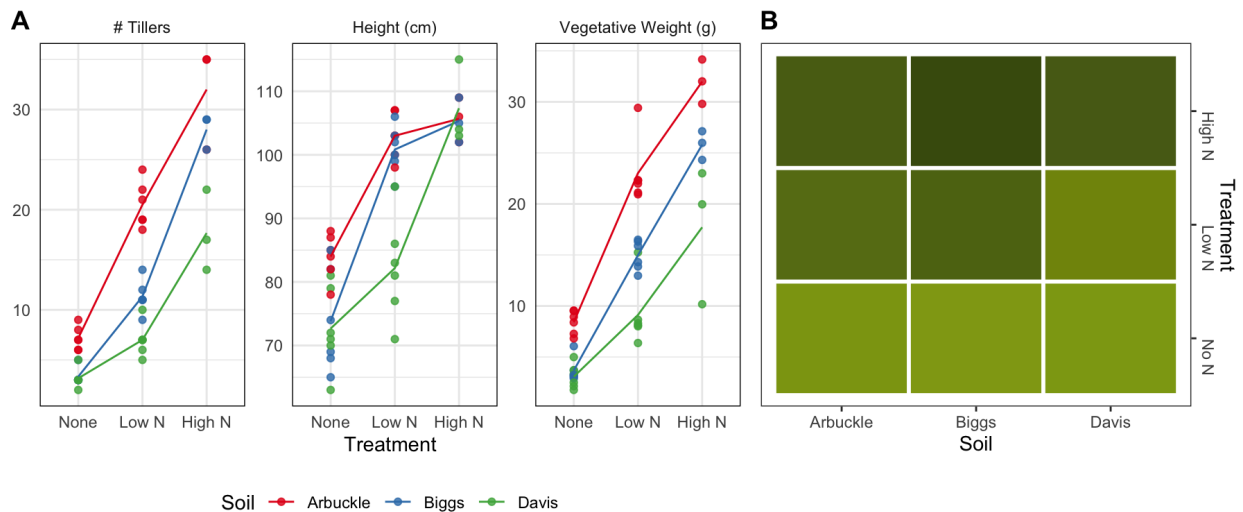Phenotypic responses to nitrogen fertilizer of plants grown in three agricultural soils. (A) The number of Tillers, height, and weight of plants grown in each condition. Colors represent the soils. Dots represent individual samples and the line represents the average. (B) Average leaf color of plants grown in each treatment combination. The columns correspond to each soil and each row corresponds to a nitrogen treatment.

Diversity patterns reveal soil-specific and soil-independent responses of the microbiome to urea at the phylum and ASV levels

Permutational multivariate analysis of variance (PERMANOVA) on Bray-Curtis dissimilarities demonstrated that the microbial composition was significantly affected by soil, compartment, and nitrogen level, as well as all second level interactions of the listed factors (Table 1). PERMANOVA ran on samples separated by compartment further demonstrated that nitrogen level significantly altered microbial composition in the endosphere and rhizosphere samples, but not the bulk soil samples (Table S3). The samples grown in Davis soil harbored a more divergent community compared to the Arbuckle and Biggs grown samples, as demonstrated by principal coordinate analysis (Figure 2A). Constrained analysis of principal coordinates with the data conditioned on soil shows a gradient response to the level of nitrogen in both the rhizosphere and endosphere samples, but not the bulk soil samples (Figure 2B), demonstrating that microbial response to nitrogen is dependent on host association.

Phyla-level analysis further revealed differences between soils and nitrogen treatments (Figure 2C). Of particular note is the Myxococcota in the endosphere of Arbuckle-grown samples compared to Biggs- and Davis-grown endospheres. To identify significant responses to nitrogen fertilizer at the phyla level, beta regression was performed within each soil and compartment, with no N, low N, and high N assigned the numbers 0, 0.5, and 1 respectively (Figure 2D). This analysis revealed similar patterns between the soil, with a significant increased relative abundance (with increasing N) of Gammaproteobacteria in both the rhizosphere and endosphere samples with all soils, as well as a significant decrease in Actinobacteria in the endospheres with all soils. Other phyla had varying responses, such as Verrucomicrobiota in the endosphere, which was not significantly affected in Arbuckle, significantly decreased in relative abundance in Biggs, and significantly increased in Davis.
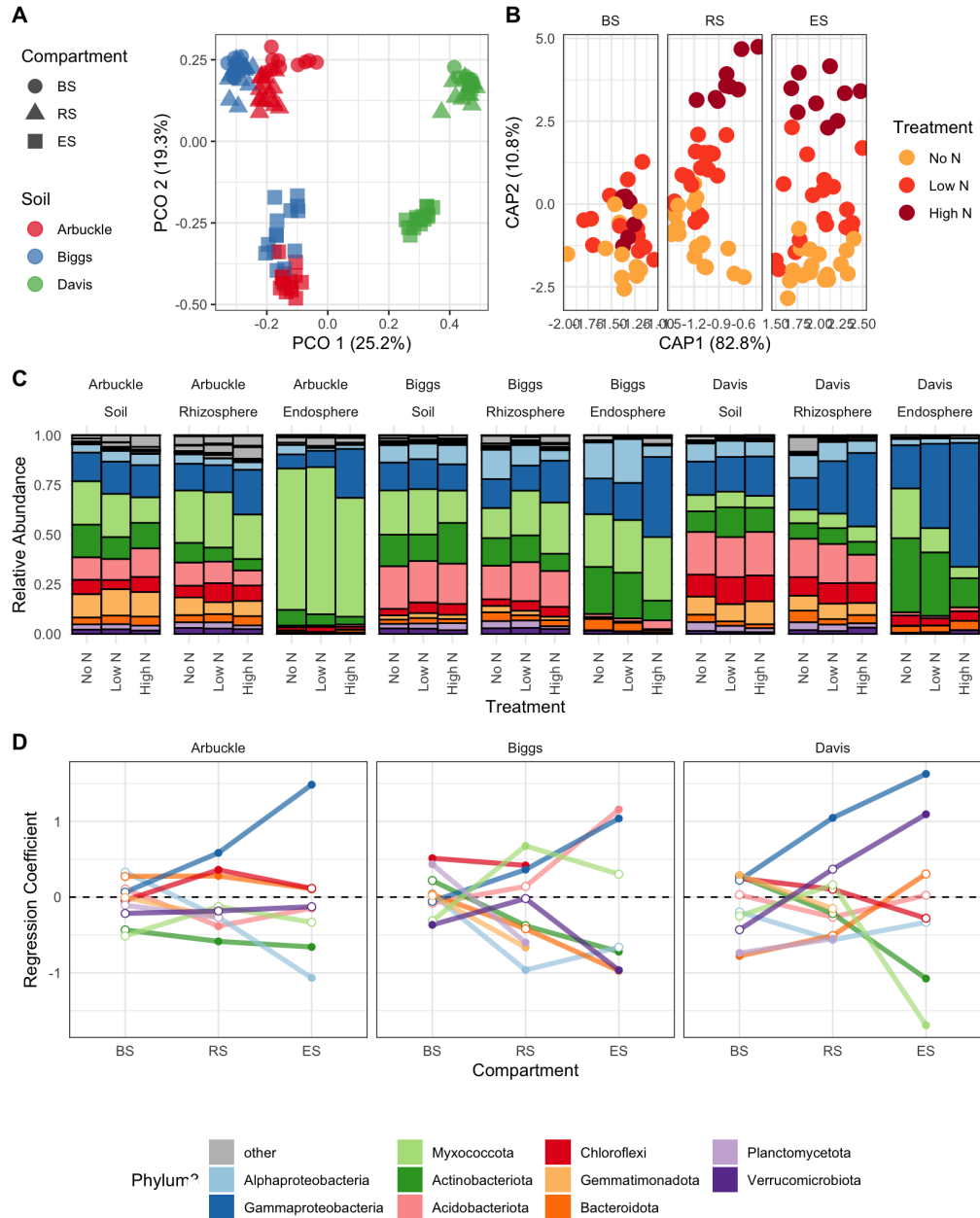
Figure 2

Beta diversity patterns show responses of the microbiome to nitrogen and soil source. (A) PCoA of Bray-Curtis distances. Shapes correspond to compartment and color corresponds to soil. (B) Constrained analysis of principal coordinates plot conditioned on soil source and colored by treatment. Facets are showing the response of the communities to nitrogen in each compartment. (C) Phylum profiles in each treatment combination. Colors correspond to percent belonging to each of the top 10 phyla in the dataset. (D) Beta regression of each phylum within each compartment and soil in response to nitrogen. The dots represent the beta regression coefficient (showing an increase in abundance in response to nitrogen with a coefficient greater than 0 and vice-versa). Filled dots are significant responses of phyla to nitrogen, and white dots are not significant (P < 0.05). Lines are connecting phyla within each soil to show the trends of that phyla through the compartments. BS = bulk soil, RS = rhizosphere, ES = endosphere.

Differential abundance analysis identified 161 ASVs that were affected by the nitrogen treatment in either the endosphere or rhizosphere in at least one soil. The nitrogen-responsive ASVs were almost entirely soil source specific, with there being two nitrogen-responsive ASVs shared between Arbuckle and Davis rhizospheres, and one ASV uniquely shared in each pair of soils in endosphere samples. Even though there was little overlap in ASVs with a significant nitrogen response between soils, we characterized the broad trends of ASVs that were nitrogen responsive in at least one soil by clustering the z score of their relative abundance across all soils to identify similar global trends among ASVs. Nitrogen-responsive ASVs were clustered into five different clusters and the cumulative relative abundance of each cluster was compared between soils (Figure 3). Clusters two and four show an increasing cumulative relative abundance with addition of nitrogen in the endosphere and the rhizosphere, whereas cluster five decreased in cumulative relative abundance with the addition of nitrogen. Clusters one and three have soil-dependent responses to the nitrogen treatment. The two clusters that increase in relative abundance have many Gammaproteobacteria, with 19 and 9 ASVs assigned to cluster two and four respectively. Many of these ASVs belong to the families Comamonadaceae and Rhodocyclaceae, with 9 and 6 ASVs respectively in cluster two and 3 and 3 in cluster four. The number of Gammaproteobacteria in these nitrogen-responsive clusters aligns with the overall increase in Gammaproteobacteria in response to nitrogen seen in the phyla profiles discussed above. Isolates from both Comamonadaceae and Rhodocyclaceae are known to use nitrate as a reducing agent in respiration, are capable of aromatic compound degradation, and produce methanogenic precursor molecules through fermentation[23,24].
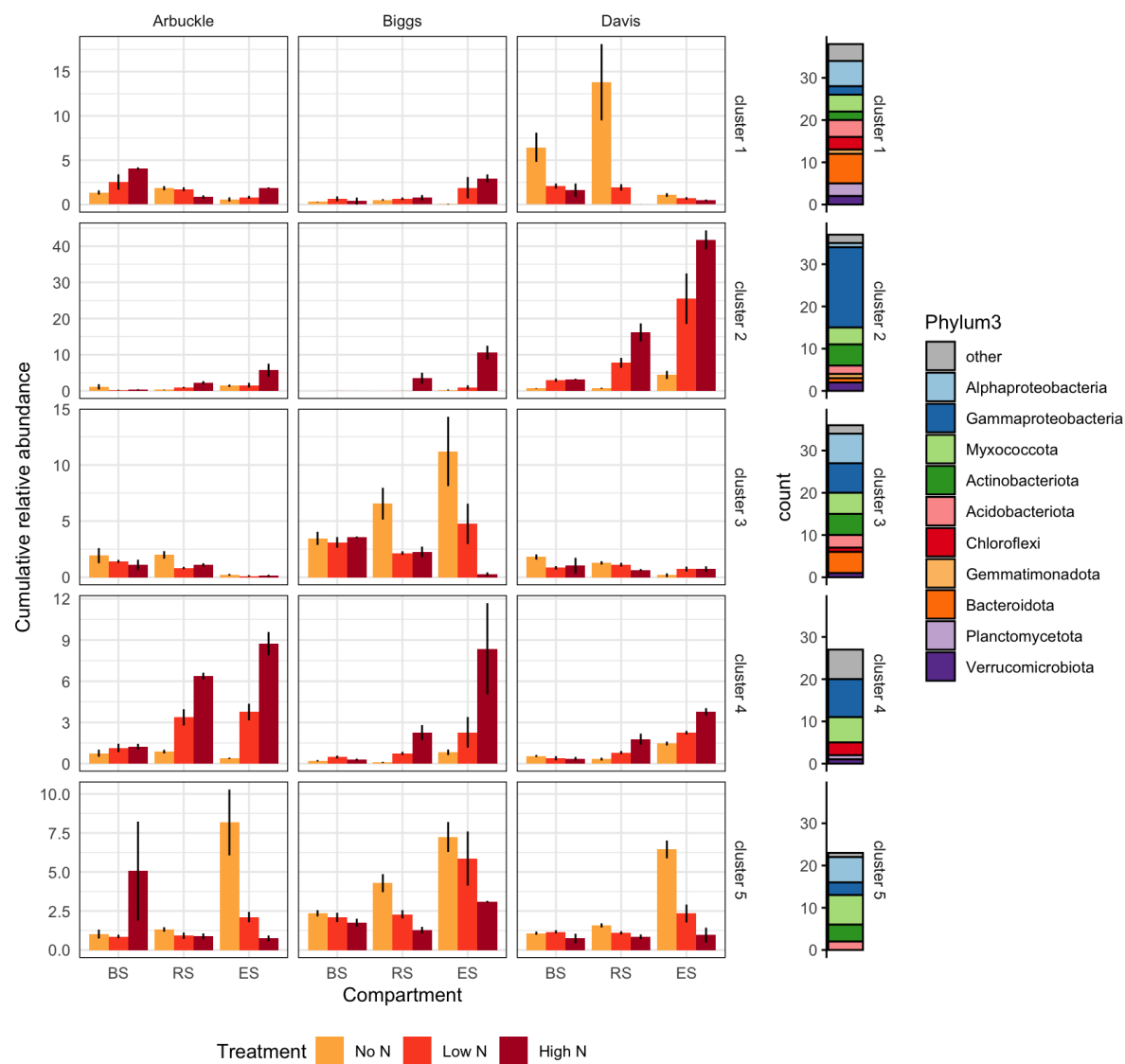
Figure 3
Responses of clusters of ASVs to nitrogen treatment. Each row represents a different cluster of nitrogen-responsive ASVs, and each column shows the trends of the cumulative relative abundance of that cluster in each soil, in each compartment. The color within each box represents the cumulative relative abundance in each treatment. The black bars represent standard error. The stacked boxplot on the right shows the count and composition of each cluster at the phylum level. BS = bulk soil, RS = rhizosphere, ES = endosphere.

Differentially abundant ASVs are not exclusively a result of a stronger rhizosphere effect in

nitrogen treatments

We next investigated some underlying drivers of the observed changes by comparing bulk soil to

rhizosphere fold changes to fold changes of nitrogen treatments within the rhizosphere. The addition of

nitrogen to bulk soils alone was not sufficient to alter the microbiome (Figure 2B), meaning the observed changes are likely also dependent on changes to carbon output from the host. The addition of nitrogen fertilizer increases the rate of exudation in the roots[25,26], so we hypothesized that the nitrogen-responsive changes we observed were either due to an overall increase in exuded carbon (i.e. a stronger rhizosphere effect), or due to specific nitrogen-induced changes to the exudate composition. To test this, we compared the rhizosphere effect (by comparing the fold change of ASVs in the no N bulk soil to the no N rhizosphere samples) to the effect of nitrogen in the rhizosphere (comparing no N, low N, and high N rhizosphere samples). If the changes in relative abundance observed in response to nitrogen were due mostly to a stronger rhizosphere response, we expected to see a positive correlation between the rhizosphere effect in the no N samples and the effect of adding nitrogen to the rhizosphere samples. Instead, we observed that almost none of the ASVs affected by the nitrogen treatment were ASVs enriched in the no N rhizospheres over the bulk soils with the exception of two Arbuckle ASVs (Figure 4). Furthermore, the ASVs in Davis and Biggs that were significantly affected in both situations had a negative correlation. The ASVs found in quadrant IV of figure 4 are ASVs that are enriched in the rhizosphere of no nitrogen samples, but then decrease in relative abundance as nitrogen is added. The lack of positive correlation found in this analysis demonstrates that the response seen in these samples is not due solely to a general stronger rhizosphere effect.
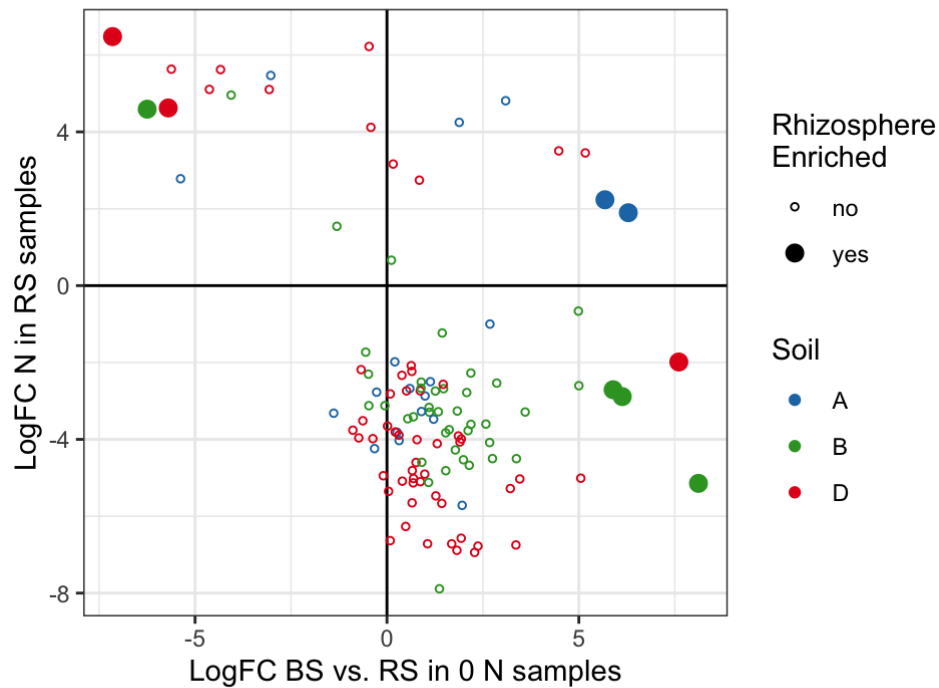
Figure 4

Comparison of log fold changes between rhizospheres and bulk soils with no nitrogen to rhizospheres in response to nitrogen. Each dot represents an ASV that is significantly affected by the nitrogen treatment in the rhizosphere. Solid larger dots represent ASVs which are also significantly enriched or depleted in the rhizosphere compared to bulk soil in the no N treatment. The x axis represents those fold changes, whereas the y axis represents the average of No N rhizosphere vs low N rhizosphere, and No N rhizosphere vs high N rhizosphere to get the average response to nitrogen in the rhizospheres.

Functional profiling reveals nitrogen, fermentation, and aromatic degradation processes

enriched in the rhizospheres of the high nitrogen treatment

       To further profile the functions affected by nitrogen treatment, full shotgun metagenome sequencing was performed on a subset of samples. Three high N and 3 no N treatments of the Arbuckle rhizosphere samples were sequenced. Using HUMAnN3, we quantified genes, enzymes corresponding to the enzyme commission numbers (ECs), and pathways in the Metacyc database[27]. In total, 400,564 genes, 2,744 ECs, and 521 pathways were identified in the samples. Principal component analysis (PCA) demonstrated there was a clear separation of the no N and high N samples in each case (Figure 5A-C).

The second axis of the PCA corresponded to the sequencing depth of each sample (Figure S2), indicating that deeper sequencing would likely reveal more diverse low-count genes in this dataset.

Differential abundance analysis was performed in order to identify differentially abundant pathways associated with the Metacyc parent classes biosynthesis, degradation/utilization/assimilation, generation of precursor metabolites and energy, and macromolecule modification. Since Metacyc pathways are often complex and branching, we explored pathways that were differentially abundant with a P cutoff value of 0.1 in order to explore more general trends in the data and capture situations where one branch of a pathway is significantly enriched where another is not (see Figure S3 for an example of this observation). In total, 11 pathways were differentially abundant at $P < 0.05$, 86 at $P < 0.07$, and 94 at $P < 0.10$ (Figure 5D). Most differentially abundant pathways were more abundant in the high N treatment. Only one pathway was enriched at $P < 0.05$ in the no N treatment: PWY-6098, the biosynthesis of the terpene diploterol. Differential abundance of individual ECs was also performed and identified 40 ECs differentially abundant at $P < 0.05$ and 394 at $P < 0.07$.

Some of the most significantly enriched pathways in the high N treatment were all related to the degradation of phenolic compounds, including the degradation of toluene, catechol, protocatuate, gallate, methylgallate, vanillin, and syringate (Table 2). Many pathways associated with fermentation and the production of short chain fatty acids (SCFAs) were also enriched in the high N treatment (Table 2). These pathways include the fermentation of glutamate, pyruvate and acetylene among others to produce methanogenic precursor molecules acetate, propionate, and butyrate. Methanogenesis was also enriched, as demonstrated by the enrichment of EC 2.8.4.1 (which is associated with Methyl coenzyme M reductase, which catalyzes the final step of methanogenesis) in the high N treatment ($P = 0.053$). Pathways associated with methanogenesis were enriched in the high N treatment, including tetrahydromethanopterin biosynthesis, a coenzyme in methanogenesis[28] ($P = 0.052$). Furthermore, the

71
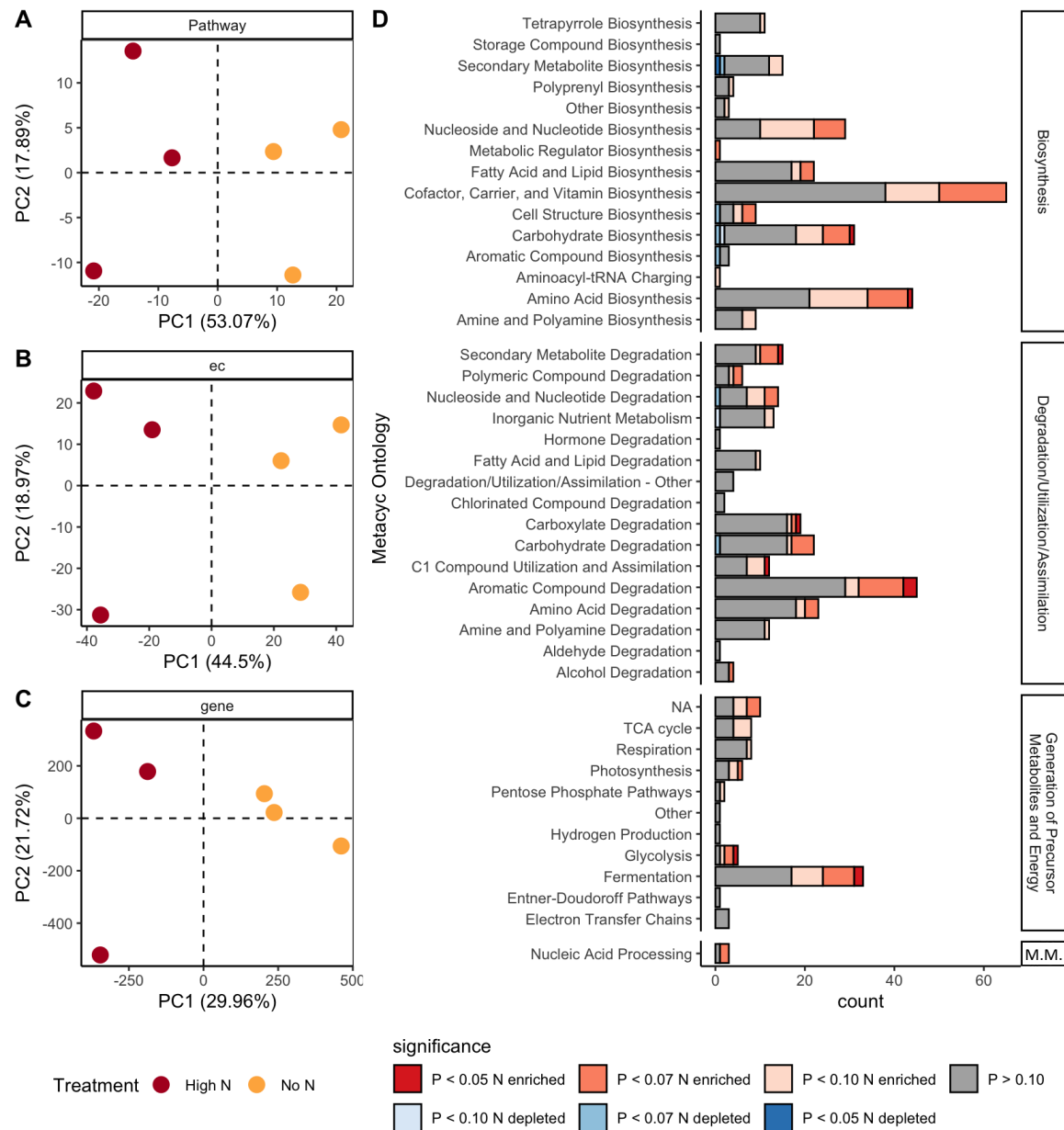
Figure 5

Beta diversity and differential abundance of nitrogen-responsive pathways in the metagenome dataset. Principal coordinate analysis of the metagenome dataset when quantified at the (A) pathway level, (B) enzyme (EC) level, and (C) gene level. Colors represent the two treatments. (D) each pathway was represented by the parent class (box on the right) and subclass (y axis). The x axis demonstrates the number of pathways identified in each subclass. Pathways are colored by significance and wheth er they were enriched in the high N treatment (red) or no N treatment (blue). M.M.= Macromolecule Modification.

methanogenesis from acetate pathway has a lower P value than the methanogenesis from H_2 and CO_2 (P=0.089 vs P=0.47 respectively).

Only a few differences were observed in pathways and ECs related to nitrogen cycling. Nitrate assimilation was more abundant in the high N treatment (P=0.078). Additionally, EC 1.7.2.4 (Nitrous-oxide reductase, which reduces nitrous oxide to nitrogen gas) was significantly enriched in the high N treatment (P=0.043), although no pathways associated with this enzyme were enriched overall. Furthermore, EC 1.18.6.1 (nitrogenase, which reduces nitrogen gas to ammonia) was enriched in the high N treatment (P=0.062). Two nitrogenase-associated enzymes, ADP-ribosyl-[dinitrogen reductase] hydrolase (EC 3.2.2.24) and NAD(+)-dinitrogen-reductase ADP-D-ribosyltransferase (EC 2.4.2.37) were also enriched in the high N treatment (P=0.053, P=0.049 respectively). These genes positively and negatively regulate the activity of nitrogenase respectively[29,30].

Assembly of Sixty metagenome-assembled genomes provide insights into the connectivity of nitrogen-responsive pathways

In total, 85 MAGs with more than 60% completeness and less than 15% contamination were recovered from the assemblies of each sample. After dereplication, 60 MAGs remained, spanning a broad taxonomic range, and covering many of the most abundant taxa in our samples (Fig 6A). Comparisons on the relative abundances of 16S genes derived from amplicon sequencing, shotgun metagenomics, and MAGs show similar taxonomic profiles among the three datasets (Figure 6B). Notably, Gammaproteobacteria increases in abundance in the high N treatment in all three datasets. Also, notably absent from the MAGs are Actinobacteria, which were found to universally decrease with the addition of nitrogen fertilizer in the 16S amplicon dataset (Figure 2B-C). In total, 743 Metacyc pathways were found across all MAGs. Notable among these pathways were multiple pathways associated with aromatic compound degradation, fermentation to SCFAs, and nitrogen cycling (Figure 6C). Thirty-nine pathways found to be differentially abundant in the HUMANn3 analysis were also present in the MAGs, 9 of which were aromatic compound degradation pathways, and 1 of which was a fermentation pathway (glutamate

73

fermentation to butanoate) (Figure 6C). In total, 28 different MAGs contained significantly enriched

pathways related to aromatic degradation. Ten of these MAGs were classified as Gammaproteobacteria,

which was the class most consistently enriched in the 16S amplicon data. Half of these

Gammaproteobacteria were also found to be significantly enriched among the MAGs, with the other half

showing no differential abundance. Many of these Gammaproteobacteria belonged to the order

Burkholderiales, which also contained enriched ASVs in the 16S amplicon analysis. The other two major

phyla found to contain significantly enriched aromatic degradation pathways were Bacteroidota and

Myxococcota, with 4 MAGs each. Many of the MAGs that contained aromatic compound degradation

pathways also contained various fermentation pathways (Figure S4).

Since we are profiling metagenomes and not metatranscriptomes, it is possible that the

differentially abundant genes, enzymes, or pathways discussed here are not directly enriched by the

treatment, but rather enriched due to hitchhiking on a function that truly responds to the nitrogen

treatment by co-occurring in the same genome. We investigated the co-occurrence of pathways found in

the MAGs to see whether differentially abundant pathways were likely direct targets of selection or

enriched as a result of hitchhiking. We measured the Jaccard similarity coefficient between each pathway

and constructed a co-occurrence network from the significant coefficients (Figure 6D). Of the 39 enriched

pathways identified in the MAGs, 21 had no significant co-occurrences with other pathways. The

differentially abundant pathways that had significant co-occurrences generally had very low betweenness

centrality (Figure S5B). Furthermore, modules of co-occurring pathways were determined (Figure S5A),

and the majority of differentially abundant pathways are not found in the same modules. Assuming that

the co-occurrence relationships observed in the MAGs is applicable to the community at large, the

differentially abundant pathways are unlikely to be differentially abundant as a result of hitchhiking.
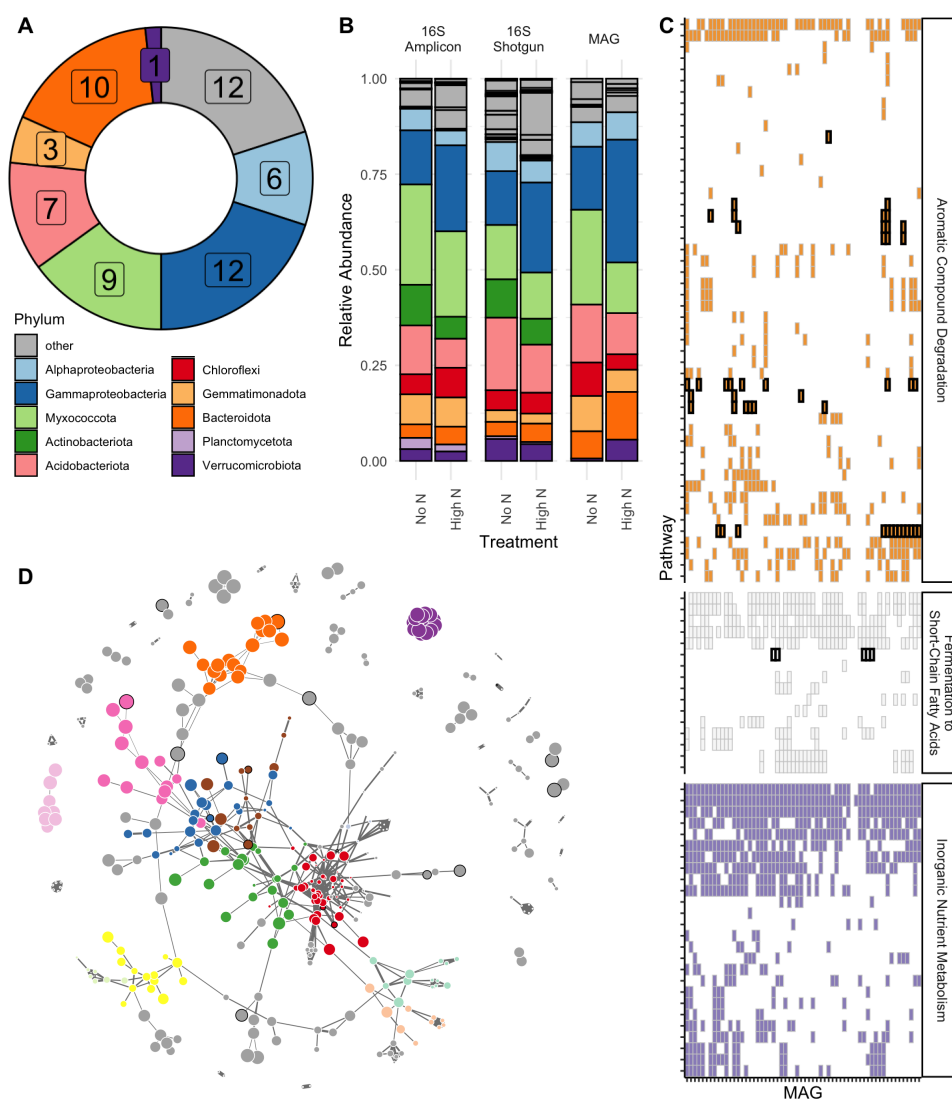
Figure 6

(A) The taxonomic classification of the 60 MAGs recovered from the metagenome dataset. (B) Taxonomic profiles derived from the 16S amplicon dataset, the 16S sequences extracted from the metagenome dataset, and MAGs. (C) Pathways belonging to the Metacyc sub classes Aromatic Compound Degradation, Fermentation to Short-Chain Fatty Acids, and Inorganic Nutrient Cycling. Each row is a different pathway, and each column is a MAG. Each box represents the presence of that pathway in the corresponding MAG. Boxes with thick black outlines represent pathways that were found to be significantly enriched in the high N treatment in the HUMAnN3 analysis. (D) Co-occurrence network of pathways found in MAGs. Only pathways with at least one significant connection are depicted. The size of the lines are weighted by the Jaccard similarity, and the size of the dots represent the number of MAGs containing that pathway. A black outline of a dot indicates that that pathway was found to be differentially abundant in the HUMAnN3 analysis. The different colors represent the 13 largest modules of pathways. The composition of these clusters can be found in Figure S5A. A grey color indicates that that pathway is not a member of one of the 13 largest clusters.

Discussion

The microbiome has soil-specific and soil-independent responses to nitrogen fertilizer

Here we provide a characterization of rice root-associated microbiomes grown in three different soils in response to nitrogen. The differences of the microbial community in response to nitrogen fertilizer observed in the endosphere and rhizosphere but not bulk soil (Figure 2B) suggests that the differences were not due solely to nitrogen, but rather the interaction of nitrogen and the carbon compounds exuded by the host. The responses to fertilizer were largely dependent on soil source, indicating that taxonomic responses to nitrogen are not as global as responses to other external factors, such as drought[19]. This could explain some of the differences in nitrogen-sensitive taxa seen here compared to other studies profiling the effects of nitrogen on rice-associated microbiomes[31,32], though differences could also be due to different methodologies, as these studies rely on methods that do not profile the community as deeply as the profiling done here.

The differential responses to nitrogen between the soils could be due to various factors, including differences in soil chemistry or differences in microbial interactions arising from the unique initial compositions of the various communities. The three soils used in this study have distinct chemical properties[20] which could interact uniquely with the microbiome upon nitrogen fertilization. The release of exudates into the soil primes the soil by liberating carbon sources previously unavailable[33], meaning that fertilizer-induced exudation could liberate different compounds depending on the soil source. However, the addition of nitrogen fertilizer increases the amount of carbon taken up by the microbiome originating from the rice plant compared to soil organic carbon[16], suggesting differences due to soil chemistry might decrease with increasing nitrogen. However, we found that comparisons of Bray-Curtis dissimilarity between the soils were just as dissimilar at no or low N levels as high N levels (Figure S6). Assuming the ratio of soil-derived to plant-derived carbon decreases upon application of fertilizer in this study, the lack of convergence of the community at high N levels perhaps indicates that the differences seen are independent of soil chemistry, or that soil chemistry directly impacts root exudate composition and is

76

thereby indirectly impacting the community. Furthermore, it is possible that while soils vary in taxa that are responsive to the treatment, the different taxa enriched in each soil could perform the same metabolic functions. Further metagenome and metatranscriptome profiling of other soils would be necessary to evaluate if these divergent taxa have convergent functions in response to nitrogen.

While there were many unique responses to nitrogen fertilizer between soil sources, some consistent patterns were observed, namely the increase of Gammaproteobacteria (specifically the families Comamonadaceae and Rhodocyclaceae) and decrease of Actinobacteria in response to nitrogen (Figure 2C-D,3). These taxa could be those most directly impacted by nitrogen fertilizer and could be interesting targets to further understand nitrogen and carbon cycling in the rice rhizosphere. However, more research is needed to understand the consistency of these trends in a variety of circumstances. For example, rice-associated microbiomes shift in composition through the growing season[21,34], meaning that the growth stage at which fertilizer is applied could significantly impact nitrogen-responsive taxa. Furthermore, the fertilizer used in this study was sown into the soil before planting, meaning that we sampled plants long after fertilization. While this experimental design allows us to evaluate the long-term impacts of nitrogen on the microbiome, it does not profile the initial responses of the microbiome to nitrogen fertilizer. For example, while urea was the fertilizer used in this study, the urease-related genes were not enriched in the high N treatment. Furthermore, fertilizer has been shown to affect the activity and abundances of methanotrophs that can use ammonia as a substrate[13,14]; in this study, we found neither differences in methanotrophic taxa in the 16S amplicon data, nor differences in the abundance of genes corresponding to methane monooxygenase. Profiling the community at multiple timepoints after fertilizer application could further elucidate microbial turnover in response to nitrogen.

Rhizosphere communities alter carbon cycling functions in response to nitrogen

The 16S amplicon data can describe which taxa are affected by nitrogen fertilizer, whereas metagenomics can describe which functions are affected. The most striking trends in the results were the alterations in aromatic compound degradation, fermentation, and methanogenesis. Increasing nitrogen

77

increases the amount of methane that is derived from plant carbon rather than soil organic carbon[16], so seeing shifts in carbon cycling pathways could provide information as to how carbon is being incorporated into the microbiome, and how carbon sources are degraded to methanogenic precursor molecules. The broad enrichment of degradation of aromatic compound pathways suggest that nitrogen fertilizer is increasing the amount of aromatic compounds in the rhizosphere. In maize, the presence of aromatic compounds (specifically phenolics) in the exudate correlates with the amount of nitrogen fertilizer applied[26], and a similar change in rice exudation could explain the enrichment of degradation pathways observed here. Furthermore, it has been shown that aromatic compound degradation is syntrophically coupled to methanogenesis in rice paddies[35]. Perhaps the enrichment of aromatic degradation pathways in these samples could be contributing to the observed increase in reads associated with Methyl coenzyme M reductase, the key enzyme involved in methanogenesis.

Further related to methanogenesis is the production of methanogenic precursor SCFAs. We found an enrichment of pathways fermenting glutamate, pyruvate and acetylene to produce acetate, propionate, and butyrate, which have all previously been shown to be produced and utilized in methanogenesis during the degradation of rice carbon sources[36]. Also of note is the greater enrichment of reads mapping to acetoclastic methanogenesis over hydrogenotrophic methanogenesis; previously it had been shown that plant-produced carbon is normally incorporated into the hydrogenotrophic methanogen[11], but here we identified an enrichment of acetoclastic methanogenesis. Perhaps this indicates that the addition of nitrogen alters which form of methanogenesis becomes dominant. This could be the result of changes in the recruitment of methanogenic syntrophs, which could contain the above-described fermentative pathways. Furthermore, many of the MAGs containing aromatic degradation pathways also contain fermentative pathways (Figure S6), meaning they could be capable of producing SCFAs and act syntrophically with methanogens. Two of the enriched fermentation pathways were glutamate fermentation to propionate and glutamate fermentation to butyrate. The majority of assimilated nitrogen often passes through the GOGAT pathway, which incorporates nitrogen into glutamine which is then catalyzed into glutamate[37]. While very few nitrogen cycling genes were differentially abundant between

78

samples, perhaps the assimilation of nitrogen before the time of sampling led to increases in glutamate, and subsequent increase of microbes containing glutamate fermentation pathways as observed in this data. While an increase in glutamate could also be due to an increased exudation of glutamate, a recent study found a reduced glutamate content in the exudates of nitrogen-fertilized rice compared to unfertilized rice[38] suggesting this response is not a direct result of altered exudation.

While we have found many differentially abundant genes and pathways in this data, the interpretation is limited since metagenomic data only counts abundances and not expression of genes. While genes can be differentially abundant, it does not mean that they are expressed or that expression of them is responding to a stimulus; rather, differentially abundant genes could be enriched due to hitchhiking off other genes that are truly responsive by occurring in the same genome. An example of this is the above mentioned enrichment of both nitrogenase, the negative regulator of nitrogenase (NAD(+)-dinitrogen-reductase ADP-D-ribosyltransferase), and the positive regulator of nitrogenase (ADP-ribosyl-[dinitrogen reductase] hydrolase). It is unlikely that all three products are simultaneously expressed to a greater degree in the high N treatment, but genomes containing nitrogenase likely contain these regulators as well, so enrichment of nitrogenase would also cause the enrichment of these associated genes. The enrichment of nitrogenase genes is unexpected, since it has been shown in multiple crops that the addition of synthetic fertilizers reduces the activity of nitrogenase, or abundances of taxa associated with nitrogenase[39–41].

While we are able to identify pathways that are overall enriched, another challenge with metagenomic datasets is that we cannot confirm that all of the relevant genes for a given pathway are found in the same microbe, and thus the identified pathway is truly complete. One way to alleviate these issues and gain further insight into differentially abundant pathways is through the construction of MAGs. We were able to confirm that some of the differentially abundant pathways were fully present in different MAGs, and that the differentially abundant pathways did not co-occur to a large degree with other pathways within the MAGs. Assuming the co-occurrence relationships observed within the MAGs are representative of the whole community, this result implies that the differentially abundant pathways were

directly enriched rather than enriched through hitchhiking. While the results obtained from this metagenome sequencing describe interesting interactions potentially stimulated by urea fertilizer, including the enrichment of methangenesis, fermentation, and aromatic compound degradation in the high N treatment, the varying results between soil of the 16S data suggests that these results might not be universal, and metagenome sequencing must be performed similarly in other soils to understand global responses of the rice microbiome to nitrogen. Further researching the effects of nitrogen on methane cycling microbes coupled with the effects of different rice cultivars on methane cycling microbes as outlined in the first chapter could lead to an improved nitrogen use efficiency while reducing methanogenesis.

Methods

Experimental Design

Kitaake seedlings were germinated on ½ murashige skoog agarose plates on June 13, 2019. Six-day old seedlings were transplanted to pots containing one of three agricultural soils originating from Arbuckle, Biggs, and Davis, California, which have all been described previously[19,20]. Three planted pots and two bulk soil pots of each soil were placed in each of six bins for a total of 9 plants and 6 bulk soils in each bin. Two bins each were treated with one of three nitrogen treatments (no N, low M, and high N). This resulted in an initial replication of 6 plants per factor combination and 4 bulk soils per factor combination for a total of 54 plants and 36 bulk soil samples. The low nitrogen treatment consisted of 1.5 g urea mixed into the soil of each pot pre-planting, and an additional 25 g urea mixed directly into the water filling the bins. The high N treatment consisted of 3 g Urea mixed in each pot, and 50 g Urea in each bin. One of the high N bins was located in a different section of the greenhouse and did not grow as well as indicated by reduced growth and leaf discoloration; for this reason, this bin was excluded from further analyses, meaning the high N treatment had a replication of three instead of six.

Plant Phenotype measurements

The plants were measured and samples collected on August 8, 2019, fifty days after transplantation. The height and number of tillers were recorded during collection. The shoot of each plant was placed in an oven, and full weight and vegetative weight (weight after removing any panicles) were measured after one week of drying. Three small leaf fragments were removed before processing and photographed using a Canon EOS 6D with an X-Rite ColorChecker Classic (MSCCC). Photographs were color corrected using the X-Rite ColorChecker software, and the average pigment of each leaf fragment and rgb values were determined using Adobe Photoshop. Hue, saturation and lightness values were determined using the rgb2hsl function in the plotwidgets package[42].

Microbiome compartment separation and collection

Rhizosphere and Endosphere samples were collected as previously described[43]. Roots were shaken to remove excess soil and placed in a 50 mL falcon tube containing 20 mL of phosphate buffered solution (PBS). The rhizosphere samples were collected by vortexing the roots and removing 500 uL of the resulting suspension. Roots were then washed three times with PBS and sonicated for 30 seconds to isolate the endosphere.

16S rRNA gene amplicon library construction

DNA was extracted from the rhizosphere, endosphere, and bulk soil samples using the PowerSoil DNA isolation kit (Qiagen) following the manufacturer's protocol. Libraries were prepared as previously described using dual-indexing primers[18]. PCR was performed using the Qiagen HotStar HiFidelity polymerase kit, and touchdown PCR was used to amplify the libraries with the following parameters: 95°C for 5 min, 35 cycles of 95°C for 45 s, 50°C for 1 min, and 72°C for 1 min, and 72°C for 10 min. Contamination was identified by running negative controls of each sample on a 1% agarose gel. Samples were purified with AMPure beads, and samples were quantified with a Qubit high-sensitivity assay

kit. AMPure beads were used to purify the samples, which were then pooled and sequenced in a 2 x 250 paired-end Illumina MiSeq run.

16S rRNA gene amplicon processing and analysis

Samples were demultiplexed using a custom script (https://github.com/RiceMicrobiome/Edwards-et-al.-2014/tree/master/sequencing_scripts). Samples were clustered into ASVs using DADA2[44], and taxonomy was assigned using the AssignTaxonomy() function in dada2 with the SILVA_138 database[45]. This update of the database includes some changes to taxonomy compared to previous studies from our lab, including splitting up the Deltaproteobacteria into the new phyla Desulfobacterota, Myxococcota, Bdellovibrionota, and SAR324, and the merging of order Betaproteobacteria into the order Gammaproteobacteria. All statistical analyses were performed in R version 4.1.1[46]. The vegan package[47] was used to perform PERMANOVA with the adonis() function, calculation of Bray-Curtis dissimilarities with the vegdist() function, and canonical analysis of principal coordinates with the capscale() function. The ape package[48] was used for unconstrained principal coordinate analysis using the pcoa() function. Beta Regression on phyla was performed using the package betareg[49]. Differentially abundant ASVs were identified through the combination of two methodologies: treating nitrogen treatment as a continuous variable and correlating ASV abundance with nitrogen treatment using DESeq2[50], and performing pairwise Wald tests (also with DESeq2) with nitrogen treatment treated as a categorical variable between the no N and low N and the no N and high N treatments. The second method was included to capture nitrogen-responsive ASVs that were responsive to nitrogen treatments, but not in a linear fashion, e.g. an increase from no N to low N, but a plateau from low N to high N. Overall, 125 ASVs were identified as differentially abundant in at least one treatment and compartment in the correlation test, and 116 ASVs were similarly identified as differentially abundant between the wald tests, with 80 ASVs overlapping between the two datasets. The results from these two methods were combined for a total of 161 nitrogen-responsive ASVs. Clustering was performed with the cutreeHybrid() function from the dynamicTreeCut package[51] using a minimum cluster size of 10.

Genome-resolved metagenome sequence processing

Libraries were constructed by the UC Davis Sequencing core using the Takara HV Thruplex kit, and sequenced in a 2 x 150 paired-end Novaseq run. Trimmomatic[52] was used to remove adapters and quality trim, with a phred score of 33, minimum length of 50, and a sliding window of 4 to 30. The PhiX reads were removed with bbduk[53] with a k value of 31. Reads from each sample were assembled independently into contigs using MEGAHIT[54] with the preset "meta-large" and a minimum contig length of 1000.

For binning contigs into MAGs, assemblies of each sample were first concatenated into a single file using the concatenate.py script from VAMB[55], then the trimmed reads for each sample were aligned to the concatenated file using minimap2[56] using the sr presets and keeping 5 secondary alignments. Bins were then generated using VAMB with default settings. Bins were quality checked using CheckM[57], then dereplicated using dRep[58], both with default settings except for setting a completeness cutoff at 60%. All bins remaining after dereplication were considered MAGs. Coverage of each of the MAGs was determined using CoverM[59] v0.6.1. Taxonomy was assigned using GTDB-Tk[60]. Each MAG was then annotated using prokka[61] using the default settings, and the complete Metacyc pathways in each MAG were determined using MinPath[62].

Assembly-independent functional characterization was performed using HUMAnN3[63] on forward and reverse reads concatenated into a single file, with default settings using the EC filtered uniref90 database. Enzyme numbers associated with each gene were determined using the humann_regroup_table function, and enzyme numbers associated with each pathway were determined using the humann_unpack_pathways function. Differential abundances of pathways and enzyme numbers were determined by general linear models using MaAsLin2[64], using log transformation and treating nitrogen treatment as a fixed effect. To extract 16S profiles from the metagenomic dataset, 16S reads were identified using SortMeRNA[65], and were classified with RDP classifier[66].

References

1. Fageria, N. K. Yield Physiology of Rice. *Journal of Plant Nutrition* (2007) doi:10.1080/15226510701374831.
2. Pittelkow, C. M., Adviento-Borbe, M. A., van Kessel, C., Hill, J. E. & Linquist, B. A. Optimizing rice yields while minimizing yield-scaled global warming potential. *Glob. Chang. Biol.* **20**, 1382–1393 (2014).
3. Ishii, S., Ikeda, S., Minamisawa, K. & Senoo, K. Nitrogen cycling in rice paddy environments: past achievements and future challenges. *Microbes Environ.* **26**, 282–292 (2011).
4. Peng, S. *et al.* Improving nitrogen fertilization in rice by sitespecific N management. A review. *Agron. Sustain. Dev.* **30**, 649–656 (2010).
5. Zhao, X. *et al.* Nitrogen runoff dominates water nitrogen pollution from rice-wheat rotation in the Taihu Lake region of China. *Agric. Ecosyst. Environ.* **156**, 1–11 (2012).
6. Fu, J. *et al.* Nationwide estimates of nitrogen and phosphorus losses via runoff from rice paddies using data-constrained model simulations. *J. Clean. Prod.* **279**, 123642 (2021).
7. Qi, D., Wu, Q. & Zhu, J. Nitrogen and phosphorus losses from paddy fields and the yield of rice with different water and nitrogen management practices. *Sci. Rep.* **10**, 9734 (2020).
8. Masson-Delmotte, V., P. Zhai, A. Pirani, S.L. Connors, C. Péan, S. Berger, N. Caud, Y. Chen, L. Goldfarb, M.I. Gomis, M. Huang, K. Leitzell, E. Lonnoy, J.B.R. Matthews, T.K. Maycock, T. Waterfield, O. Yelekçi, R. Yu, B. Zhou. Climate Change 2021: The Physical Science Basis.
9. Kuypers, M. M. M., Marchant, H. K. & Kartal, B. The microbial nitrogen-cycling network. *Nat. Rev. Microbiol.* **16**, 263–276 (2018).
10. Simmonds, M. B. *et al.* Seasonal methane and nitrous oxide emissions of several rice cultivars in direct-seeded systems. *J. Environ. Qual.* **44**, 103–114 (2015).
11. Lu, Y. & Conrad, R. In situ stable isotope probing of methanogenic archaea in the rice rhizosphere. *Science* **309**, 1088–1090 (2005).
12. Neue, H.-U. Methane Emission from Rice Fields. *Bioscience* **43**, 466–474 (1993).
13. Hu, A. & Lu, Y. The differential effects of ammonium and nitrate on methanotrophs in rice field soil. *Soil Biol. Biochem.* **85**, 31–38 (2015).
14. Shrestha, M., Shrestha, P. M., Frenzel, P. & Conrad, R. Effect of nitrogen fertilization on methane oxidation, abundance, community structure, and gene expression of methanotrophs in the rice rhizosphere. *ISME J.* **4**, 1545–1556 (2010).
15. Benckiser, G., Santiago, S., Neue, H. U., Watanabe, I. & Ottow, J. C. G. Effect of fertilization on exudation, dehydrogenase activity, iron-reducing populations and Fe++ formation in the rhizosphere of rice (Oryza sativa L.) in relation to iron toxicity. *Plant Soil* **79**, 305–316 (1984).
16. Zhu, Z. *et al.* Rice rhizodeposits affect organic matter priming in paddy soil: The role of N fertilization and plant growth for enzyme activities, CO2 and CH4 emissions. *Soil Biol. Biochem.* **116**, 369–377 (2018).
17. Banger, K., Tian, H. & Lu, C. Do nitrogen fertilizers stimulate or inhibit methane emissions from rice fields? *Glob. Chang. Biol.* **18**, 3259–3267 (2012).
18. Edwards, J. *et al.* Structure, variation, and assembly of the root-associated microbiomes of rice. *Proc. Natl. Acad. Sci. U. S. A.* **112**, E911–20 (2015).
19. Santos-Medellín, C., Edwards, J., Liechty, Z., Nguyen, B. & Sundaresan, V. Drought Stress Results in a Compartment-Specific Restructuring of the Rice Root-Associated Microbiomes. *MBio* **8**, (2017).
20. Edwards, J. *et al.* Soil domestication by rice cultivation results in plant-soil feedback through shifts in soil microbiota. *Genome Biol.* **20**, 221 (2019).
21. Edwards, J. A. *et al.* Compositional shifts in root-associated bacterial and archaeal microbiota track the plant life cycle in field-grown rice. *PLoS Biol.* **16**, e2003862 (2018).

22. Wang, Y., Wang, D., Shi, P. & Omasa, K. Estimating rice chlorophyll content and leaf nitrogen concentration with a digital still color camera under natural light. *Plant Methods* **10**, 36 (2014).

23. Willems, A. The Family Comamonadaceae. in *The Prokaryotes: Alphaproteobacteria and Betaproteobacteria* (eds. Rosenberg, E., DeLong, E. F., Lory, S., Stackebrandt, E. & Thompson, F.) 777–851 (Springer Berlin Heidelberg, 2014).

24. Oren, A. The Family Rhodocyclaceae. in *The Prokaryotes: Alphaproteobacteria and Betaproteobacteria* (eds. Rosenberg, E., DeLong, E. F., Lory, S., Stackebrandt, E. & Thompson, F.) 975–998 (Springer Berlin Heidelberg, 2014).

25. Chang, E.-H., Zhang, S.-F., Wang, Z.-Q., Wang, X.-M. & Yang, J.-C. Effect of Nitrogen and Phosphorus on the Amino Acids in Root Exudates and Grains of Rice During Grain Filling. *Acta Agronomica Sinica* **34**, 612–618 (2008).

26. Zhu, S., Vivanco, J. M. & Manter, D. K. Nitrogen fertilizer rate affects root exudation, the rhizosphere microbiome and nitrogen-use-efficiency of maize. *Appl. Soil Ecol.* **107**, 324–333 (2016).

27. Caspi, R. *et al.* The MetaCyc database of metabolic pathways and enzymes and the BioCyc collection of pathway/genome databases. *Nucleic Acids Res.* **44**, D471–80 (2016).

28. Hallam, S. J. *et al.* Chapter four - Molecular Tools for Investigating ANME Community Structure and Function. in *Methods in Enzymology* (eds. Rosenzweig, A. C. & Ragsdale, S. W.) vol. 494 75–90 (Academic Press, 2011).

29. Fitzmaurice, W. P., Saari, L. L., Lowery, R. G., Ludden, P. W. & Roberts, G. P. Genes coding for the reversible ADP-ribosylation system of dinitrogenase reductase from Rhodospirillum rubrum. *Mol. Gen. Genet.* **218**, 340–347 (1989).

30. Lowery, R. G. & Ludden, P. W. Purification and properties of dinitrogenase reductase ADP-ribosyltransferase from the photosynthetic bacterium Rhodospirillum rubrum. *J. Biol. Chem.* **263**, 16714–16719 (1988).

31. Ikeda, S. *et al.* Low nitrogen fertilization adapts rice root microbiome to low nutrient environment by changing biogeochemical functions. *Microbes Environ.* **29**, 50–59 (2014).

32. Chen, J. *et al.* Nitrogen Fertilizer Amendment Alter the Bacterial Community Structure in the Rhizosphere of Rice (Oryza sativa L.) and Improve Crop Yield. *Front. Microbiol.* **10**, 2623 (2019).

33. Bastida, F. *et al.* Global ecological predictors of the soil priming effect. *Nat. Commun.* **10**, 3481 (2019).

34. Liechty, Z. *et al.* Comparative analysis of root microbiomes of rice cultivars with high and low methane emissions reveals differences in abundance of methanogenic Archaea and putative upstream fermenters. *mSystems* **5**, (2020).

35. Glissmann, K., Hammer, E. & Conrad, R. Production of aromatic compounds during methanogenic degradation of straw in rice field soil. *FEMS Microbiol. Ecol.* **52**, 43–48 (2005).

36. Conrad, R. & Klose, M. Selective inhibition of reactions involved in methanogenesis and fatty acid production on rice roots. *FEMS Microbiol. Ecol.* **34**, 27–34 (2000).

37. Reitzer, L. Nitrogen assimilation and global regulation in Escherichia coli. *Annu. Rev. Microbiol.* **57**, 155–176 (2003).

38. Tawaraya, K., Horie, R., Wagatsuma, T., Saito, K. & Oikawa, A. Metabolite profiling of shoot extract, root extract, and root exudate of rice under nitrogen and phosphorus deficiency. *Soil Sci. Plant Nutr.* **64**, 312–322 (2018).

39. Bahulikar, R. A. *et al.* Nitrogen Fertilization Reduces Nitrogen Fixation Activity of Diverse Diazotrophs in Switchgrass Roots. *Phytobiomes Journal* **5**, 80–87 (2021).

40. Jha, P. N. *et al.* Alterations in the Endophyte-Enriched Root-Associated Microbiome of Rice Receiving Growth-Promoting Treatments of Urea Fertilizer and Rhizobium Biofertilizer. *Microb. Ecol.* **79**, 367–382 (2020).

41. Reinprecht, Y. *et al.* Effects of Nitrogen Application on Nitrogen Fixation in Common Bean Production. *Front. Plant Sci.* **11**, 1172 (2020).

42. Weiner, J. *plotwidgets: Spider Plots, ROC Curves, Pie Charts and More for Use in Other Plot.* https://CRAN.R-project.org/package=plotwidgets (2016).

43. Edwards, J., Santos-Medellín, C. & Sundaresan, V. Extraction and 16S rRNA Sequence Analysis of Microbiomes Associated with Rice Roots. *Bio Protoc* **8**, e2884 (2018).
44. Callahan, B. J. *et al.* DADA2: High-resolution sample inference from Illumina amplicon data. *Nat. Methods* **13**, 581–583 (2016).
45. Quast, C. *et al.* The SILVA ribosomal RNA gene database project: improved data processing and web-based tools. *Nucleic Acids Res.* **41**, D590–6 (2013).
46. R Core Team. R: A Language and Environment for Statistical Computing. (2021).
47. Oksanen, J. *et al.* vegan: Community Ecology Package. (2020).
48. Paradis, E. & Schliep, K. ape 5.0: an environment for modern phylogenetics and evolutionary analyses in R. *Bioinformatics* vol. 35 526–528 (2019).
49. Cribari-Neto F, Z. A. Beta Regression in R. *Journal of Statistical Software* **34**, 1–24 (2010).
50. Love, M. I., Huber, W. & Anders, S. Moderated estimation of fold change and dispersion for RNA-seq data with DESeq2. *Genome Biology* vol. 15 550 (2014).
51. Langfelder, P., Zhang, B. & from Steve Horvath, W. C. dynamicTreeCut: Methods for Detection of Clusters in Hierarchical Clustering Dendrograms. (2016).
52. Bolger, A. M., Lohse, M. & Usadel, B. Trimmomatic: a flexible trimmer for Illumina sequence data. *Bioinformatics* **30**, 2114–2120 (2014).
53. Bushnell, B. *BBTools software package*. (2014).
54. Li, D., Liu, C.-M., Luo, R., Sadakane, K. & Lam, T.-W. MEGAHIT: an ultra-fast single-node solution for large and complex metagenomics assembly via succinct de Bruijn graph. *Bioinformatics* **31**, 1674–1676 (2015).
55. Nissen, J. N. *et al.* Improved metagenome binning and assembly using deep variational autoencoders. *Nat. Biotechnol.* **39**, 555–560 (2021).
56. Li, H. Minimap2: pairwise alignment for nucleotide sequences. *Bioinformatics* **34**, 3094–3100 (2018).
57. Parks, D. H., Imelfort, M., Skennerton, C. T., Hugenholtz, P. & Tyson, G. W. CheckM: assessing the quality of microbial genomes recovered from isolates, single cells, and metagenomes. *Genome Res.* **25**, 1043–1055 (2015).
58. Olm, M. R., Brown, C. T., Brooks, B. & Banfield, J. F. dRep: a tool for fast and accurate genomic comparisons that enables improved genome recovery from metagenomes through de-replication. *ISME J.* **11**, 2864–2868 (2017).
59. Woodcroft, B. J. *CoverM: Read coverage calculator for metagenomics*. (Github).
60. Chaumeil, P.-A., Mussig, A. J., Hugenholtz, P. & Parks, D. H. GTDB-Tk: a toolkit to classify genomes with the Genome Taxonomy Database. *Bioinformatics* **36**, 1925–1927 (2019).
61. Seemann, T. Prokka: rapid prokaryotic genome annotation. *Bioinformatics* **30**, 2068–2069 (2014).
62. Ye, Y. & Doak, T. G. A parsimony approach to biological pathway reconstruction/inference for genomes and metagenomes. *PLoS Comput. Biol.* **5**, e1000465 (2009).
63. Beghini, F. *et al.* Integrating taxonomic, functional, and strain-level profiling of diverse microbial communities with bioBakery 3. *Elife* **10**, (2021).
64. Mallick, H. *et al.* Multivariable Association Discovery in Population-scale Meta-omics Studies. *bioRxiv* 2021.01.20.427420 (2021) doi:10.1101/2021.01.20.427420.
65. Kopylova, E., Noé, L. & Touzet, H. SortMeRNA: fast and accurate filtering of ribosomal RNAs in metatranscriptomic data. *Bioinformatics* **28**, 3211–3217 (2012).
66. Wang, Q., Garrity, G. M., Tiedje, J. M. & Cole, J. R. Naive Bayesian classifier for rapid assignment of rRNA sequences into the new bacterial taxonomy. *Appl. Environ. Microbiol.* **73**, 5261–5267 (2007).

Supplemental Figures and Tables
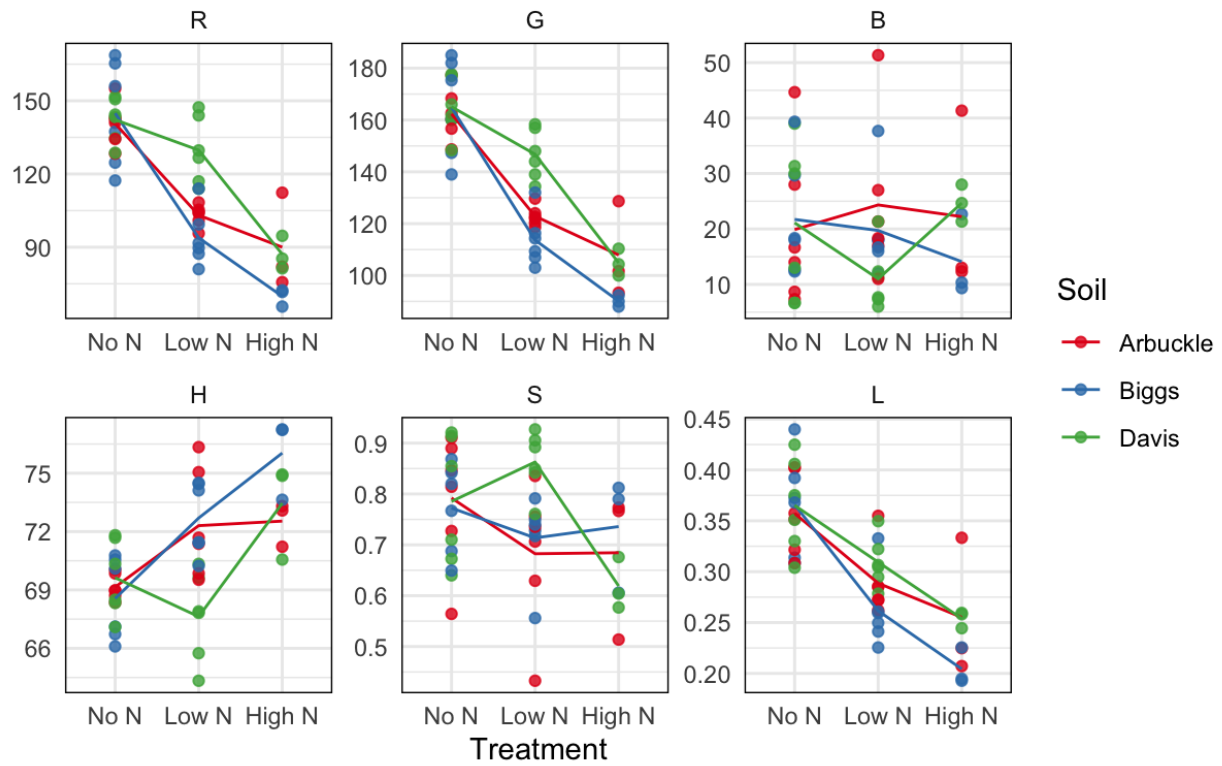
Supplemental Figure 1
RGB (red, green, blue) and HSL (hue, saturation, lightness) of the leaf values in each soil (colors) at each treatment level (x axis).
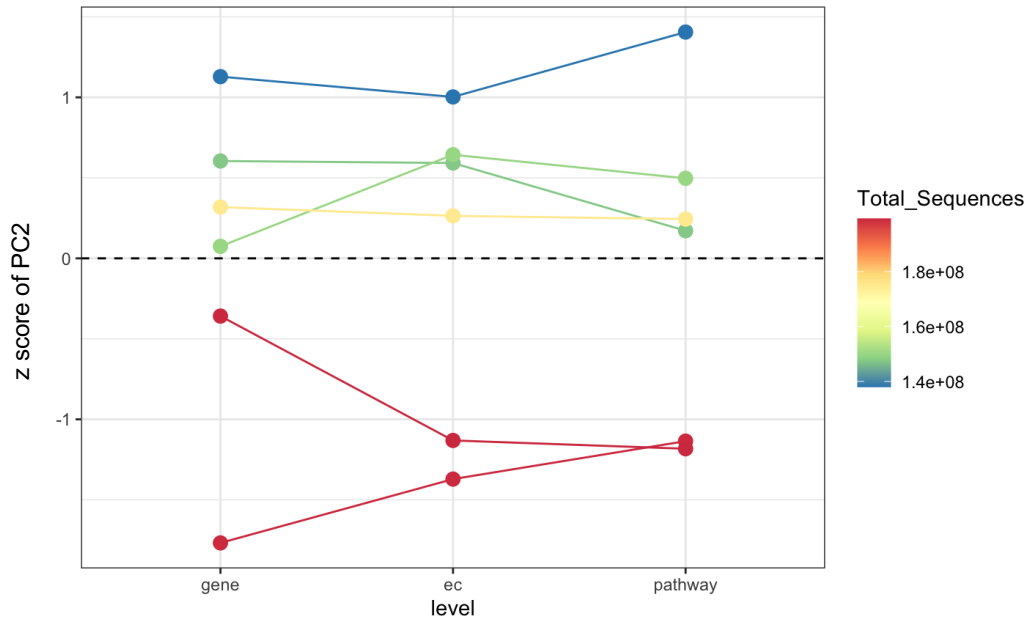
Supplemental Figure 2
Depiction of the relationship between the second axis of PCAs from figure 5 A-C and sequencing depth. The x axis represents which PCA was is being depicted, and the y axis is the z score of the second axis of the corresponding PCA. The z score was calculated in order to normalize values between the different PCAs. The color represents the sequencing depth, and lines connecting dots represent the same samples in each of the different PCAs.

PWY-5100: pyruvate fermentation to acetate and lactate II
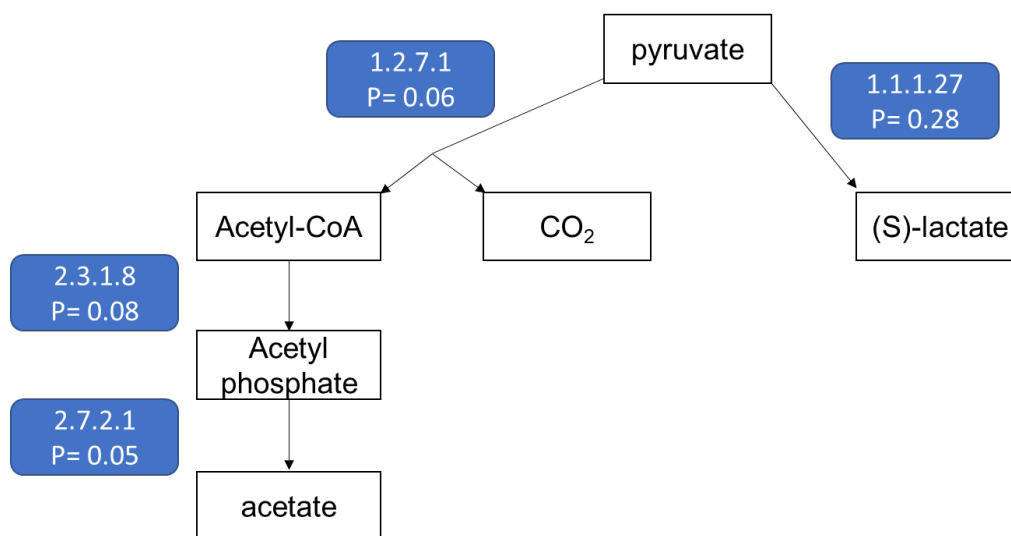
Supplemental Figure 3
An example of a branching Metacyc pathway. White boxes represent different compounds and blue boxes represent enzymes that catalyze reactions along the black arrows. The EC number as well as the corresponding p value are provided. All enzymes in this pathway had a greater abundance in the high N treatment than the no N treatment.
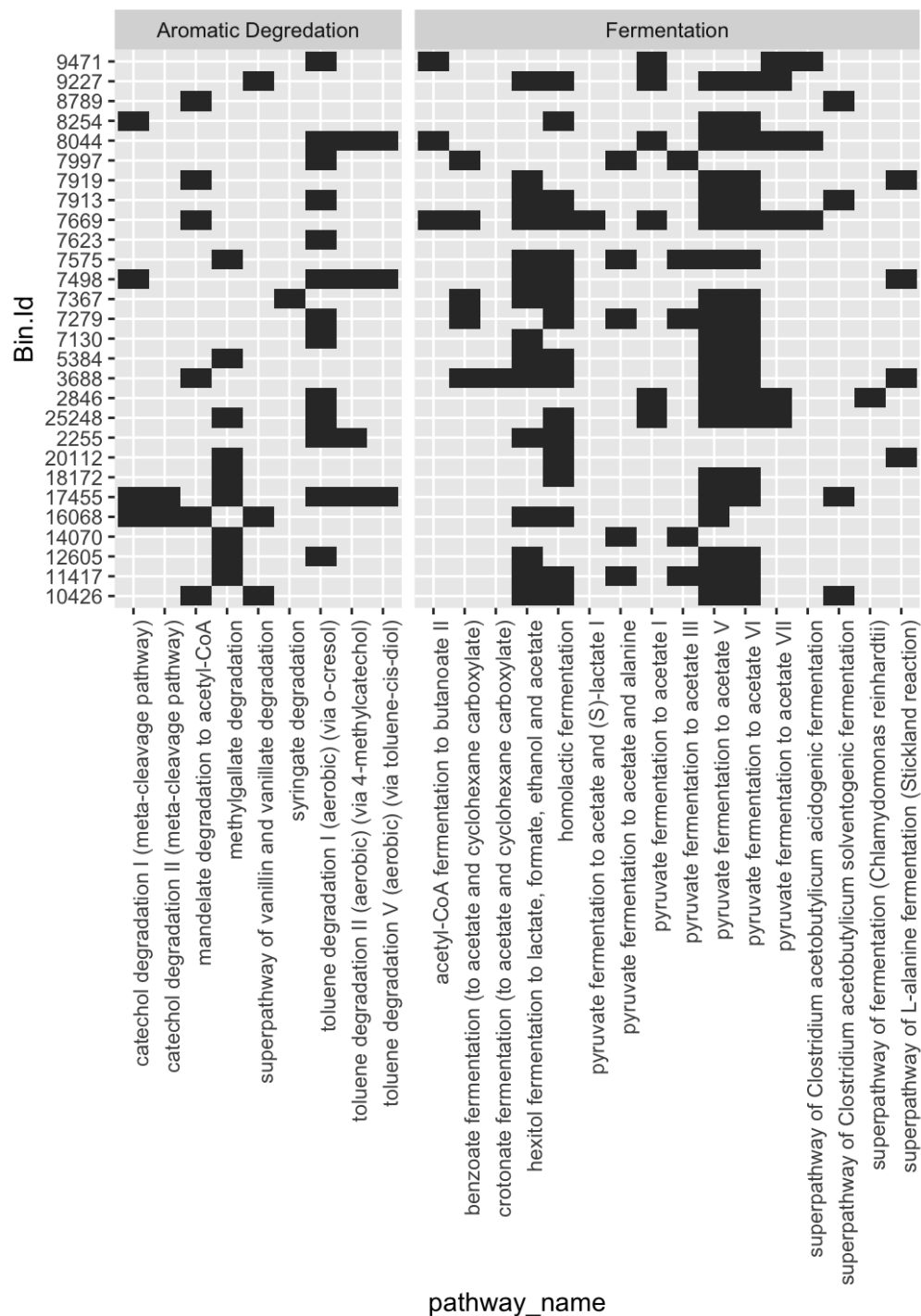
Supplemental Figure 4
MAGs that contain both aromatic degradation pathways and fermentation pathways, as depicted by the two titles at the top. Black boxes mean that the corresponding MAG (y axis) contains the specific pathway (x axis).
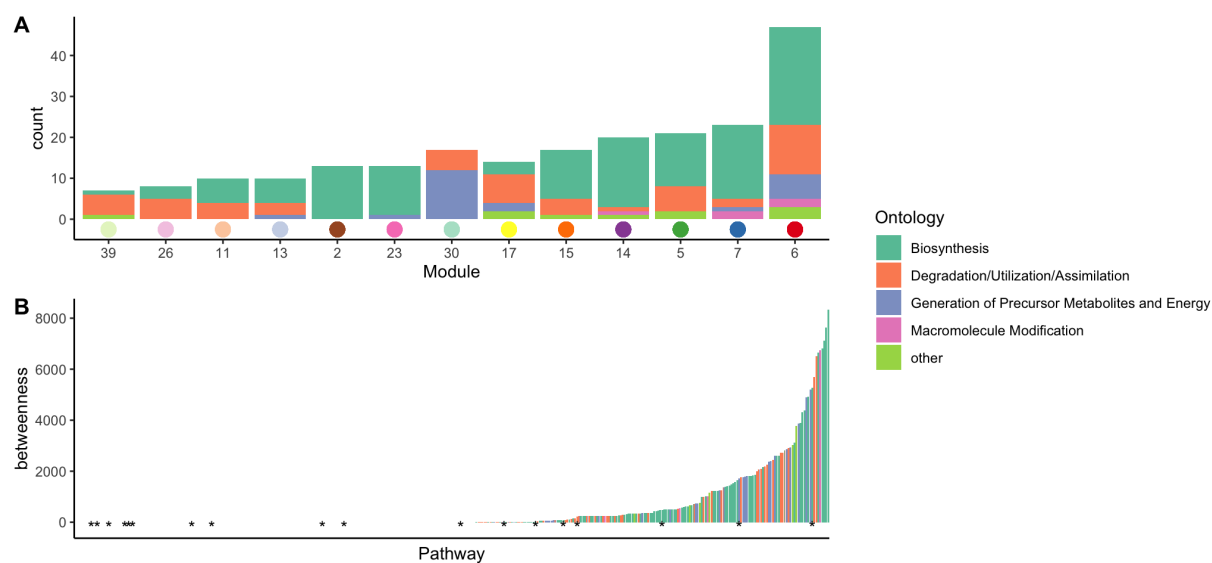
Supplemental Figure 5

(A) The thirteen most abundant modules identified in the co-occurrence network. The height of each bar corresponds to how many pathways are present in each module. The colored dot below the bar corresponds to the colors in the co-occurrence network (Figure 6D). The colors of each bar shows the parent class of each pathway in the module. (B) the betweenness centrality of each pathway in the co-occurrence network (Figure 6D). The color of the bar depicts the metacyc parent class that the pathway belongs to. Asterisks on the bottom highlight pathways that were differentially abundant in the HUMAnN3 analysis.
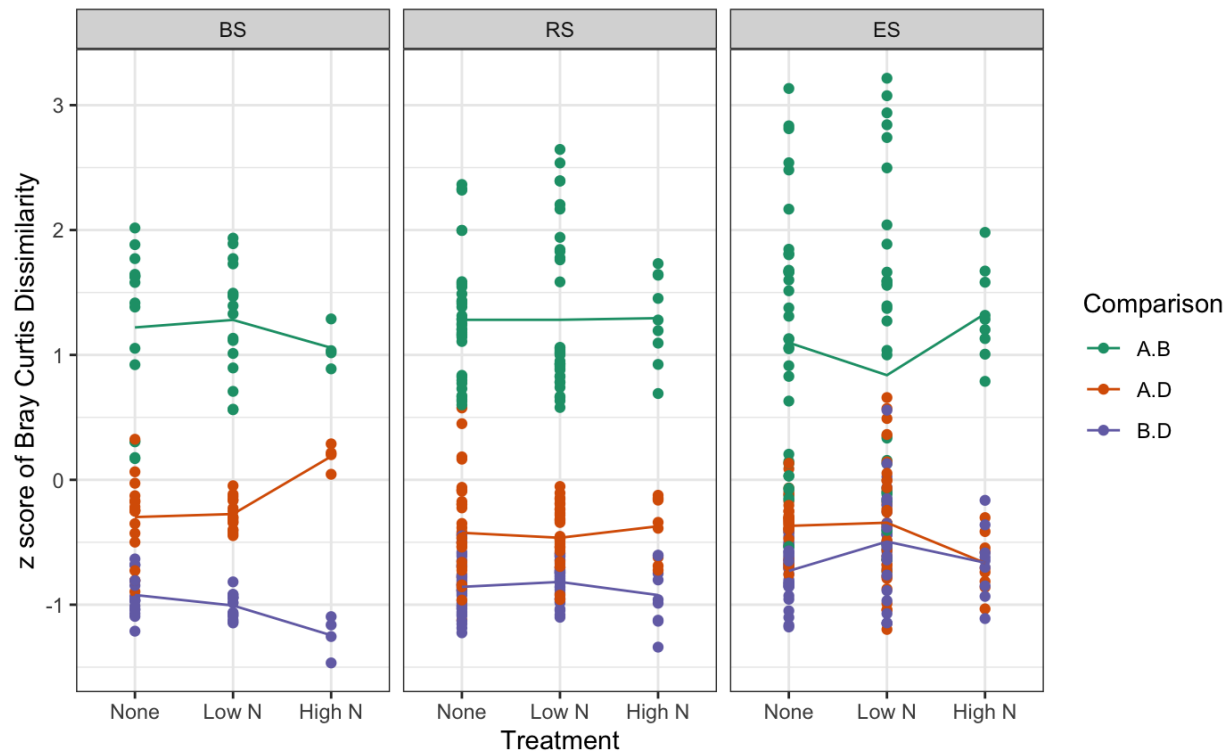
Supplemental Figure 6

Comparison of Bray-Curtis dissimilarity between soils at each time point. Each color represents a pairwise comparison between the three soils. Dots represent a comparison of two individual samples and the line is the average.

	Df	SumsOfSqs	MeanSqs	F.Model	R2	Pr(>F)	
Soil	2	10.7859	5.393	60.494	0.35817	0.001	***
Compartment	1	5.6141	5.6141	62.974	0.18643	0.001	***
N_level	1	0.9463	0.9463	10.615	0.03142	0.001	***
Soil:Compartment	2	4.4256	2.2128	24.821	0.14696	0.001	***
Soil:N_level	2	0.8753	0.4376	4.909	0.02907	0.001	***
Compartment:N_level	1	0.2257	0.2257	2.532	0.00749	0.016	*
Soil:Compartment:N_level	2	0.2875	0.1437	1.612	0.00955	0.061	.
Residuals	78	6.9536	0.0891		0.23091		
Total	89	30.114			1		

Table 1
PERMANOVA results testing the effects of Nitrogen treatment (N_level), Soil, and Compartment on the Bray-Curtis distances.

Pathway	Pathway Description	Metacyc Class	logFC	log.stderr	p.adjusted
PWY-5180	toluene degradation I (aerobic) (via o-cresol)	A.C.D.	1.0559	0.0410	0.0030
PWY-5182	toluene degradation II (aerobic) (via 4-methylcatechol)	A.C.D.	1.0559	0.0410	0.0030
PWY-5415	catechol degradation I (meta-cleavage pathway)	A.C.D.	0.7621	0.0476	0.0079
GALLATE-DEGRADATION-I-PWY	gallate degradation II	A.C.D.	1.7742	0.2913	0.0521
P184-PWY	protocatechuate degradation I (meta-cleavage pathway)	A.C.D.	1.9248	0.3171	0.0521
METHYLGALLATE-DEGRADATION-PWY	methylgallate degradation	A.C.D.	2.1590	0.3759	0.0536
PWY-6338	superpathway of vanillin and vanillate degradation	A.C.D.	0.9958	0.1899	0.0602
PWY-7097	vanillin and vanillate degradation I	A.C.D.	0.9958	0.1899	0.0602
PWY-7098	vanillin and vanillate degradation II	A.C.D.	0.9664	0.1833	0.0602
PWY-6339	syringate degradation	A.C.D.	2.0335	0.3941	0.0604
PWY-5179	toluene degradation V (aerobic) (via toluene-cis-diol)	A.C.D.	1.4500	0.2903	0.0622
PWY-5420	catechol degradation II (meta-cleavage pathway)	A.C.D.	1.0317	0.2132	0.0622
PWY-6957	mandelate degradation to acetyl-CoA	A.C.D.	2.4556	0.5072	0.0622
PWY-5183	superpathway of aerobic toluene degradation	A.C.D.	2.8686	0.7195	0.0739
PWY-5419	catechol degradation to 2-hydroxypentadienoate II	A.C.D.	1.0887	0.2996	0.0780
PWY-6210	2-aminophenol degradation	A.C.D.	2.4779	0.8138	0.0954
PWY-7383	anaerobic energy metabolism (invertebrates, cytosol)	Fermentation	0.6562	0.0718	0.0395
P161-PWY	acetylene degradation (anaerobic)	Fermentation	1.4644	0.1782	0.0486
CENTFERM-PWY	pyruvate fermentation to butanoate	Fermentation	1.6664	0.2265	0.0514
PWY-6590	superpathway of Clostridium acetobutylicum acidogenic fermentation	Fermentation	1.6185	0.2207	0.0514

PWY-5497	purine nucleobases degradation II (anaerobic)	Fermentation	1.1218	0.1788	0.0521
PWY-7003	glycerol degradation to butanol	Fermentation	1.6361	0.2718	0.0521
GLUDEG-II-PWY	L-glutamate degradation VII (to butanoate)	Fermentation	2.0342	0.3792	0.0602
PWY-5088	L-glutamate degradation VIII (to propanoate)	Fermentation	2.0231	0.3714	0.0602
P164-PWY	purine nucleobases degradation I (anaerobic)	Fermentation	3.1012	0.7079	0.0625
PWY-5100	pyruvate fermentation to acetate and lactate II	Fermentation	0.6274	0.1599	0.0742
FERMENTATION-PWY	mixed acid fermentation	Fermentation	0.5247	0.1472	0.0780
PWY-7111	pyruvate fermentation to isobutanol (engineered)	Fermentation	0.3481	0.0994	0.0780
PWY-7389	superpathway of anaerobic energy metabolism (invertebrates)	Fermentation	0.2750	0.0777	0.0780
ANAEROFRUCAT-PWY	homolactic fermentation	Fermentation	0.2870	0.0831	0.0784
PWY-5109	propanoate fermentation to 2-methylbutanoate	Fermentation	0.7354	0.2180	0.0797

Table 2
Pathways belonging to the Metacyc classes fermentation and aromatic compound degradation (A.C.D.). A log fold change greater than zero indicates the pathway is enriched in the high N treatment.

Measurement	term	df	sumsq	meansq	statistic	p.value
# Tillers	Soil	2	7.42E+02	3.71E+02	83.1601246	3.20E-14
# Tillers	Treatment	2	2.75E+03	1.37E+03	308.2205607	2.25E-23
# Tillers	Soil:Treatment	4	2.18E+02	5.46E+01	12.2392523	2.21E-06
# Tillers	Residuals	36	1.61E+02	4.46E+00	*NA*	*NA*
Height (cm)	Soil	2	1.19E+03	5.97E+02	17.7085267	4.42E-06
Height (cm)	Treatment	2	5.97E+03	2.98E+03	88.5035837	1.27E-14
Height (cm)	Soil:Treatment	4	8.53E+02	2.13E+02	6.3273926	5.80E-04
Height (cm)	Residuals	36	1.21E+03	3.37E+01	*NA*	*NA*
Vegetative Weight (g)	Soil	2	8.46E+02	4.23E+02	65.1016653	1.10E-12
Vegetative Weight (g)	Treatment	2	2.59E+03	1.30E+03	199.6397873	3.28E-20
Vegetative Weight (g)	Soil:Treatment	4	1.48E+02	3.70E+01	5.6893599	1.18E-03
Vegetative Weight (g)	Residuals	36	2.34E+02	6.50E+00	*NA*	*NA*
H	Soil	2	3.56E+01	1.78E+01	4.2710141	2.17E-02
H	Treatment	2	1.44E+02	7.21E+01	17.2987715	5.44E-06
H	Soil:Treatment	4	8.30E+01	2.08E+01	4.9831951	2.66E-03
H	Residuals	36	1.50E+02	4.17E+00	*NA*	*NA*
S	Soil	2	2.56E-02	1.28E-02	1.0862279	3.48E-01
S	Treatment	2	6.44E-02	3.22E-02	2.7352363	7.84E-02
S	Soil:Treatment	4	1.08E-01	2.69E-02	2.2866062	7.90E-02
S	Residuals	36	4.24E-01	1.18E-02	*NA*	*NA*
L	Soil	2	6.32E-03	3.16E-03	2.0262749	1.47E-01
L	Treatment	2	1.07E-01	5.33E-02	34.1321091	4.86E-09
L	Soil:Treatment	4	5.89E-03	1.47E-03	0.943839	4.50E-01
L	Residuals	36	5.62E-02	1.56E-03	*NA*	*NA*
R	Soil	2	2.16E+03	1.08E+03	6.7894542	3.15E-03
R	Treatment	2	2.38E+04	1.19E+04	74.7582487	1.52E-13
R	Soil:Treatment	4	2.78E+03	6.96E+02	4.3728652	5.52E-03
R	Residuals	36	5.73E+03	1.59E+02	*NA*	*NA*
G	Soil	2	2.03E+03	1.02E+03	7.7653759	1.57E-03
G	Treatment	2	2.64E+04	1.32E+04	101.0109909	1.72E-15
G	Soil:Treatment	4	2.04E+03	5.11E+02	3.905302	9.82E-03
G	Residuals	36	4.71E+03	1.31E+02	*NA*	*NA*
B	Soil	2	1.45E+02	7.27E+01	0.5421969	5.86E-01
B	Treatment	2	6.23E+01	3.12E+01	0.2325293	7.94E-01
B	Soil:Treatment	4	5.99E+02	1.50E+02	1.1161664	3.64E-01
B	Residuals	36	4.83E+03	1.34E+02	*NA*	*NA*

Table S1

ANOVAs testing the effects of soil and treatment on different plant phenotypes (first column)

Measurement	contrast	Soil	estimate	SE	df	t.ratio	p.value	p.adjusted
# Tillers	Low N - None	Arbuckle	13.33333333	1.21906157	36	10.9373748	9.50E-13	5.70E-12
# Tillers	High N - None	Arbuckle	24.83333333	1.49303941	36	16.6327381	0.00E+00	0.00E+00
# Tillers	Low N - None	Biggs	8	1.21906157	36	6.5624249	2.47E-07	1.48E-06
# Tillers	High N - None	Biggs	24.66666667	1.49303941	36	16.5211089	0.00E+00	0.00E+00
# Tillers	Low N - None	Davis	3.83333333	1.21906157	36	3.1444953	6.48E-03	3.89E-02
# Tillers	High N - None	Davis	14.5	1.49303941	36	9.711733	2.68E-11	1.61E-10
Height (cm)	Low N - None	Arbuckle	19	3.35249124	36	5.6674272	3.85E-06	2.31E-05
Height (cm)	High N - None	Arbuckle	21.66666667	4.10594646	36	5.2768995	1.28E-05	7.67E-05
Height (cm)	Low N - None	Biggs	27	3.35249124	36	8.0537123	2.86E-09	1.72E-08
Height (cm)	High N - None	Biggs	31.5	4.10594646	36	7.6718	8.79E-09	5.27E-08
Height (cm)	Low N - None	Davis	9.5	3.35249124	36	2.8337136	1.45E-02	8.68E-02
Height (cm)	High N - None	Davis	34.66666667	4.10594646	36	8.4430391	9.29E-10	5.57E-09
Vegetative Weight (g)	Low N - None	Arbuckle	14.59833333	1.47179045	36	9.918758	1.53E-11	9.18E-11
Vegetative Weight (g)	High N - None	Arbuckle	23.57333333	1.80256781	36	13.0776403	3.11E-15	1.87E-14
Vegetative Weight (g)	Low N - None	Biggs	11.29333333	1.47179045	36	7.6731938	8.75E-09	5.25E-08
Vegetative Weight (g)	High N - None	Biggs	22.12333333	1.80256781	36	12.2732323	2.00E-14	1.20E-13
Vegetative Weight (g)	Low N - None	Davis	6.04666667	1.47179045	36	4.1083747	4.33E-04	2.60E-03
Vegetative Weight (g)	High N - None	Davis	14.63833333	1.80256781	36	8.1208226	2.36E-09	1.41E-08
H	Low N - None	Arbuckle	3.15597971	1.17833614	36	2.6783357	2.13E-02	1.28E-01
H	High N - None	Arbuckle	3.38960329	1.44316115	36	2.3487351	4.63E-02	2.78E-01
H	Low N - None	Biggs	4.13526924	1.17833614	36	3.5094139	2.40E-03	1.44E-02
H	High N - None	Biggs	7.4755661	1.44316115	36	5.179994	1.72E-05	1.03E-04
H	Low N - None	Davis	-1.99793071	1.17833614	36	-1.6955524	1.77E-01	1.00E+00
H	High N - None	Davis	3.82798109	1.44316115	36	2.6524973	2.27E-02	1.36E-01
S	Low N - None	Arbuckle	-0.10959732	0.06264677	36	-1.7494487	1.60E-01	9.62E-01
S	High N - None	Arbuckle	-0.10756264	0.07672632	36	-1.4019002	2.92E-01	1.00E+00
S	Low N - None	Biggs	-0.05874721	0.06264677	36	-0.9377531	5.51E-01	1.00E+00
S	High N - None	Biggs	-0.03646858	0.07672632	36	-0.4753073	8.38E-01	1.00E+00
S	Low N - None	Davis	0.07743783	0.06264677	36	1.2361025	3.75E-01	1.00E+00
S	High N - None	Davis	-0.16633845	0.07672632	36	-2.1679452	6.90E-02	4.14E-01
L	Low N - None	Arbuckle	-0.06862745	0.02280737	36	-3.009003	9.24E-03	5.55E-02
L	High N - None	Arbuckle	-0.10217865	0.02793321	36	-3.6579627	1.59E-03	9.51E-03
L	Low N - None	Biggs	-0.10424837	0.02280737	36	-4.5708188	1.10E-04	6.57E-04
L	High N - None	Biggs	-0.16143791	0.02793321	36	-5.7794251	2.73E-06	1.64E-05
L	Low N - None	Davis	-0.05577342	0.02280737	36	-2.4454119	3.71E-02	2.22E-01
L	High N - None	Davis	-0.11111111	0.02793321	36	-3.977742	6.34E-04	3.81E-03
R	Low N - None	Arbuckle	-37.55555556	7.28181727	36	-5.1574427	1.84E-05	1.11E-04
R	High N - None	Arbuckle	-50.66666667	8.91836836	36	-5.6811588	3.69E-06	2.21E-05

R	Low N - None	Biggs	-51.05555556	7.28181727	36	-7.0113755	6.33E-08	3.80E-07
R	High N - None	Biggs	-75	8.91836836	36	-8.40961	1.02E-09	6.13E-09
R	Low N - None	Davis	-12.44444444	7.28181727	36	-1.7089751	1.73E-01	1.00E+00
R	High N - None	Davis	-55.11111111	8.91836836	36	-6.179506	7.97E-07	4.78E-06
G	Low N - None	Arbuckle	-39.44444444	6.60383197	36	-5.9729631	1.50E-06	9.02E-06
G	High N - None	Arbuckle	-54.44444444	8.08800934	36	-6.7315012	1.48E-07	8.86E-07
G	Low N - None	Biggs	-51.16666667	6.60383197	36	-7.7480267	7.02E-09	4.21E-08
G	High N - None	Biggs	-74.72222222	8.08800934	36	-9.2386419	9.84E-11	5.90E-10
G	Low N - None	Davis	-18.33333333	6.60383197	36	-2.7761659	1.67E-02	1.00E-01
G	High N - None	Davis	-60.22222222	8.08800934	36	-7.4458646	1.72E-08	1.03E-07
B	Low N - None	Arbuckle	4.44444444	6.68467219	36	0.664871	7.25E-01	1.00E+00
B	High N - None	Arbuckle	2.33333333	8.18701798	36	0.2850041	9.30E-01	1.00E+00
B	Low N - None	Biggs	-2	6.68467219	36	-0.2991919	9.24E-01	1.00E+00
B	High N - None	Biggs	-7.61111111	8.18701798	36	-0.9296561	5.56E-01	1.00E+00
B	Low N - None	Davis	-10.11111111	6.68467219	36	-1.5125814	2.44E-01	1.00E+00
B	High N - None	Davis	3.55555556	8.18701798	36	0.4342919	8.60E-01	1.00E+00

Table S2
Contrasts derived from linear models testing the effects of nitrogen treatment (high N and low N compared to no N) for the various plant phenotypes.

Bulk Soil:

	Df	SumsOfSqs	MeanSqs	F.Model	R2	Pr(>F)	
Soil	2	5.5202	2.7601	32.576	0.69452	0.001	***
N_level	1	0.1489	0.14886	1.757	0.01873	0.117	
Soil:N_level	2	0.2457	0.12286	1.45	0.03091	0.162	
Residuals	24	2.0335	0.08473		0.25584		
Total	29	7.9482			1		

Rhizosphere:

	Df	SumsOfSqs	MeanSqs	F.Model	R2	Pr(>F)	
Soil	2	8.1133	4.0566	54.097	0.67741	0.0001	***
N_level	1	0.4619	0.4619	6.16	0.03857	0.0006	***
Soil:N_level	2	0.4772	0.2386	3.182	0.03985	0.0046	**
Residuals	39	2.9245	0.075		0.24418		
Total	44	11.977			1		

Endosphere:

	Df	SumsOfSqs	MeanSqs	F.Model	R2	Pr(>F)	
Soil	2	7.0982	3.5491	34.354	0.56682	0.0001	***
N_level	1	0.7101	0.7101	6.873	0.0567	0.0001	***
Soil:N_level	2	0.6855	0.3428	3.318	0.05474	0.0018	**
Residuals	39	4.0291	0.1033		0.32174		
Total	44	12.523			1		

Table S3
PERMANOVA results testing the effects of Nitrogen treatment (N_level) and Soil on the Bray-Curtis distances of each compartment individually.